

NANO CALCIUM PHOSPHATES DOPED WITH TITANIUM AND FLUORIDE IONS:
SINTERABILITY AND STABILITY OF PHASES

A THESIS SUBMITTED TO
THE GRADUATE SCHOOL OF NATURAL AND APPLIED SCIENCES
OF
MIDDLE EAST TECHNICAL UNIVERSITY

BY

SERAP GÜNGÖR GERİDÖNMEZ

IN PARTIAL FULFILLMENT OF THE REQUIREMENTS
FOR
THE DEGREE OF DOCTOR OF PHILOSOPHY
IN
ENGINEERING SCIENCES

JUNE 2012

Approval of the thesis:

**NANO CALCIUM PHOSPHATES DOPED WITH TITANIUM AND FLUORIDE
IONS: SINTERABILITY AND STABILITY OF PHASES**

submitted by **SERAP GÜNGÖR GERİDÖNMEZ** in partial fulfillment of the
requirements for the degree of **Doctor of Philosophy in Engineering Sciences**
Department, Middle East Technical University by,

Prof. Dr. Canan Özgen

Dean, Graduate School of **Natural and Applied Sciences**

Prof. Dr. Murat Dicleli

Head of Department, **Engineering Sciences Dept.**

Assoc. Prof. Dr. Zafer Evis

Supervisor, **Engineering Sciences Dept.**

Examining Committee Members:

Prof. Dr. Turgut Tokdemir.

Engineering Sciences Dept., METU

Assoc. Prof. Dr. Zafer Evis

Engineering Sciences Dept., METU

Assoc. Prof. Dr. Dilek Keskin

Engineering Sciences Dept., METU

Assoc. Prof. Dr. Hasan Okuyucu

Materials Engineering Dept., YBU

Assoc. Prof. Dr. Ayşen Tezcaner

Engineering Sciences Dept., METU

Date: 14.06.2012

I hereby declare that all information in this document has been obtained and presented in accordance with academic rules and ethical conduct. I also declare that, as required by these rules and conduct, I have fully cited and referenced all material and results that are not original to this work.

Name, Last Name : Serap GÜNGÖR GERİDÖNMEZ
Signature :

ABSTRACT

NANO CALCIUM PHOSPHATES DOPED WITH TITANIUM AND FLUORIDE IONS: SINTERABILITY AND STABILITY OF PHASES

GÜNGÖR GERİDÖNMEZ, Serap

Ph.D., Department of Engineering Sciences

Supervisor: Assoc. Prof. Dr. Zafer EVİS

June 2012, 129 pages

The purpose of this study was to synthesize calcium phosphates doped with titanium and fluoride ions in different combinations. Pure and doped calcium phosphates were synthesized by a precipitation method. The synthesized materials were sintered at 1100°C and 1300°C for 1h. The ceramics were characterized by density measurements to determine the effect of sintering temperature. Presence of phases and bonds were characterized by XRD diffraction and FTIR spectroscopy. Grain sizes of the samples were obtained by SEM. Microhardness test was applied on the samples to determine the mechanical properties of the samples. It was observed that Ti^{4+} addition decreased the density of samples significantly at 1100°C, whereas increasing the sintering temperature to 1300°C caused an increase. Increasing the F^- ion amount increased the densification at 1100°C when molar ratios were 1.0, 1.25, 1.50 and decreased the density at 1300°C when Ca /P molar ratios were 1.0, 1.25, 1.67 and 2.0. Ti^{4+} and F^- co-doped samples showed variety in their density behaviour after the sintering at 1100°C and 1300°C.

The XRD analyses demonstrated that for Ca to P ratio 1 at 1100°C, β -CPP phase, when sintering temperature was raised to 1300°C, as a second phase of β -CPP and α -TCP observed. Increasing the molar ratio to 1.25 and 1.50 demonstrated β -TCP and/or β -CPP and β -TCP/ HA at 1100°C and β -TCP and/or β -CPP, α -TCP, TiO_2 and HA, α -TCP, TiO_2 phases at 1300°C, respectively. In higher Ca/P molar ratios of 1.67 and 2.0, HA, β -TCP, α -

TCP, CaO, TiO₂, CaTiO₃ and HA, CaO, α -TCP, CaTiO₃ phases were determined. Increasing the sintering temperature to 1300°C resulted in transformation to α -TCP.

In FTIR spectroscopy analysis, when the samples with molar ratio of 1, 1.25, 1.50, 1.67 and 2.0, sintered at 1100°C, the characteristic bands of β -CPP, OCP/ β -TCP, β -TCP/HA, HA and HA were observed, respectively. With increasing the sintering temperature to 1300°C, samples with molar ratio of 1.0 and 1.25 revealed additional secondary characteristic peaks of HA and β -TCP. SEM images revealed that sintering temperature and ion amounts of dopants had significant effect on grain sizes of the samples. The grain sizes were generally increased when sintering temperature rose from 1100°C to 1300°C. The μ -hardness test demonstrated that Ti⁴⁺ and F⁻ ions in large amounts had positive effect on the mechanical properties at the sintering temperatures of 1100°C and 1300°C.

Keywords: Hydroxyapatite; Calcium phosphate; Titanium; Fluoride.

ÖZ

TİTANYUM VE FLOR İYONLARI İLAVE EDİLMİŞ NANO-KALSIYUM FOSFATLAR: SİNERLENME VE FAZLARIN KARARLILIĞI

GÜNGÖR GERİDÖNMEZ, Serap

Doktora, Mühendislik Bilimleri Bölümü

Tez yöneticisi: Doç. Dr. Zafer EVİS

Haziran 2012, 129 sayfa

Bu çalışmanın amacı farklı kombinasyonlarda titanyum ve flor eklenmiş kalsiyum fosfatların sentezlenmesidir. Saf ve iyon eklenmiş kalsiyum fosfatlar bir çöktürme metodu ile sentezlenmiştir. Sentezlenen malzemeler 1100°C ve 1300°C de bir saat sinterlenmiştir. Seramikler sinterleme sıcaklığının etkisini belirlemek için yoğunluk ölçümleri ile incelenmiştir. Fazların ve bağların varlığı XRD kırınımı ve FTIR spektrometresi ile karakterize edilmiştir. Örneklerin tane boyutları taramalı elektron mikroskobu (SEM) ile elde edilmiştir. Örneklerin mekanik özelliklerinin belirlenebilmesi için numunelere mikrosertlik testi uygulanmıştır. 1100°C de Ti^{4+} katkısının örneklerin yoğunluğu önemli derecede düşürdüğü, sinterleme sıcaklığının 1300°C ye yükseltilmesinin ise bir azalmaya neden olduğu gözlemlenmiştir. F^- iyonunun miktarının artırılması Ca/P mol oranları 1.0, 1.25, 1.50'de yoğunlaşmayı arttırmış ve yoğunlukları 1300 °C de Ca/P mol oranları 1.0, 1.25, 1.67 ve 2.0 de yoğunluklar azalmıştır. Ti^{4+} ve F^- birlikte ilave edilmiş numunelerin yoğunluk davranışları 1100°C ve 1300°C'de sinterlendikten sonra farklılık göstermiştir.

XRD analizleri Ca/P oranı 1.0 iken, 1100°C de β -CPP fazı, sinterleme sıcaklığı 1300°C yükseltildiğinde ikincil fazlar olarak β -CPP ve α -TCP gözlenmiştir. Mol oranları 1.25 ve 1.50'ye artırılmasıyla sırasıyla 1100°C'de β -TCP ve/veya β -CPP, β -TCP/ HA ve 1300°C'de β -TCP ve/veya β -CPP, α -TCP, TiO_2 ve HA, α -TCP, TiO_2 fazlarını göstermiştir. 1.67 ve 2.0 olan daha yüksek Ca/P mol oranlarında, HA, β -TCP, α -TCP, CaO, TiO_2 , $CaTiO_3$ ve HA,

CaO, α -TCP, CaTiO₃ fazları belirlenmiştir. Sinterleme sıcaklığı 1300°C'ye yükseltildiğinde α -TCP'ye dönüşümle sonuçlanmıştır.

FTIR spektroskopi analizinde, mol oranları 1, 1.25, 1.50, 1.67 ve 2,0 olan numunelerde, 1100°C'de sinterlendiğinde sırasıyla, β -CPP, OCP/ β -TCP, β -TCP/HA ve HA karakteristik bantları gözlemlenmiştir. Sinterleme sıcaklığının 1300°C'ye yükseltilmesiyle, mol oranları 1.0 ve 1.25 olan numunelerde HA ve β -TCP ek ikincil karakteristik faz tepeleri olarak ortaya çıkmaktadır. SEM görüntüleri sinterleme sıcaklığı ve ilave edilmiş iyon katkı miktarlarının tane boyutları üzerinde önemli etkisi olduğunu göstermiştir. Tane boyutları genellikle sinterleme sıcaklığı 1100°C'den 1300°C'ye çıkartıldığında artmıştır. Mikrosertlik testi, 1100°C ve 1300°C sinterleme sıcaklıklarında yüksek miktarlarda Ti⁴⁺ ve F⁻ iyonlarının mekanik özellikler üzerinde olumlu etkisinin olduğunu göstermiştir.

Anahtar Kelimeler: Hidroksiapatit; Kalsiyum fosfat; Titanyum; Flor.

To my father and mother

ACKNOWLEDGMENTS

I would like to express my sincere gratitude to my supervisor Assoc. Prof. Dr. Zafer Evis for his enthusiastic guidance and patience throughout this study. I am also so grateful to my advisor for encouraging me in this interesting field, continuous encouragement and confidence in me and my work throughout the research.

I would also like to thank to Prof Dr. Turgut Tokdemir, Prof. Dr. Ruşen Geçit and Prof. Dr. Setsuo Maeda for their sincere support and guidance during my thesis.

I would like to express my gratitude thanks to my advisor Assoc. Prof. Dr. Zafer Evis, Assoc. Prof. Dr. Ayşen Tezcaner and Assoc. Prof. Dr. Dilek Keskin for allowing me to work in their Biomaterials laboratory. I owe my thanks to my lab friends Aydın Tahmasebifar and İdil Uysal for their guidance during my experiments. I also would like to thank my other dear lab friends; Ayşegül Kavas, Özge Erdemli and Ömer Aktürk for their support, friendship and the lovely environment they created in our lab.

I would like to express my special thanks to my dearest friends Dr. Ebru Önlü Dural, Dr. Rezan Sevinik Adıgüzel, Yasemin Kaya, and Ünal Tongür for their precious friendship. I am also grateful to my friends for their moral support and good will. With their presence, the joy they bring into my life and their constant support, they mean more than friends to me.

I would like to give my greatest thanks to my parents and my brother for the values they taught and the endless support they provided through my entire life. Their respect and belief in what I do is precious for me.

I offer my special thanks to my spouse Fatih Geridönmez for his unconditional love, continuous encouragement and support that provide me during my thesis.

TABLE OF CONTENTS

ABSTRACT	IV
ÖZ.....	VI
ACKNOWLEDGMENTS.....	IX
TABLE OF CONTENTS	X
LIST OF TABLES.....	XII
LIST OF FIGURES	XIV
LIST OF ABBREVIATIONS	XVI
CHAPTERS	
1 INTRODUCTION.....	1
1.1 BONE	1
1.1.1 Composition of Bone	2
1.1.2 Bone Mineral	5
1.2 APATITES	7
1.2.1 Calcium Phosphates	9
1.2.1.1 Calcium Phosphate Types	10
1.3 HYDROXYAPATITE	13
1.3.1 Synthesis Methods of HA.....	14
1.3.1.1 Solid State Sintering Process of HA	15
1.3.1.2 Emulsion and Micro-emulsion Techniques of HA	16
1.3.1.3 Hydrothermal Reactions of HA.....	17
1.3.1.4 Sol-gel Synthesis Technique of HA.....	18
1.3.1.5 Precipitation Method of HA	20
1.3.2 Microstructure and Phase Transformations of HA	21
1.3.3 Biological Properties of HA	22
1.3.4 Mechanical Properties HA	24
1.3.5 Nanophase Hydroxyapatite.....	24
1.4 HYDROXYAPATITE DOPED BY TITANIUM.....	26
1.5 HYDROXYAPATITE DOPED BY FLUORIDE.....	28

1.6	AIM OF THE THESIS	29
2	METHODS	30
2.1	MATERIALS.....	30
2.2	SYNTHESIS OF CALCIUM PHOSPHATES.....	30
2.2.1	Synthesis of Doped Calcium Phosphates	32
2.3	CHARACTERIZATION METHODS.....	33
2.3.1	Density Measurements	33
2.3.2	X-ray Diffraction	33
2.3.3	Fourier Transform Infrared Spectroscopy (FTIR)	34
2.3.4	Scanning Electron Microscopy (SEM).....	34
2.3.5	Mechanical Measurements	34
2.3.5.1	Vickers Micro-Hardness	34
3	RESULTS AND DISCUSSION	36
3.1	STRUCTURAL ANALYSIS.....	36
3.1.1	Density of the Samples.....	36
3.2	STRUCTURAL INVESTIGATION OF THE SAMPLES.....	40
3.2.1	X-Ray Diffraction	40
3.2.1.1	Lattice Parameter Measurements of Pure and Doped Hydroxyapatite ..	63
3.2.2	Fourier Transform Infrared Spectroscopy	66
3.2.3	Scanning Electron Microscopy	91
3.3	MECHANICAL INVESTIGATION OF THE SAMPLES	108
3.3.1	Micro-hardness Measurements	108
4	CONCLUSION	112
	REFERENCES	115
	VITA.....	129

LIST OF TABLES

TABLES

Table 1.1: The basic functions of the bone (adapted from [1]).	1
Table 1.2: The classification of bones according to shapes in the body and the properties [6].	4
Table 1.3: Composition of the dentine, enamel and bone given by weight % [17].	9
Table 1.4: Calcium phosphate types, abbreviation and Ca/P ratio [24].	11
Table 1.5: Comparative mechanical properties of cortical bone and HA.....	25
Table 1.6: Parameters in controlling crystal size, morphology chemical stability and sinterability of HA.	27
Table 2.1: List of the synthesis products with Ca/P ratio of 1.0, 1.25, 1.50, 1.67, 2.0.....	32
Table 2.2: Theoretical densities of CaP used in the relative density calculations [16].	33
Table 3.1: Sintered densities of calcium phosphates after the sintering at 1100°C and 1300°C for 1h	37
Table 3.2: ICDD files for CPP, DCPA, HA, TTCP and TCP.	40
Table 3.3: Hexagonal lattice parameters of pure and doped CaPs with a Ca/P ratio of 1.67 sintered at 1100°C and 1300°C.	64
Table 3.4: Z positions of the ions of OH and F [66].	65
Table 3.5: Frequencies and assignment and frequencies of CPP.....	67
Table 3.6: FTIR band locations in the samples with Ca/P molar ratio 1.0 at 1100°C.	67
Table 3.7: FTIR band locations in the samples with Ca/P molar ratio 1.0 at 1300°C.	69

Table 3.8: FTIR band locations in the samples with Ca/P molar ratio 1.25 at 1100°C.	72
Table 3.9: FTIR band locations in the samples with Ca/P molar ratio 1.25 at 1300°C.	74
Table 3.10: FTIR band locations in the samples with Ca/P molar ratio 1.50 at 1100°C.....	75
Table 3.11: FTIR band locations in the samples with Ca/P molar ratio 1.50 at 1300°C.....	79
Table 3.12: Frequencies and assignments of CaPs.	81
Table 3.13: FTIR band locations in the samples with Ca/P molar ratio 1.67 at 1100°C.....	82
Table 3.14: FTIR bands of HA and HA-TiO ₂ [105]	83
Table 3.15: FTIR band locations in the samples with Ca/P molar ratio 1.67 at 1300°C.....	84
Table 3.16: FTIR band locations in the samples with Ca/P molar ratio 2.0 at 1100°C.....	87
Table 3.17: FTIR band locations in the samples with Ca/P molar ratio 2.0 at 1300°C.....	88
Table 3.18: Average grain size of CaPs with molar ratios of 1,1.25, 1.50, 1.67, 2 sintered at 1100°C and 1300 °C.....	107
Table 3.19: Micro-hardness of CaPs with Ca/P ratios of 1,1.25, 1.50, 1.67 and 2 sintered at 1100°C and 1300 °C.....	111

LIST OF FIGURES

FIGURES

Figure 1.1: Composition of the bone [63].	2
Figure 1.2: Hierarchically organized structure of the bone [7].	5
Figure 1.3: Alignment of mineral crystals between collagen fibrils, fibers and bone mineral crystals [13].	7
Figure 1.4: Setting of carbonate HA and collagen molecules [15].	8
Figure 1.5: Crystal structure of HA a) c-axis b) off-axis c) with some atoms removed [119].	14
Figure 1.6: Experimental procedure of the sol-gel synthesis of HA powders [45].	19
Figure 1.7: Ca (I) and Ca (II) atoms in the microstructure of HA [52].	21
Figure 2.1: Synthesis process of pure CaPs.	31
Figure 3.1: XRD patterns of CaPs with Ca to P ratio of 1.0 sintered at 1100°C.	42
Figure 3.2: XRD patterns of CaPs with Ca to P ratio of 1.0 sintered at 1300°C.	45
Figure 3.3: XRD patterns of CaPs with Ca to P ratio of 1.25 sintered at 1100°C.	46
Figure 3.4: XRD patterns of CaPs with Ca to P ratio of 1.25 sintered at 1300°C.	48
Figure 3.5: XRD patterns of CaPs with Ca to P ratio of 1.50 sintered at 1100°C.	50
Figure 3.6: XRD patterns of CaPs with Ca to P ratio of 1.50 sintered at 1300°C.	52
Figure 3.7: XRD patterns of CaPs with Ca to P ratio of 1.67 sintered at 1100°C.	55
Figure 3.8: XRD patterns of CaPs with Ca to P ratio of 1.67 sintered at 1300°C.	58
Figure 3.9: XRD patterns of CaPs with Ca to P ratio of 2.0 sintered at 1100°C.	60

Figure 3.10: XRD patterns of CaPs with Ca to P ratio of 2.0 sintered at 1300°C.	62
Figure 3.11: FTIR patterns of CaPs with Ca to P ratio of 1 sintered at 1100°C.	70
Figure 3.12: FTIR patterns of CaPs with Ca to P ratio of 1 sintered at 1300°C.	71
Figure 3.13 : FTIR patterns of CaPs with Ca to P ratio of 1.25 sintered at 1100°C.	73
Figure 3.14: FTIR patterns of CaPs with Ca to P ratio of 1.25 sintered at 1300°C.	76
Figure 3.15: FTIR patterns of CaPs with Ca to P ratio of 1.50 sintered at 1100°C.	77
Figure 3.16: FTIR patterns of CaPs with Ca to P ratio of 1.50 sintered at 1300°C.	80
Figure 3.17: FTIR patterns of CaPs with Ca to P ratio of 1.67 sintered at 1100°C.	85
Figure 3.18: FTIR patterns of CaPs with Ca to P ratio of 1.67 sintered at 1300°C.	86
Figure 3.19: FTIR patterns of CaPs with Ca to P ratio of 2.0 sintered at 1100°C.	89
Figure 3.20: FTIR patterns of CaPs with Ca to P ratio of 2.0 sintered at 1300°C.	90
Figure 3.21: SEM images of CaPs with Ca to P ratio of 1.0 sintered at 1100°C.	93
Figure 3.22: SEM images of CaPs with Ca to P ratio of 1.0 sintered at 1300°C.	94
Figure 3.23: SEM images of CaPs with Ca to P ratio of 1.25 sintered at 1100°C.	96
Figure 3.24: SEM images of CaPs with Ca to P ratio of 1.25 sintered at 1300°C.	97
Figure 3.25: SEM images of CaPs with Ca to P ratio 1.50 sintered at 1100°C.	100
Figure 3.26: SEM images of CaPs with Ca to P ratio of 1.50 sintered at 1300°C.	101
Figure 3.27: SEM images of CaPs with Ca to P ratio of 1.67 sintered at 1100°C.	102
Figure 3.28: SEM images of CaPs with Ca to P ratio of 1.67 sintered at 1300°C.	103
Figure 3.29: SEM images of CaPs with Ca to P ratio of 2.0 sintered at 1100°C.	105
Figure 3.30: SEM images of CaPs with Ca to P ratio of 2.0 sintered at 1300°C.	106

LIST OF ABBREVIATIONS

<i>ACP</i>	: Amorphous Calcium Phosphate
<i>DCPD</i>	: Dicalcium phosphate dihydrate
<i>FA</i>	: Fluorapatite
<i>FHA</i>	: Fluoridated Hydroxyapatite
<i>FTIR</i>	: Fourier Transfer Infrared Spectroscopy
<i>HA</i>	: Hydroxyapatite
<i>RT</i>	: Room Temperature
<i>SEM</i>	: Scanning Electron Microscopy
<i>TTCP</i>	: Tetracalcium phosphate
<i>α-TCP</i>	: α -Tricalcium phosphate
<i>β-TCP</i>	: β -Tricalcium phosphate
<i>XRD</i>	: X-Ray Diffraction
<i>HLB</i>	: Hydrophile–lipophile balance
<i>FGM</i>	: Functionally-graded biomaterial

CHAPTER 1

INTRODUCTION

1.1 Bone

Bone is the most consequential biological tissue for mechanical support, protection and locomotion of a human and composed of complex and excellently organized hard living tissues. They function as to move, support, and protect the various organs of the body and to produce red and white blood cells and store minerals. Basic functions of the bone are summarized in Table 1.1.

Table 1.1: The basic functions of the bone (adapted from [1]).

Mechanical Support	Maintain points of attachment for most skeletal muscles and build up the softer tissues.
Protection	Contribute as mechanical protection for many of the body's internal organs.
Supporting in Movement	Skeletal muscles are attached to bones when the associated muscles contract they cause bones to move.
Storage of Minerals	Calcium (Ca) and phosphorus (P) stored in the bone tissues. These minerals are released when required into the blood which is simplifying the balance of minerals in the body.
Production of Blood Cells	Blood cells are produced in the red bone marrow.

1.1.1 Composition of Bone

Bone is considered as a natural composite material which consists of an organic protein; collagen and the inorganic mineral hydroxyapatite (HA, $\text{Ca}_{10}(\text{PO}_4)_6(\text{OH})_2$) whose primary elements are calcium and phosphate [2]. The organic matrix consist of 90% collagen and 10% of various noncollagenous proteins. Composition of the bone is given in Figure 1.1.

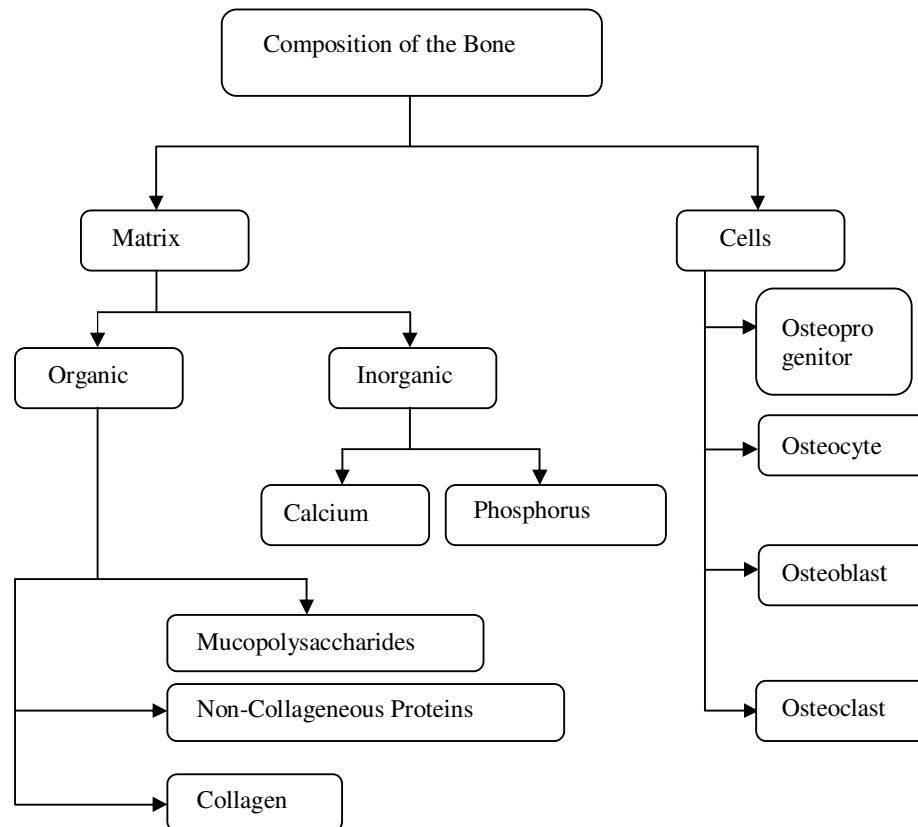


Figure 1.1: Composition of the bone [63].

Osteoblasts, osteoclasts and osteocytes are the bone lining cells which cover all surfaces of the bone. Bone lining cells control the activity of the ions (Ca^{2+} , PO_4^{3-} , etc.) among body and the bone. Osteoblasts, formed from bone lining cells, are cuboidal mononucleate cells that are responsible for bone formation [76]. Osteoblasts lay down the collagenous matrix osteoid which plays a role in the deposition of minerals. Osteoclasts resorb the bone tissue

by removing its mineralized matrix and breaking up the organic bone. Osteoclasts resorb bone by secreting H^+ and acids for matrix dissolution and enzymes for degradation of the matrix. Osteoclasts and osteoblasts are instrumental in controlling the amount of bone tissue. Osteocytes derived from osteoblasts function as bone maintaining cells. Osteocyte occupies a small chamber called lacuna which is used for exchange of nutrients and waste. The osteocyte is capable of bone deposition, resorption, formation, and matrix maintenance and calcium homeostasis. Osteocytes transmit the signals to other osteocytes in response to bone remodeling an even slight deformation of bone is caused by muscular activity [77]. Bones have different shapes according to their locations and functions throughout the body as seen in Table 1.2.

Table 1.2: The classification of bones according to shapes in the body and the properties [6].

Shape	Properties
Long Bones	Bones having long posture. Elongated shaft and two expanded ends one on either side of the shaft (shaft known as diaphysis and the ends called epiphysis). Shafts has a central medullary cavity where lies the bone marrow. Humerus, metacarpals, metatarsals, etc.
Short Bone	Short in posture and can be of any shape. Cuboid, cuneiform, scaphoid, trapezoid.
Flat Bone	Flat in appearance and have two prominent surfaces. They resemble shallow plates and form boundaries of certain body cavities. Scapula, ribs, sternum.
Irregular bones	Shape of the bones is fully irregular and they do not fit. Vertebrae, hip bone and bones in the base of skull.
Pneumatic bones	Characteristic is the presence of large air spaces which make them light in weight. Besides making skull light in weight also help in resonance of sound and as air conditioning chambers for the inspired air. Major portion of the skull in the form of sphenoid, ethmoid and maxilla.
Sesamoid bones	In the form of nodules embedded in tendons and joint capsules. Not possess any periosteum and their ossifications also take place after birth. Resist pressure, minimize friction, and maintain the local circulation. Patella, pisiform and fabella
Accessory bone	Accessory bones are not always present. One of their common occurrences is in the form of un-united epiphysis developed from extra centres of ossification. Sutural bones, os-trigonum, etc.

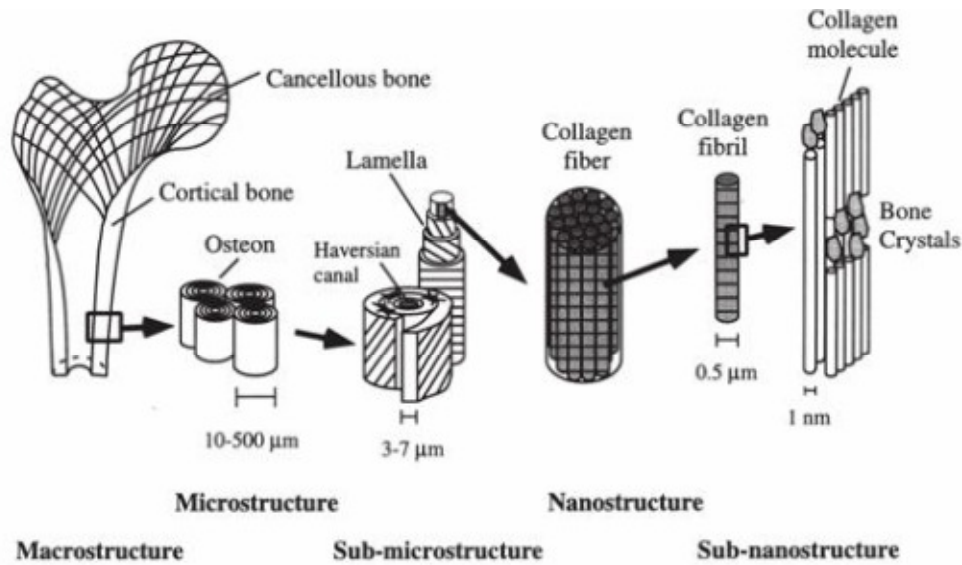


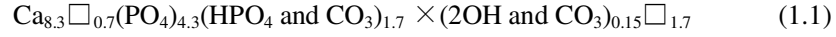
Figure 1.2: Hierarchically organized structure of the bone [7].

Porosity is the main parameter that effects the mechanical properties of the bone. As stated previously, bone consists of compact and cancellous parts in macroscopic level. Compact bone has a high density while cancellous bone exhibits a high level of porosity [7]. Porosity in cancellous bone enables metabolic activity besides its negative effect on the stiffness. Active remodeling provides cancellous bone to remain younger. The mechanical properties of these two different structures are influenced with different maturation properties. After maturation a reduction is observed in tensile strength of cortical bone due to the decrease in bone density [8]

1.1.2 Bone Mineral

Bone mineral is an heterogeneous material. Its composition varies based upon species, type of bone, diet, etc [9]. Minerals found in bones are: calcium, potassium, manganese, etc. Bone consists of calcium phosphates in the forms of crystallized HA and/or ACP which are formed of various ions like Na^+ , Sr^{2+} , C^{2+} , Mg^{2+} , K^+ , CO_3^{2-} , Cl^- and F^- . Bone is composed of 65% mineral, 35% organic matrix, cells, and water. The bone minerals are formed as in small crystals which are in the shape of needles, plates and rods located within and between collagen fibers. Foreign substances such as tetrocyclines, polyphosphates,

bisphosphonates and bone-seeking radionuclides can also be incorporated with high affinity [10]. Bone chemical composition is shown in chemical formula:



In which \square represents a vacancy. With maturation, the bone crystal get close, but never reaches, to the perfect HA structure [9].

The organic matrix produced by osteoblasts is composed of 90% collagen and 10% of various noncollagenous proteins [11]. The mechanical properties and the ability to regulate mineral ion homeostasis are implemented with the mineral component. The collagen type 1 fibrils whose function is to create an inorganic/organic composite structure, store the bone mineral which consists of tiny HA crystals [12]. Bone mineral growth and proliferation are controlled by the spatial limitation of the collagen fibers and by the absorption of matrix proteins [11]. The osteoblasts store the triphelical collagen molecule into the extra cellular space and fibrils produced with self-assembling process with dimensions of 300 nm length and 1.5 nm thickness. The mineral particles nucleated with a 67 nm periodicity in the collagen matrix is given in Figure 1.3.

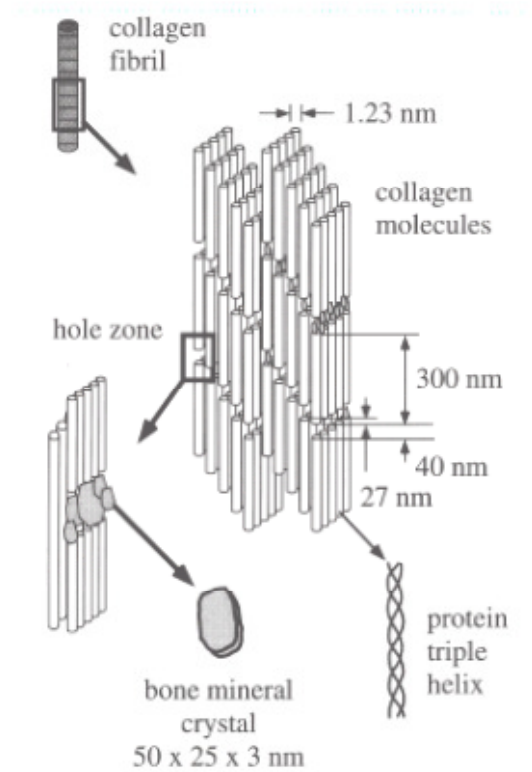


Figure 1.3: Alignment of mineral crystals between collagen fibrils, fibers and bone mineral crystals [13].

The plate-like apatite crystals formed within the discrete spaces of the collagen fibrils by which the crystal growth is limited and forced to be discrete and discontinuous with dimensions of 50×25 nm width and 2-3 nm crystal thickness [11].

1.2 Apatites

Apatite is a group of phosphate minerals usually referring to HA, chlorapatite etc. that has an hexagonal structure with the general chemical formula of $X_{10}(YO_4)_6Z_2$. In general chemical formula, X^{2+} can be partly or completely replaced by Ca^{2+} , Ba^{2+} , Sr^{2+} , Pb^{2+} , Ca^{2+} ions and YO_4^{3-} can be replaced by PO_4^{3-} , AsO_4^{3-} , VO_4^{3-} , SiO_4^{4-} , CO_3^{2-} ions whereas, Z^- can be replaced by F^- , OH^- , Cl^- or CO_3^{2-} ions [14]. The main inorganic constituent of hard

tissues of animal and human is known as apatite [15]. The biological apatites, in the form of needle or plate, are spreaded all around the organic matrix (see Figure 1.4).

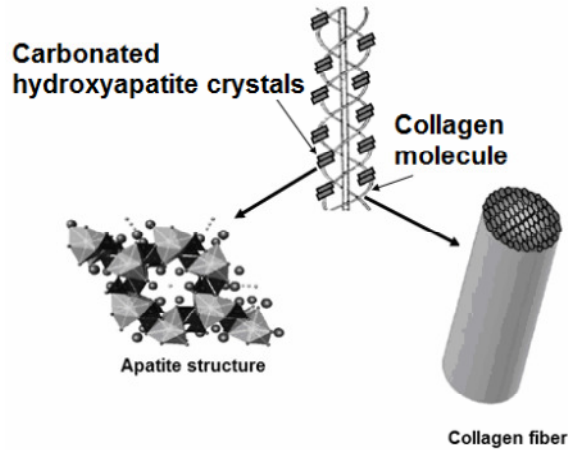


Figure 1.4: Setting of carbonate HA and collagen molecules [15].

Biological apatites are nonstoichiometric with vacant frame sites. Lowering of the symmetry and/or a small variance from the hexagonal structure is resulted from the lattice substitutions [16]. The structure of biological apatite is poorly crystalline because of the existence of the carbonate ions. Carbonate ions are known to have a considerable effect on the growth of the apatite crystals in solution; resulting in smaller crystals or even distorted products [16]. Ca/P ratios of dentine, enamel and bone and their composition of the inorganic components are given in Table 1.3.

Table 1.3: Composition of the dentine, enamel and bone given by weight % [17].

Component	Dentin	Enamel	Bone
Ca	40.3	37.6	36.6
P	18.6	18.3	17.1
CO ₃ ²⁻	4.8	3	4.8
Na	0.1	0.7	1
K	0.07	0.05	0.07
Mg	1.1	0.2	0.6
Sr	0.04	0.03	0.05
Cl	0.27	0.4	0.1
F	0.07	0.01	0.1
Ca/P (molar)	1.67	1.59	1.65

From Table 1.3, it can be concluded that;

- Stoichiometric Ca to P ratio of 1.67 is significantly higher than that ratio of enamel
- In bone and dentin the Mg quantity is higher than that in enamel and twice as much in the dentin compared to the bone.
- CO₃²⁻ amount of dentin and bone are same but higher than that of enamel.

It is concluded that when PO₄³⁻ is replaced by CO₃²⁻ in human enamel, the Ca/P ratio is completely different than that in pure HA [18]. HA is the most used CaP in biomedical applications because of its similarity to the mineral part of the bone.

1.2.1 Calcium Phosphates

Calcium phosphates (CaP) are the minerals involving calcium ions (Ca²⁺) with orthophosphates (PO₄³⁻) and frequently hydrogen or hydroxide ions. CaPs are used frequently in medical applications due to their high biocompatibility in the human body. Different CaPs are used for different biomedical applications, depending on the bioactivity

or resorption rates of the material. CaPs are used in hard tissue repair for a long time because of their similar inorganic form with the hard tissues. Many studies revealed that CaP biomaterials (HA, TCP and HA / TCP composite) and CaP-based biomaterials (CaP apatite-coated metals, calcium carbonate apatite and bioglass ceramics) are biocompatible and osteoconductive. When these materials are implanted in vivo, the results showed non-toxic, antigenically inactive, not inducing cancer and bonding directly to bone without any intervening connective tissue layer [19]. However, mechanical properties of CaPs are poor against to heavy loads due to their brittle nature.

HA and TCP are the most crucial CaPs due to superior biocompatibility of HA and its slow dissolution rate in the body and high resorption rate of TCP. Toth et al. revealed that bone formation in dogs induced by HA/TCP, α -CPP, and β -CPP (CPP: calcium pyrophosphate) [20]. Yang et al. revealed that HA / TCP phosphate ceramic-induced osteogenesis in dogs [21]. Yuan et al. showed that β -TCP ceramic and CaP cement can induce bone formation in soft tissues of dogs [22]. The coincident cases of CaP biomaterial induced osteogenesis represent the possibility to develop CaP biomaterials with fundamental osteoinductive property. Yuan et al. demonstrated that the osteoinduction of CaP biomaterials is material dependent [22]. The micropores on the macropore walls of the materials are important for osteoinduction. The material dependent properties of CaP-induced osteogenesis strongly suggest the possibility to develop CaP-based biomaterials with intrinsic osteoinductive property [19]

1.2.1.1 Calcium Phosphate Types

CaP ceramics have excellent osteoconductivity, bioactivity and ability to form strong bone–CaP interface. CaPs, especially HA and β -TCP, have been widely studied and used as bone substitute materials because of their similar molecular composition to bone [23]. There are many kinds of CaPs whose bioactivity and osteoconductivity are different [16]. CaPs can be found in the form of composites containing H_2PO_4^- , HPO_4^{2-} , and PO_4^{3-} ions [16].

The properties of CaPs can be characterized according to their Ca/P ratio in their structures.

HA is one of the most widely used synthetic CaP because of its chemical similarity to the inorganic component of hard tissues. In HA, Ca to P molar ratio is 1.67. The material properties are influenced by various Ca/P ratios at different aspects. When Ca to P ratio of hydroxyapatite is lower than 1.67, α or β -TCP phases may be revealed after the processing. If Ca to P ratio is higher than 1.67, calcium oxide may appear along with the hydroxyapatite phase [24]. In Table 1.4, various CaPs with their abbreviation and Ca/P ratios are presented.

Table 1.4: Calcium phosphate types, abbreviation and Ca/P ratio [24].

Name	Ca/P	Abbreviation	Formula
Calcium Metaphosphates (α , β , γ)	0.5	CMP	$\text{Ca}(\text{PO}_3)_2$
Calcium Pyrophosphates (α , β , γ)	1	CPP	$\text{Ca}_2\text{P}_2\text{O}_7$
Calcium Pyrophosphate Dihydrate	1	CPPD	$\text{Ca}_2\text{P}_2\text{O}_7 \cdot 2\text{H}_2\text{O}$
Calcium-deficient Hydroxyapatite	1.5	CDHA	$\text{Ca}_9(\text{HPO}_4)(\text{PO}_4)_5\text{OH}$
Dicalcium Phosphates	1	DCPA	CaHPO_4
Dicalcium Phosphates Dihydrate	1	DCPA	$\text{CaHPO}_4 \cdot 2\text{H}_2\text{O}$
Hepta Calcium Phosphate	0.7	HCP	$\text{Ca}_7(\text{P}_5\text{O}_{16})_2$
Hydroxyapatite	1.67	HA	$\text{Ca}_{10}(\text{PO}_4)_6(\text{OH})_2$
Monocalcium Phosphate Monohydrate	0.5	MCPM	$\text{Ca}(\text{H}_2\text{PO}_4)_2$
Tetracalcium Dihydrogen Phosphate	0.67	TDHP	$\text{Ca}_4\text{H}_2\text{P}_6\text{O}_{20}$
Tetracalcium Phosphate	2	TTCP	$\text{Ca}_4(\text{PO}_4)_2\text{O}$
Tricalcium Phosphate (α , β , γ)	1.5	TCP	$\text{Ca}_3(\text{PO}_4)_2$
Octacalcium Phosphate	1.33	OCP	$\text{Ca}_8\text{H}_2(\text{PO}_4)_6 \cdot 5\text{H}_2\text{O}$

Apatites are generally used as hard tissue implants such as coatings on metal prosthesis or in composites [16].

Ryu et al. studied TCP ceramic composite to overcome low biodegradability of HA [25]. Tricalcium phosphates has three polymorphs, such as: β -TCP is stable below 1180°C , α -TCP is stable between 1180°C and 1400°C , and α' -TCP is stable above 1470°C [25].

Among the three allotropic forms, β -TCP is preferred as a bioceramic on account of its chemical stability, mechanical strength, and proper bioresorption rate [25].

Tetracalcium phosphate is the only CaP phase with Ca to P ratio greater than stoichiometric hydroxyapatite. Different from other calcium orthophosphates such as hydroxyapatite or monetite, which are widely used as food ingredients, in tooth pastes, in pharmaceutical applications or in chromatography, phase-pure tetracalcium phosphate has found application only as a bioceramic [26]. Tetracalcium phosphate is an essential component of low-temperature setting inorganic biocements. Nevertheless, it is a metastable compound and various reaction routes are used to obtain phase-pure material in monolithic or particulate form [26]. Chow et al. demonstrated that TTCP/DCPA bioceramics can be hardened satisfactory and developed reasonable strengths when the TTCP/DCPA molar ratio was as low as 0.5 [27].

Amorphous calcium phosphate (ACP) is an intermediate phase in the preparation of several CaPs. Amorphous calcium phosphate is easily converted into poorly crystalline apatite analogous to bone mineral crystals. ACP used in plasma sprayed coatings on metal prostheses and injectable cements for orthopedic applications as a commercial substitute bone materials involved in the transient or constitutive phase. Amorphous calcium phosphate is also used in dental applications such as filler or colloidal suspension in toothpaste to promote demineralization [28].

For biomedical applications, sintered dicalcium pyrophosphate (SDCP) seems to be biocompatible to bone tissue in vivo animal model. Sintered dicalcium pyrophosphate has been demonstrated to be more biocompatible than HA in vitro model. Research with ovariectomized rats revealed that ingestion of either bisphosphonate or SDCP lessen the bone porosity and raise the bone mineral contents in the long bones [23]. Later works showed that Sintered dicalcium pyrophosphate can lead to apoptosis of osteoclasts in an ultrastructural model characterized by changes of the nucleus accompanied by degradation of cellular organelles [29]. Sun et al. showed that increased concentration of calcium and pyrophosphate ions can activate genes of the bone cells [29].

Dicalcium phosphates dehydrate (DCPD) is the major component of hard tissues like bone, teeth and used as a medicine for calcium supply. The crystallization of DCPD was obtained mainly by gel method [31].

Synthetic octacalcium phosphate (OCP) is used as a bone substitute material in various forms like coating on metallic implants and granules [31]. OCP is proposed to be a precursor of biological apatite crystals in bones and teeth. Transformation of synthetic OCP to HA has been studied in various physiological environments like body fluid and ultra filtered human serum, and by murine tissue implantation. The apatite converted from OCP under in vitro physiological conditions was a Ca-deficient HA, which has a chemical composition with a lower Ca/P molar ratio and higher acid phosphate content. Suzuki et al. revealed that the implantation of OCP markedly enhanced bone formation compared to the implantation of hydrolyzed Ca-deficient HA from OCP [31]. Osteoblastic cell proliferation and the differentiations were also simplified on OCP in vitro. Also Suzuki et al. confirmed that OCP as a bone substitute material increases the bone regeneration [31].

1.3 Hydroxyapatite

HA is the major component and an essential material of bone and teeth. HA forms the bone mineral and matrix of teeth. It has been widely used among various biocompatible materials in orthopedic applications because of its superior biocompatibility, bioactivity and similarity of its chemical resemblance to natural hard tissues [24]. HA is one of the few bioactive materials which support the bone growth and osseointegration when it is used in orthopedic, dental and maxillofacial applications. Mechanical properties of bone and HA are different in terms of their strength, hardness and toughness. Discrepancy limits its applications in load bearing areas [32]. Non-load bearing areas like middle ear, replacement for tooth roots places where HA has been frequently used. The physical, chemical, and biological properties of HA are controlled by its crystal structure (given in Figure 1.5) and composition. Insertion of Ca^{2+} with other metal ions into the HA structure improves the properties of HA, metal ions such as Ag^+ , Cu^{2+} , Zn^{2+} in the HA structure can affect its crystallinity, morphology, lattice parameters, stability and antibacterial property [33].

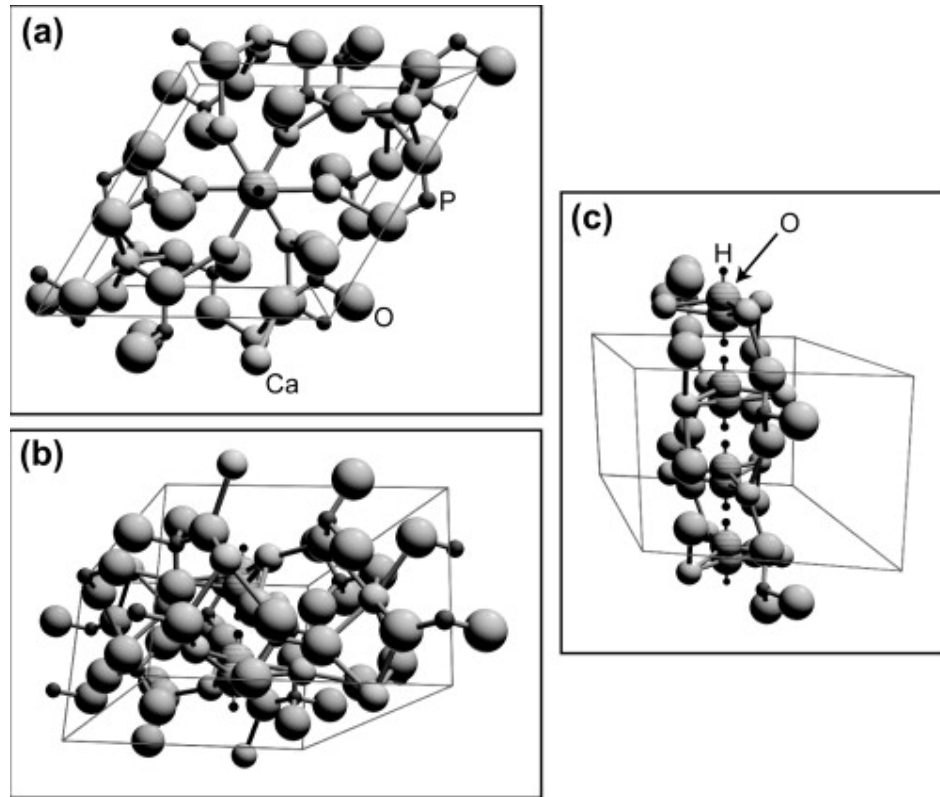


Figure 1.5: Crystal structure of HA a) c-axis b) off-axis c) with some atoms removed [119].

Muralithran and Ramesh demonstrated that the sintering temperature of HA is a critical factor influencing its phase stability, densification behavior, microstructure and hardness [34]. The optimum sintering temperature of HA was found to be 1250°C. A decrease in density was observed at lower temperature (<1250°C) sintering. The stability of HA phase in the sintered body was found to be dependent on the sintering temperature. Decomposition occurred above 1320°C. There is a correlation between hardness and grain size. Decomposition of HA is detrimental to its sinterability, densification and hardness [34].

1.3.1 Synthesis Methods of HA

HA is a potential material for various biomedical applications which can be produced by different synthesis methods and techniques. Techniques to prepare HA are classified in

three groups: wet, dry and hydrothermal processes [35]. Benefits of the wet processes are that the secondary product is almost water and the probability of contamination during processing is very low. The drawbacks are that with little difference in the reaction conditions in which the composition of the resulting product is affected sorely and the time needed for producing HA takes many days [36]. Wet method is very complicated and needs a special attention to control the Ca/P ratio as well as the crystallinity. Various methods have been employed to prepare the nano-sized HA, including precipitation, hydrothermal, sol-gel, crystal conversion and microwave techniques.

1.3.1.1 Solid State Sintering Process of HA

Solid state reaction is a simple and cheap method to synthesize HA. In the solid-state-reaction process, the samples were prepared by mixing the inorganic components in the presence of acetone or water [37]. The inorganic component mixture is then milled, compacted under pressure and sintered at a high temperature [37]. In solid state sintering method, milling is important because the amount of absorbed water is critically dependent on it and also milling influences the surface area of the powders [35]. The risk of contamination in the product is induced with milling. Another parameter in solid state sintering process is heat treatment. According to the results, HA produced by solid state sintering process reveals good biocompatibility and mechanical properties [35]. Also single phase of HA could be produced only in the powder milled in water [35]. As a result of low cost solid state sintering process a large amount of high crystalline HA can be obtained economically [35]. However, the powders synthesized by this method usually have irregular forms and large grain sizes.

Pramanik et al. synthesized HA by low cost solid-state sintering method [37]. After the sintering at 380, 600, and 1063°C, the material demonstrated structural phase transitions. Moreover, presence of α -TCP was observed after the sintering at 1250°C. Mechanical properties of HA were improved by an increase in cold compaction pressure during pelletization. Samples crushed and resintered at 1250°C demonstrated significant improvement in the mechanical properties and good biocompatibility. The density of HA was found to be lower than that of the conventional ceramic materials [37]. The surface

hardness of the samples was found to be 15-16 times larger than natural femoral bone and no change in the sample weight (dry state) was observed [37].

1.3.1.2 Emulsion and Micro-emulsion Techniques of HA

HA powders can be synthesized in bicontinuous micro emulsion, inverse micro emulsion and emulsion techniques by the reaction of CaCl_2 and $(\text{NH}_4)_2\text{HPO}_4$ [38]. Different proportion of cyclohexane surfactant is used during the reactions in order to determine if the solution acts as an emulsion structure, inverse microemulsion or bicontinuous microemulsion. As a result, bicontinuous and inverse microemulsion initiate the formation of much finer HA powders than from the emulsion composition [38].

Jarudilokkul et al. synthesized nanosized HA particles with emulsion liquid membrane (ELM) method [39]. The synthesized particles were calcium deficient apatite with an amorphous morphology. The initial Ca/P molar ratio had no effects on the particle sizes. When reaction temperature was increased, the surface area of prepared particles decreased resulting in an increase in particle size, transformation of HA particles to β -TCP [39].

Microemulsion processing techniques are used to prepare nanoparticles of metals, superconductors and bioceramics. Koumoulidis et al. applied the pH-shock wave method using an emulsion technique to produce phosphate particles, with a grain size of 40-120 nm [40]. Samples consist of mesoporosity with a narrow pore size and maximum pore diameters between 292 and 350 Å. After a heating at 650°C, the solid is crystallized in particles of similar size and shape, with no internal porosity. Significant amount of β -TCP was observed after the calcination at 900°C [40].

Yang et al. synthesized luminescent Eu^{3+} doped HA particles with high purity and crystallinity under mild reaction conditions with microwave assisted microemulsion process [41]. pH of the solution affects the morphologies and the particle size of the final products [41].

Guo et al. synthesized nanosized HA particles with a reverse microemulsion technique [42]. HA particles produced with microemulsion route compared with conventional precipitation

method had a smaller size and less particle agglomeration. HA particle diameter and length were increased with the increase of HLB (hydrophile–lipophile balance) values [42].

1.3.1.3 Hydrothermal Reactions of HA

Hydrothermal method is often used to prepare HA with good crystallinity and homogeneous size and shapes, which can be achieved at low temperatures. In hydrothermal reactions in order to synthesize HA, calcium hydrogen phosphate dehydrate ($\text{CaHPO}_4 \cdot 2\text{H}_2\text{O}$) and calcium carbonate (CaCO_3) or $\text{Ca}(\text{OH})_2$ powders were mixed in a high speed agitator [43]. The molar ratio of $\text{CaHPO}_4 \cdot 2\text{H}_2\text{O}$ to $\text{Ca}(\text{OH})_2$ was 3:7 [14] also mixture in another work prepared at a Ca/P ratio of 1.67 [43]. After hydrolyzation, the aggregates were filtered and rinsed in the de-ionized water. Subsequently the synthetic products were dried and grounded. Finally the powders with different Ca/P ratios hydrolysis were annealed at different temperatures [43]. In another study HA powders with good crystallinity, sinterability, high strength and biocompatibility were produced with heating the powders of $\text{Ca}(\text{OH})_2$ and $\text{Ca}(\text{H}_2\text{PO}_4)_2 \cdot 2\text{H}_2\text{O}$ with distilled water in a pressurized pot [14]. The drawback of this method is small amounts can be produced in the laboratory, limited commercial use and moderately expensive.

Zhang and Vecchio synthesized HA rods with the hydrothermal reaction of DCPA and cuttlebone powder or CaCO_3 from 120°C to 180°C for different durations [44]. The synthesis is observed to be a nucleation-growth process. The nucleation and growth of HA rods mainly occurred on DCPA particles. Because of the low stability of DCPA and calcite, the concentration of calcium and phosphate ions in the solution was low [44]. So HA can grow slowly and preferably along c-axis and form hexagonal shape in hydrothermal conditions. β -TCP as calcite nucleated and grew on the surface of calcite particles at the beginning of the reaction. When the reaction time was increased, formation of β -TCP slowed down. HA with lower solubility, grew larger into rod-shape particles on DCPA with the depletion of the starting materials. A small amount of β -TCP was produced as a side product. Synthesized large HA rods have potential applications for protein purification in liquid chromatography [44].

1.3.1.4 Sol-gel Synthesis Technique of HA

In sol-gel method, HA powder was prepared by using phosphoric pentoxide (P_2O_5) and calcium nitrate tetrahydrate ($Ca(NO_3)_2 \cdot 4H_2O$) [45]. A designed amount of phosphoric pentoxide (P_2O_5) and calcium nitrate tetrahydrate are dissolved in ethanol to form the solution. Then two solutions were mixed in a Ca/P molar ratio of 1.67 as an initial mixed precursor solution. In order to obtain white transparent gel, the mixture was continuously stirred at ambient temperature and dried in an oven. Resultant powders are obtained with crushed sintered products [45]. A simple sol-gel synthesis method of HA is presented in Figure 1.8.

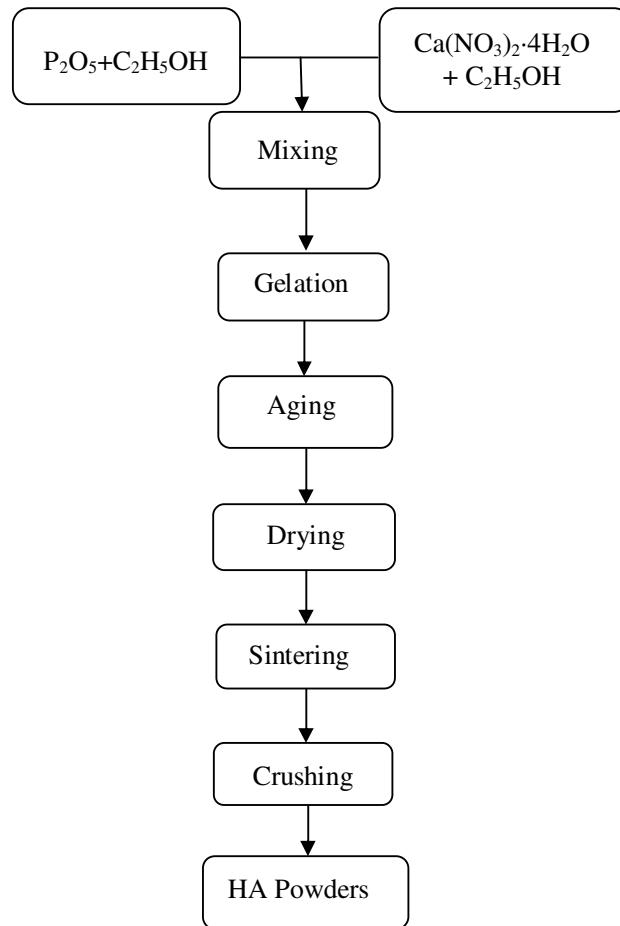


Figure 1.6: Experimental procedure of the sol-gel synthesis of HA powders [45].

Sintering temperature and time determine the crystallinity degree, morphology and the particle size of HA obtained by the sol-gel synthesis technique [45]. Controlling the grain size and morphology with sintering temperature, sol-gel synthesis of HA is similar to other HA production methods [45]. As a drawback during drying, cracks might occur due to the capillary forces. Some studies about sol-gel synthesis methods and the outcomes are summarized below.

Padmanabhan et al. synthesized HA nanorods of 70-90 nm diameter and 400-500 nm length. The pH during synthesis was 9 [46]. With increasing the temperature, the crystallite size of the HA nanoparticles increased. At 700°C, anisotropic crystal elongation was emerged.

With increasing the temperature, the crystallinity of the powders was also increased. HA nanorods with an aspect ratio value between 6 and 7 were obtained. Final calcined product was pure HA. Rietveld analysis demonstrated high purity and hexagonal structure of calcined HA, demonstrate hexagonal structure [46].

Liu et al. produced HA ceramics with sol-gel route using triethyl phosphate and calcium nitrate as phosphorous and calcium precursors [47]. Water and anhydrous ethanol were used as diluting environment for HA sol preparation. The sols were stable and no gelling was occurred in surrounding environment over 5 days. After the solvent was removed from the solution at 60°C, it became a white gel. When calcination temperature was increased, the crystal size and the HA content in both gels increased. The microstructure and crystallinity of the resulting HA ceramic were not affected with the initial diluting media. After ethanol-based sol dip-coating onto a Ti^{4+} substrate, and calcination at 450°C, resulted in porous coating with pore size ranging from 0.3 to 1 μm [47].

1.3.1.5 Precipitation Method of HA

Precipitation is one of the most used techniques in order to prepare HA powders. In this method, HA compounds are prepared with calcium nitrate tetra hydrate and di-ammonium hydrogen phosphate $((\text{NH}_4)_2\text{HPO}_4)$ as the starting materials and ammonia solution as pH adjustment agent [48]. A suspension of $\text{Ca}(\text{NO}_3)_2 \cdot 4\text{H}_2\text{O}$ with distilled water and di-ammonium hydrogen phosphate with distilled water was prepared. The solutions were stirred and the temperature was maintained at 25°C. A solution of di-ammonium hydrogen phosphate in distilled water solution is added drop wise to the calcium nitrate tetra hydrate. The pH of the $\text{Ca}(\text{NO}_3)_2 \cdot 4\text{H}_2\text{O}$ solution is adjusted to be 11 [48]. Afterwards the precipitated HA is removed by centrifugation method. The obtained HA is then dried and calcined. It has been observed that with increasing the temperature grain, size of the product increased. As a result the grain size of HA can be controlled by a precipitation method and nano-sized crystals can be obtained by applying a heat treatment at a suitable temperature. In biomedical applications, nano-sized HA crystals are significant due to their increased bioactivity and osseointegration [48]. Consequently, precipitation method is significant in order to synthesize HA especially used in biomedical area. A study about precipitation method and its outcomes are summarized below.

Cengiz et al. synthesized HA using CaPTris solution as a calcium phosphate medium by precipitation method [49]. The synthesized crystallites range from 15.88 to 16.12 nm. The (d002/d300) ratio was found as 0.99 for the particles. The length and the width of the particles were found to be less than 500 and 100 nm. Composition of the product produced from CaPTris (1.58) is closer to that of the ideal HA (1.67) [49].

Among all these methods the precipitation method is a simple and low cost process in industrial applications. HA prepared by precipitation method also has the feature of small size, low crystallinity and high surface activity, which can meet different demands.

1.3.2 Microstructure and Phase Transformations of HA

The structure of HA is hexagonal which belongs to the space group P63/m. This is defined by a six fold c-axis perpendicular to three a-axes (a_1 , a_2 , a_3) whose angles are 120° [50]. In HA structure four of the ten Ca atoms intercept Ca (I) position and the remaining six calcium atoms occupy the Ca (II) position. In the structure the OH groups are located at the corners of the unit cells (Figure 1.9) [52]. Network is made up of (PO_4^{3-}) group constituting the skeletal stability in the HA structure in which from level $z = 0.25$ to $z = 0.75$ of six (PO_4^{3-}) groups constituting form a helical formation.

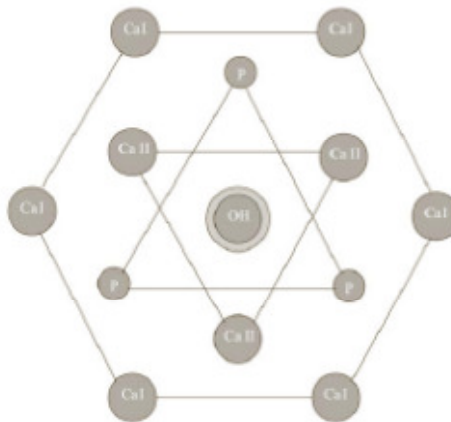
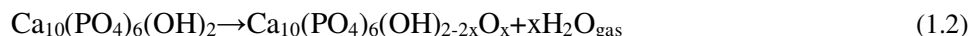


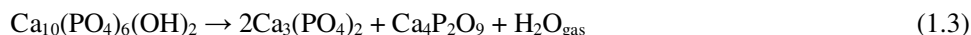
Figure 1.7: Ca (I) and Ca (II) atoms in the microstructure of HA [52].

Phase transformation is generally happened during sintering of HA in which, decomposition of HA to secondary phases like TCP and TTCP occurs at high temperatures [53]. Phase transformation of HA is seen in different synthesis methods such that in solid state reaction, the newly formed phases are β - $\text{Ca}_2\text{P}_2\text{O}_7$, $\text{CaP}(\text{HPO}_4)(\text{PO}_4)_5\text{OH}$, β -TCP and α -TCP at temperatures of 500°C, 800°C and 1250°C, respectively. Similarly in micro emulsion synthesis method, β -TCP is formed at 1200°C [35]. Likewise with sol-gel synthesis method β -TCP and CaO formed above 800°C [36]. Finally with precipitation method β -TCP was formed at above 1300°C [37].

In hydrothermal synthesis of HA, thermal decomposition occurs in two steps during sintering: dehydroxylation and decomposition. At temperatures around 850-900°C, HA dehydroxylates to oxyhydroxyapatite [54]:



The decomposition of HA to TCP and TTCP occurs at above 900°C.



Another factor causing the phase transformation besides sintering temperature is the calcium deficiency of the synthetic apatite [34]. Deviation from the Ca/P ratio which is 1.67 would probably result in formation of new phases [24]. The rate of the dehydroxylation and decomposition reactions depends on the humidity in the furnace because of existence of water vapor which resulted in a slow decomposition rate by preventing the dehydration of the OH group. Sintering temperature, atmosphere and Ca/P ratio of HA are important factors contributing to phase transformations. Furthermore, formation of second phases during the sintering can be suppressed by controlling the moisture content in the sintering environment. Also addition of the sintering additives into HA can control the presence of second phases [54].

1.3.3 Biological Properties of HA

In biomaterials research HA takes the particular attention because of its biocompatibility and bioactivity characteristics. HA is the ideal phase for an application inside the human

body because it is a thermodynamically stable material to be used in physiological pH, temperature and composition [55]. HA is crystallographically similar to natural bone mineral which represents the bone growth on the material [56]. For the bioactivity, consequential parameters of HA are the cell behaviors like adhesion, proliferation and morphology. In a research morphology and resorption activity of osteoclast-like cells on conventional and nanophase HA and alumina were examined [57]. The cellular activity of the osteoclast like cells was arranged by the synthesis of tartrate resistant acid phosphatase (TRAP) and the resorption pits formed on material surfaces by the cells. During 13-day time period, TRAP synthesis was the highest on conventional and nanophase of HA. For the formation of resorption pits, both conventional and nanophase HA exhibited a similar behavior to the bone reference material, however a higher resorption activity was observed on nanophase HA. As a result higher osteoclast-like cell function was observed on nanophase HA compared to conventional HA, this is consequent of increased roughness, higher surface wettability and the improved solubility of nanophase HA [57]. In a different study, osteoblast functions including on HA were investigated; proliferation, alkaline phosphatase synthesis and extracellular matrix calcium concentration on HA ceramics [58]. Resultant osteoblast cell functions were greater on nanophase HA with longer cell culture periods compared to conventional HA. As a result for these two studies, nanophase HA offers improved biological properties by enhanced osteoclast and osteoblast cell activity on the material [58].

When nano-HA powder was synthesized at room temperature (RT), in vitro experiments demonstrated that the produced material was biocompatible with osteoblastic-like MG63 cells and possess osteo-conductive properties [59].

With hot pressing technique, HA-based composite reinforced with 40 vol.% Ti particles were produced [60]. In vivo studies revealed that HA-40 vol.% Ti composite had excellent biocompatibility and could integrate with bone. There weren't any fibrous tissues with the interface between the composite implant and new born bone.

1.3.4 Mechanical Properties HA

The applicability of HA is restricted to non-stressed regions of the skeleton because of its inferior strength and low fracture toughness [37]. HA which is used under load bearing applications such as artificial joints has been restricted by its low fracture toughness (0.8-1.2 MPa m^{1/2}) and low flexural strength (<140 MPa) [61]. Also mechanical properties of HA diminishes because of the decomposition of HA into other phases [61]. Elastic modulus of HA is much higher than that of natural bone tissues which causes to greater stress concentration and fracture at the bone and material interface [62].

One additional important parameter that affects the mechanical properties of HA is the porous structure which provides a network for the growth of bone tissue and accelerates the replacement of the material by bone tissue [62]. It is observed that porosity affects the elastic modulus and hardness of HA exponentially [62]. After a sintering at 1200°C, flexural strength of HA was 120 MPa [35]. In another study, it was found to be between 58 and 80 MPa depending on the pressing geometry and load applied to the powders [63]. Another work revealed that HA nanopowders synthesized with controlled morphology resulted in rod-shaped particles into spherical nanopowders. The amount of rod-shaped particles caused a decrease in the micro hardness and an increase in indentation fracture toughness of the samples. In SEM pictures, an increase in porosity was detected with the addition of rod-shaped particles. Results demonstrated that the reported mechanical properties such as increased porosity limits crack propagation and increases indentation fracture toughness and low micro-hardness values [64]. It can be concluded that while producing HA some variables must be taken into account in order to obtain optimum mechanical properties which are mechanical synthesis methods, heat treatment temperature, porosity, microstructure and stoichiometry of the sample.

1.3.5 Nanophase Hydroxyapatite

HA has been widely used as a biomaterial because of its nano grain size which is more desirable in clinical applications [66]. Nanocrystalline HA shows improved sinterability and densification because of its greater surface area, with increase in its mechanical properties [67].

Nanostructured HA is expected to have superior mechanical performance in comparison with conventional HA as used for multifunctional implant systems by controlling important parameters such as particle size and shape, particle distribution and agglomeration. Because of the insufficient properties of HA, many measurements and studies have been implemented to improve both its mechanical and biological properties by producing nano-sized HA and doping the HA with various ions [62].

Table 1.5: Comparative mechanical properties of cortical bone and HA.

Properties	Cortical Bone	HA
Density (g/cm ³)	1.9	3.156
Tensile Strength (MPa)	124-174	40-300
Compressive Strength (MPa)	170-193	300-900
Bending Strength (MPa)	160	115-200
Youngs Modulus (GPa)	17-27	80-120
Poissons Ratio	-	0.28
Hardness (GPa)	0.396	3.79-5.0
Fracture Toughness (MPa·m ^{1/2})	2-12	0.6-1.3

By controlling the powder characteristics such as particle size, shape, particle distribution and agglomeration various properties of HA can be improved [68]. However, mechanical properties of HA do not conform with mechanical properties of bone (Table 1.5) and limit the application of HA in load-bearing areas. HA has been used in non-load bearing areas such as ossicles in middle ear and replacements for tooth roots [65].

The hexagonal structure of HA contains calcium and phosphorus elements which are the same elements in the inorganic parts of the bone and teeth. Consequently, the host reactions against HA are minimum where strong bonds are generated between bone and implant material surface due to the high bioactivity of HA. Concernment about nano crystalline HA was given in order to provide improvements both biologically and mechanically. The studies and researches on nano HA have been developing because the bone minerals are in nano scale [67].

It has been observed that in order to obtain crystalline HA with a uniform morphology aging is an important parameter. For aging up to 100 h, samples synthesized by precipitation method became more stable against decomposition to second phases. Small crystalline sizes around 50 nm could be produced from the HA powders calcined at 550°C which were confirmed by transmission electron microscopy (TEM) and XRD peak broadening analysis. The aging time and temperature were inspected of some important parameters such as precursor pH, in order to achieve nano-HA particles with tailored composition, crystal size, morphology and surface chemistry to optimize their chemical stability, sinterability and mechanical properties [67]. Resulting effects of these parameters are summarized in Table 1.6.

1.4 Hydroxyapatite Doped by Titanium

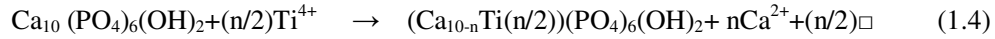
Huang et al. doped two levels of Ti^{4+} ions into HA by a co-precipitation method [69]. Rietveld refinement analysis revealed that there was a proportional increase in a and c axes with doping of Ti^{4+} into HA. Doping of Ti^{4+} into the HA structure was found to suppress grain growth without comprising the densification. Surface activity was increased with increasing the Ti^{4+} content in HA which reduced the grain size and increased the number of surface grain boundaries per unit length. Doping of Ti^{4+} into HA didn't affect the ability to bring on bone like apatite formation. This study exposed that 0.8 wt.% of Ti^{4+} doped HA have potential for the in biomedical applications, like bioactive scaffolds and coatings on Ti^{4+} implants [69].

Table 1.6: Parameters in controlling crystal size, morphology chemical stability and sinterability of HA.

Parameters		Resulting Effect
Aging time	As increasing;	Smaller crystal sizes, more uniform morphology, reduction in phase decomposition during sintering
Aging temperature	0°C; 25°C; 80°C;	Highly non-stoichiometric HA, decomposed to coarser grained β -TCP during sintering. Stoichiometric HA, spherical morphology; increased sinterability. Whisker-like HA particles with preferential growth along the <002> axis
Precursor pH	As increases; As decreases;	Preferential growth along the <002> axis of HA, rod-like morphology, larger average particle size, non-stoichiometric HA, phase decomposition during sintering. Non-stoichiometric HA, phase decomposition during Sintering

C. Ergun examined the interaction of titanium ions with HA structure [70]. In the different part of the experiment tetraethyl orthotitanate, HA/CaTiO_3 and tri-calcium phosphate/ CaTiO_3 were added, respectively. HA doped with titanium ions was produced by precipitation method. The precipitated materials were dried and sintered in air at various temperatures for 2h. The result revealed that when Ti^{4+} was incorporated into the structure, the lattice parameters got smaller. The grain size of the doped HA was smaller than that of the pure HA. When the amount of the Ti^{4+} ions in HA increased, α -TCP and CaTiO_3 formed and resulted in an increase in porosity in Ti^{4+} containing HA [70]. In another work chemical reactions between HA and titanium were examined [71]. Hot isostatic pressing was used to bond HA powder to a titanium rod. As a reaction product perovskite (calcium titanate, CaTiO_3) was found on the HA surface [71].

In the crystal structure of HA, one ion can be replaced with another with a minimal effect on its crystal structure. Ribeiro et al. demonstrated that Ca^{2+} ions were replaced with Ti^{4+} ions as seen in Equation 1.4 [9].



(where \square represents a vacancy).

1.5 Hydroxyapatite Doped by Fluoride

The incorporation of fluorine into the HA matrix enhanced the phase formation and crystallinity [72]. Thermal stability and biological properties of HA were enhanced with addition of fluoride ions (F^-) which impose the physical and biological characteristics of HA [73]. In the crystal structure of HA OH^- ions and F^- ions compete to occupy the same location. When F^- ions partially altered with OH^- ions in HA, fluoridated hydroxyapatite (FHA; $\text{Ca}_5(\text{PO}_4)_3(\text{OH})_{1-x}\text{F}_x$ $0 \leq x \leq 1$) is produced. If OH^- ions are completely changed with F^- ions, fluorapatite (FA; $\text{Ca}_5(\text{PO}_4)_3\text{F}$) is produced [74]. Properties of FHA of low solubility, high thermal stability and biological potential leads to FHA as a new alternative biomaterial for bone applications [75].

Excessive amounts of F^- ions could raise the number of adverse effects which range from mild dental fluorosis to crippling skeletal fluorosis (osteomalacia, decreasing osteoconductivity) as the level and period of exposure increases [72] and also inhibit the cell proliferation by releasing Ca^{+2} ions in HA due to decreased solubility [76]. When high concentrations of fluoride added into HA led to abnormal tissue growth and poor mechanical properties but lower fluoride levels improved the mechanical properties of HA, such as hardness, fracture toughness, elastic modulus and brittleness [77]. Also the thermal stability of HA was improved by adding fluoride ions [78]. Consequently, the optimum fluoride concentrations in HA for biomaterials applications were reported as 0.033-0.4 mol F^- [76].

In a study the influence of fluoride on the preparation and properties of HA grown in the same gel medium along with DCPD (dicalcium phosphate dihydrate) crystals were reported. The formation of HA retarded with the presence of fluoride. The microstructural morphology of HA changed from fibrous to granular structure and the crystallinity of the hydroxyapatite increased due to fluoride substitution [72]. Pure HA grown by gel method decomposed into β -TCP and CaO when sintered at a high temperature. Because of the fluoride substitution, higher thermal stability of the HA matrix was observed [72].

In another study with wet chemical technique, nanocrystalline HA and fluorhydroxyapatite powder was produced [74]. The thermal stability, mechanical property, solubility and biocompatibility of the powders were tested. XRD analysis of the calcined powders showed that all the produced materials were pure [74]. In vitro studies of cell cultures behaviors of HA were affected when F^- content raised cell attachment on HA surface but reduction of Ca^{2+} release in culture increased the F^- content which inhibited the cell proliferation [74].

Song et al. [18] showed that F^- is very stable in the lattice sites and doping of F^- ions stabilizes the crystal structure of HA because structural energy of F^- ions is much lower than that of other ions [18]. Furthermore, the presence of F^- ions has a decreasing effect on the acid dissolution of HA [16].

1.6 Aim of the Thesis

The purpose of this study is to synthesize calcium phosphates doped with Ti^{4+} and F^- ions to develop new nanocomposite bioceramics for biomedical applications and to investigate their microstructures, mechanical and biocompatibility properties. No study has been found in literature regarding to co-doping of Ti^{4+} and F^- ions into the CaPs. CaPs doped with Ti^{4+} and F^- were synthesized by a precipitation method and sintered from 1100°C to 1300°C for 1 h. Composites were characterized by density measurements to determine the effect of sintering temperature. Presence of phases and bonding properties of the samples were characterized by X-ray diffraction (XRD) and Fourier transforms infrared spectroscopy (FTIR). Microstructure and the grain sizes of the samples were investigated by scanning electron microscopy (SEM). Consequently, microhardness test was applied on the samples to determine their mechanical properties.

CHAPTER 2

METHODS

2.1 Materials

In order to synthesize calcium phosphates, the main precursors were calcium nitrate tetra hydrate ($\text{Ca}(\text{NO}_3)_2 \cdot 4\text{H}_2\text{O}$) and di-ammonium hydrogen phosphate ($(\text{NH}_4)_2\text{HPO}_4$) (Merck, Germany). In the synthesis of titanium and fluoride doped calcium phosphates and ammonium fluoride (NH_4F) Aldrich, USA and titanium diisopropoxide were used. Ammonia solution (Merck, Germany) was utilized as to adjust the pH values of the solution.

2.2 Synthesis of Calcium Phosphates

Nano-calcium phosphate powders were synthesized by a precipitation method [48]. Precursors of calcium nitrate tetra hydrate ($\text{Ca}(\text{NO}_3)_2 \cdot 4\text{H}_2\text{O}$) and di-ammonium hydrogen phosphate ($(\text{NH}_4)_2\text{HPO}_4$) were added into distilled water in order to prepare $\text{Ca}(\text{NO}_3)_2 \cdot 4\text{H}_2\text{O}$ and $(\text{NH}_4)_2\text{HPO}_4$ solutions with a certain molar ratio. The Ca/P ratio was kept at 1.0, 1.25, 1.50, 1.67 and 2.0. Ammonia was added into the di-ammonium hydrogen phosphate solution after previous solutions were stirred for 1 h where ammonia solution was added into both solutions to bring the pH level to 11-12. Ammonia solution, calcium nitrate solutions and titanium diisopropoxide were added at the same time into the di-ammonium hydrogen phosphate-ammonia mixture in a drop wise manner after stirring for 10 minutes. After 1 hour stirring the final mixture was heated until boiling in order to increase the reaction. After boiling, the mixture was left for stirring for 24 h. Later stirring, the mixture was filtered with a fine filter paper to obtain a wet cake. The wet cake was

dried in an oven at 200 °C to remove the excess water. Samples were sintered at 1100°C and 1300°C in air for 1 h. The synthesis process of pure CaPs is given in the Figure 2.1.

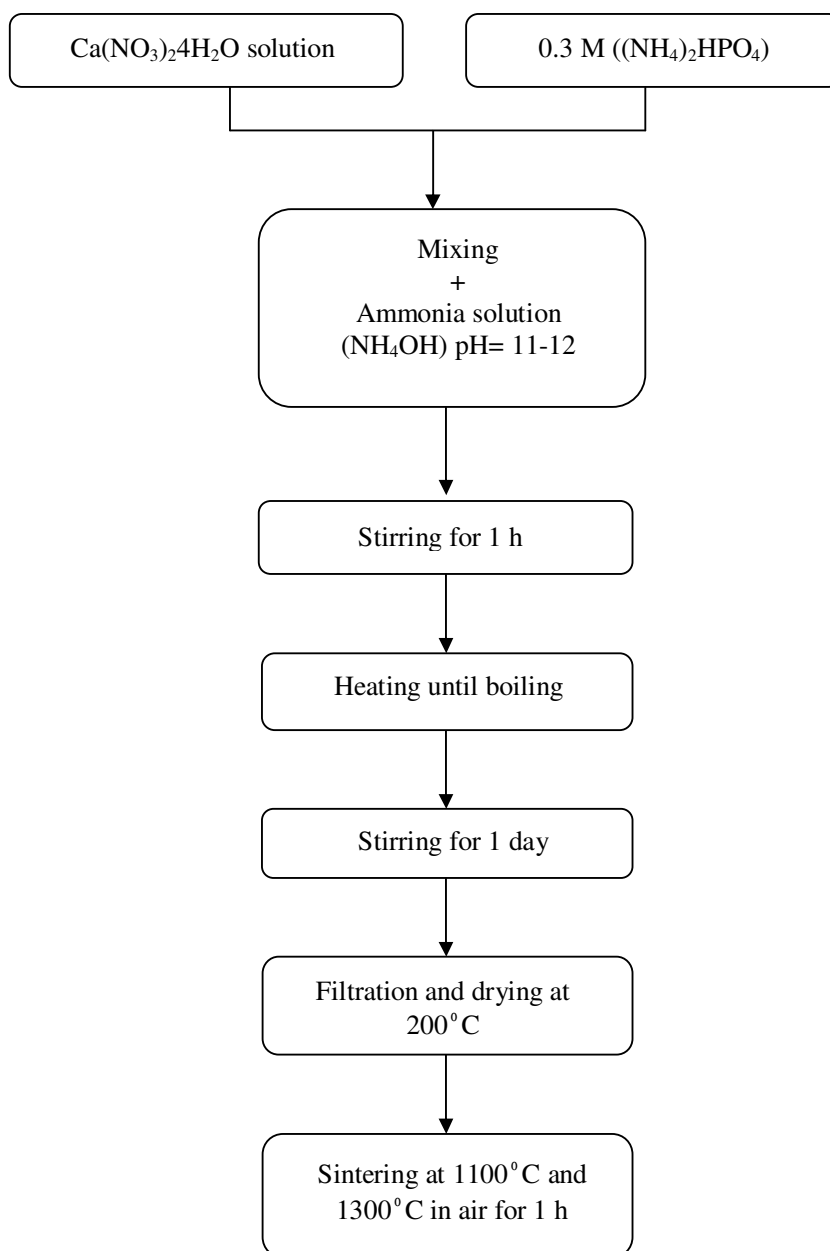


Figure 2.1: Synthesis process of pure CaPs.

2.2.1 Synthesis of Doped Calcium Phosphates

In addition to main precursors used in the synthesis of pure calcium phosphates, titanium diisopropoxide and ammonium hydroxide were used to obtain titanium and fluoride doped calcium phosphates. 75 different compositions were prepared. Same synthesis technique was used for the production of the samples. Additionally, ammonium fluoride and titanium diisopropoxide were used as F^- and Ti^{4+} . The mol. % of the dopants with different Ca/P molar ratio is given in the Table 2.1. Titanium diisopropoxide was added into calcium nitrate solution in five different mole compositions: 0%, 0.5%, 1.0%, 2.5% and 5%. The ammonium fluoride was added into di-ammonium phosphate solution in the compositions of 0%, 0.5% and 2.5 %. The following formula was used to identify the composition of the CaPs used in this study: $xxCaP\ yyTi\ zzF$, where xx represents the Ca to P ratio of the samples: 1.00, 1.25, 1.50, 1.67 and 2.00, respectively. In this formula, yy represents the mole amount (0.5, 1.0, 2.5) of Ti^{4+} ions present in the system with respect to 100 moles of Ca ions present in the system. zz represents the mole amount (0.5, 2.5) of F^- ions per 100 mole of OH^- ions in the system.

Table 2.1: List of the synthesis products with Ca/P ratio of 1.0, 1.25, 1.50, 1.67, 2.0.

Sample ID (n = 1.0, 1.25, 1.50, 1.67, 2.0)
nCaP
nCaP0.5Ti
nCaP1.0Ti
nCaP2.5Ti
nCaP5.0Ti
nCaP0.5F
nCaP2.5F
nCaP0.5Ti0.5F
nCaP1.0Ti0.5F
nCaP2.5Ti0.5F
nCaP5.0Ti0.5F
nCaP0.5Ti2.5F
nCaP1.0Ti2.5F
nCaP2.5Ti2.5F
nCaP5.0Ti2.5F

The ratios of elements insertion were adjusted according to atomic percentage of precursors. After mixing the solution, the products were filtered, dried and sintered. The filtered and dried materials were sintered at temperature of 1100 °C and 1300 °C.

2.3 Characterization Methods

2.3.1 Density Measurements

Densities of the sintered materials were derived by Archimedes method [79] :

$$d = \text{dry weight} / (\text{dry weight} - \text{wet weight}) \quad (2.1)$$

Theoretical densities of the CaPs are given in Table 2.2.

Table 2.2: Theoretical densities of CaP used in the relative density calculations [16].

Ca/P	Theoretical Density (g/cm ³)
1	3.090
1.25	2.610
1.5	3.067
1.67	3.156
2	3.100

Five different densities for each sample were obtained to determine its mean density.

2.3.2 X-ray Diffraction

Phases present in the samples were investigated by X-ray diffraction (XRD) method using a Rigaku DMAX 2200 machine. XRD was performed on the samples with a Cu-K α radiation at 40 kV/ 40 mA and samples were scanned from 10° to 80° in 2 θ with a scan speed of % 2.0 min. International Centre For Diffraction Data (ICDD) files were used for comparison with the positions of diffracted planes taken from XRD results. The amount of phases present in pure and doped calcium phosphates was calculated by using relative intensity measurements of diffracted planes.

2.3.3 Fourier Transform Infrared Spectroscopy (FTIR)

In order to assess the presence of OH⁻ and F⁻ bonds formed in the structure of calcium phosphates FTIR spectra were used. The samples were first crushed into the powder form with the use of ball mill. Ceramic powders were mixed with potassium bromide (KBr) with a weight ratio of 1 to 300. The obtained powder mixture was then cold pressed in order to obtain transparent pellets. The spectra were performed from 4000 cm⁻¹ to 400 cm⁻¹ with a 512 scan on FTIR spectrometer (Brukers IFS 66/S; Bruker Optics, Germany).

2.3.4 Scanning Electron Microscopy (SEM)

SEM JEOL JSM-6400 (JEOL Ltd., Japan) analysis was conducted in order to determine the average grain sizes of the sintered samples. The samples were polished with SiC papers (Buehler Ltd., USA) with grids from 240 to 1200 grit before examination. Final polishing was performed with a 1µm monocrystalline diamond suspension (Buehler Ltd., USA). Grain size and morphology of the prepared samples were determined with SEM (QUANTA 400F Field Emission) at a voltage of 20 kV. Before to the SEM analysis, the samples were coated with gold.

2.3.5 Mechanical Measurements

2.3.5.1 Vickers Micro-Hardness

Micro-hardness of the samples was acquired by a Vickers micro-hardness tester (HMV-2, Shimadzu, Japan). The sintered discs embedded into epoxy molds were used to determine the micro-hardness of the materials. The molds were polished with SiC paper (Buehler Ltd. USA) in order to obtain a flat surface. A load of 200 g was applied for 20 seconds onto the surface of the samples. The micro-hardness of the samples was acquired by measuring the length of the diagonal indent shape, which was formed after the indentation. The formula for the calculation of µ-hardness is as follows:

$$HV = 0.001854 P/d^2 \quad (2.2)$$

Where : HV: Vickers hardness (GPa), P: Applied load (N) and d: Diagonal indent length (mm).

CHAPTER 3

RESULTS AND DISCUSSION

3.1 Structural Analysis

3.1.1 Density of the Samples

Densities of CaPs doped with Ti^{4+} and F^- ions sintered at 1100°C and 1300°C are given in Table 3.1.

According to Table 3.1, when Ca to P ratio was 1.0, higher densities were obtained for most of the compositions after sintering at 1100°C when compared with 1300°C. Increasing the amount of Ti^{4+} ions led to decrease in the density of samples doped with Ti^{4+} ions after the sintering at 1100°C. Though, densities of Ti^{4+} doped samples (1CaP1.0Ti, 1CaP5.0Ti) went up with increasing the sintering temperature from 1100°C to 1300°C, densities of doped samples (1CaP0.5Ti, 1CaP2.5Ti) with Ti^{4+} ions went down with increasing sintering temperature. Nevertheless, there was no correlation between the density and the Ti^{4+} content after sintering temperature differ from 1100°C to 1300°C. Increasing the F^- ion amount in the ceramics from 0.5 to 2.5 mol.% led to increase in their density at 1100°C. However, the opposite case was observed after sintering at 1300°C. In a previous study, addition of F^- ion resulted in less dense materials because the bond that forms between F^- and OH^- groups reduces the rate of diffusion regulating the densification [83]. Therefore, increasing the F^- ion substitution decreased the densification [83] similar as in the samples sintered at 1300°C. For most of the ceramics doped with Ti^{4+} and F^- ions at same time, their densities decreased after increasing the sintering temperature from 1100°C to 1300°C. Therefore, these results demonstrated that co-doped samples were more dense at 1100°C

than 1300°C. These results indicated that sintered density of the CaPs with a Ca/P ratio of 1, sintered densities were influenced by the sintering temperature.

For pure 1.25 CaP , increasing the sintering temperature from 1100°C to 1300°C resulted in an increase in its density. Changing the sintering temperature of the samples (1.25CaP0.5F, 1.25CaP2.5F, 1.25CaP2.5Ti0.5F, 1.25CaP2.5Ti2.5F, 1.25CaP5.0Ti0.5F and 1.25CaP5.0Ti2.5F) from 1100°C to 1300°C showed an increase in their sintered densities.

Table 3.1: Sintered densities of calcium phosphates after the sintering at 1100°C and 1300°C for 1h .

Sample ID	Density (g/cm ³), 1100°C					Density (g/cm ³), 1300°C				
	n=1.0	n=1.25	n=1.50	n=1.67	n=2.0	n=1.0	n=1.25	n=1.50	n=1.67	n=2.0
nCaP	3.05	2.79	3.04	3.14	3.13	2.86	2.83	2.94	3.12	2.96
nCaP0.5Ti	2.93	3	2.92	3.1	2.86	2.85	2.92	2.89	2.91	2.86
nCaP1.0Ti	2.88	2.99	3.01	3.09	3.08	2.89	2.95	2.85	3.01	3.07
nCaP2.5Ti	2.87	2.96	2.93	2.98	3.07	2.86	3.03	2.75	2.93	2.98
nCaP5.0Ti	2.73	2.87	3.06	2.87	3.09	2.92	3.25	2.83	2.75	2.94
nCaP0.5F	2.86	3.03	2.93	3.09	3.08	2.78	2.88	2.82	3.11	3.04
nCaP2.5F	2.92	2.95	3.07	3.05	2.97	2.73	2.84	2.9	3.05	2.98
nCaP0.5Ti0.5F	2.95	3.03	3.01	2.84	3.2	2.88	2.78	2.9	3.02	3.1
nCaP1.0Ti0.5F	2.85	2.94	3	2.67	3.08	2.96	2.92	2.82	3.15	3.12
nCaP2.5Ti0.5F	2.85	2.94	3.02	3.14	3.06	3.03	2.97	2.78	2.91	3.11
nCaP5.0Ti0.5F	3.08	2.91	3.01	2.79	3.04	2.82	2.99	2.92	2.86	3.09
nCaP0.5Ti2.5F	3.03	2.86	2.98	2.93	3.14	2.92	2.97	2.9	2.98	3.07
nCaP1.0Ti2.5F	2.86	2.97	3	2.99	3	2.81	2.94	2.92	3.09	3.08
nCaP2.5Ti2.5F	2.99	2.99	3.03	3.1	3.09	2.89	3.01	2.89	2.93	3.08
nCaP5.0Ti2.5F	2.87	2.83	3.08	3.01	3.05	2.64	2.92	2.88	2.84	3.07

Although densities of Ti^{4+} doped samples decreased with increasing the Ti^{4+} amount from 0.5 to 5.0 mol.% after the sintering at 1100°C, densities of these samples at 1300°C improved with increasing the Ti^{4+} content. F^- doped samples had smaller densities after sintering at 1300°C. Ti^{4+} and F^- co-doped samples showed varieties in their densification behaviours after the sintering at 1100°C and 1300°C. High sintering temperature resulted in high densities when compared to low sintering temperature for most of the Ti^{4+} and F^- co-doped samples.

Densities of the CaPs with a Ca to P ratio of 1.5 are presented in Table 3.1. When sintering temperature was increased from 1100°C to 1300°C, densities of all samples were decreased. These results indicated that all the samples with Ca/P ratio of 1.5 were denser after sintering at 1100°C. Increasing the amount of Ti^{4+} from 0.5 to 5 mol.%, samples had inconsistent behaviours after sintering at both temperatures. Studies demonstrated that doping of CaPs with F^- ions resulted in a decrease in density because of the reduction of decomposition rate of the synthesized materials by formation of fluorapatite, which shows high thermal and chemical stability after the sintering [77]. Different from the study by Gross et al. [77], increasing the amount of F^- ions in the samples resulted in an increase in their densities after changing the temperature from 1100°C to 1300°C. In 0.5 mol.%F and 2.5 mol.%F co-doped samples, increasing the amount of Ti^{4+} ions did not contribute too much difference in their densities. Samples doped with 2.5 mol.%F had high densities after the sintering at 1100°C when Ti^{4+} amount increased from 0.5 to 5 mol.%.

For the sample 1.67CaP (pure HA), increasing the sintering temperature from 1100°C to 1300°C resulted in a slight decrease in its density. Increasing the Ti^{4+} amount from 0.5 to 5.0 mol.% showed a decreasing trend in the density of the materials. In previous studies, increasing the amount of Ti^{4+} doping ions in HA changed the density in a decreasing manner [118]. Moreover, Ergun showed that increasing Ti^{4+} ion amount in the ceramic decreased the densities when Ca to P ratio was close to pure HA [70]. In the literature, Chenglin et al. [84] stated that density of the sintered samples decreases with the increase in the amount of HA when (HA)–Ti system was developed by an optimized powder metallurgical process. Moreover, a functionally-graded biomaterial (FGM) of HA and Ti^{4+} interlayers had low relative densities, which resulted in high amount of porosities in the FGM's [84]. As distinct from these results, Huang et al. demonstrated that density of doped

samples raised with increasing Ti^{4+} amount in HA structure which is contradictory to this study and studies of Chenglin et al. and C. Ergun [69].

In this thesis, when F^- ion concentration was increased, density of the F^- doped samples decreased. In another study, increased F^- ion amount triggers the thermal stability of HA [93]. Nevertheless, when the F^- ion content was increased up to 57 mole% of OH ions, porous samples were achieved after sintering at various temperatures which resulted in a decrease in the density of the samples [93]. Gross et al. demonstrated that as the F^- ion content goes up, the sinterability of the samples goes down [77]. Furthermore, when F^- ion content increased the sintered density and mechanical properties such as hardness, Young's Modulus and brittleness of HA decreased at a constant sintering temperature [77]. At high sintering temperatures, different apatite phases were obtained. Different from these, fluoridated samples had only HA phase, which means F^- ion increases the stability of HA. As a consequence of increased stability of the phases in the samples, their dissolution rate decreased and density increased [95]. Former studies revealed that small amount of F^- ions into HA structure increased the density because of the increase in stability and decrease in dissolution rate [77].

Co-doped samples with Ti^{4+} and 0.5% F ions had mixed behaviours after the sintering at 1100°C and 1300°C. Increasing the F^- amount to 2.5 mol.% in Ti^{4+} and F^- co-doped samples, resulted in an increase in the densities at 1100°C and a decrease at 1300°C.

In another study, density of Ti^{4+} doped HAs increased by raising the amount of Ti^{4+} in the system [69]. Raising the temperature up to 700°C resulted in a decrease in density due to loosing of structural water from HA. Afterwards, with increasing temperature, density showed a continuous increase which can be explained as the volume shrinkage during sintering [70]. Due to the a study in the literature 1100°C was required for the best sintering temperature for HA system [85].

According to Table 3.1 for pure 2CaP, increasing the sintering temperature from 1100°C to 1300°C resulted in a decrease in its density. Increasing the Ti^{4+} amount from 0.5 to 5.0 mol.%, samples had mixed behaviours after the sintering at 1100°C and 1300°C. At two different sintering temperatures, addition of increased amount of F^- ions led to a decrease in their densities. When Ti^{4+} ions were added to 0.5 mol.% F doped sample, their densities

decreased after the sintering at 1100°C whereas their densities increased after the sintering at 1300°C. Density of the samples with Ti^{4+} ions at 1300°C was higher than that at 1100°C. When the amount of F^- ions increased, density of the samples decreased at 1100°C but very similar densities were obtained at 1300°C.

In this study, densities of most of the materials decreased by increasing the sintering temperature. Increasing the temperature up to 1300°C showed a decrease in the density due to the losing structural water from the CaPs. High densities were obtained after the sintering at 1100°C.

3.2 Structural Investigation of the Samples

3.2.1 X-Ray Diffraction

XRD patterns of the samples sintered at 1100°C and 1300°C were used to investigate the presence of the phases. The XRD patterns of the samples are compared with the ICDD files given in Table 3.2.

Table 3.2: ICDD files for CPP, DCPA, HA, TTCP and TCP.

Name	Abbreviation	Formula	ICDD File (≠)
β -Calcium Pyrophosphates	CPP	$\text{Ca}_2\text{P}_2\text{O}_7$	11-0177
Dicalcium Phosphates	DCPA	Ca_2HPO_4	70-1425
Hydroxyapatite	HA	$\text{Ca}_{10}(\text{PO}_4)_6(\text{OH})_2$	9-432
Tetracalcium Phosphate	TTCP	$\text{Ca}_4(\text{PO}_4)_2\text{O}$	25-1137
α -Tricalcium Phosphate	α -TCP	$\text{Ca}_3(\text{PO}_4)_2$	9-348
β -Tricalcium Phosphate	β -TCP	$\text{Ca}_3(\text{PO}_4)_2$	9-169

XRD patterns of the samples with a Ca to P ratio of 1 sintered at 1100°C are presented in Figure 3.1. XRD peaks of the sample 1CaP sintered at 1100°C revealed that the first phases that precipitated are consistent with the (ICDD file # 11-0177) for β -CPP which is in agreement with the result of Linghong et al. [94]. They demonstrated that when sintering

temperature was above 700°C, sintered sample contained only β -CPP which is the most stable structure.

The characteristic peaks of β -CPP come out in the range of 2θ (27.9, 31.12, 34.48, 47.06, 52.98) for β -CPP compounds. After the sintering at 1100°C, addition of Ti^{4+} ion in the samples decreased the β -CPP peak intensities when compared with pure 1CaP. Narrow peaks of all of the samples show that they were highly crystalline. The XRD patterns of the co-doped samples with F^- ions are compatible with the standard (ICDD file # 11-0177) for β -CPP. Samples co-doped with Ti^{4+} and 0.5F ions show that the intensity of the peaks of the samples increased by increasing the Ti^{4+} amount. However, as 0.5 mol.%F amount increased to 2.5 mol.%F, the intensity of the peak decreased. It was previously stated that addition of F^- ions improves the structural stability of the calcium phosphates [93]. However, when the addition amount of F^- ion increased to 2.5 mol. %, a decrease in the intensity of the peaks of the CaP structure was observed in our study. The XRD results demonstrated that all samples sintered at 1100°C showed a single-phase CPP.

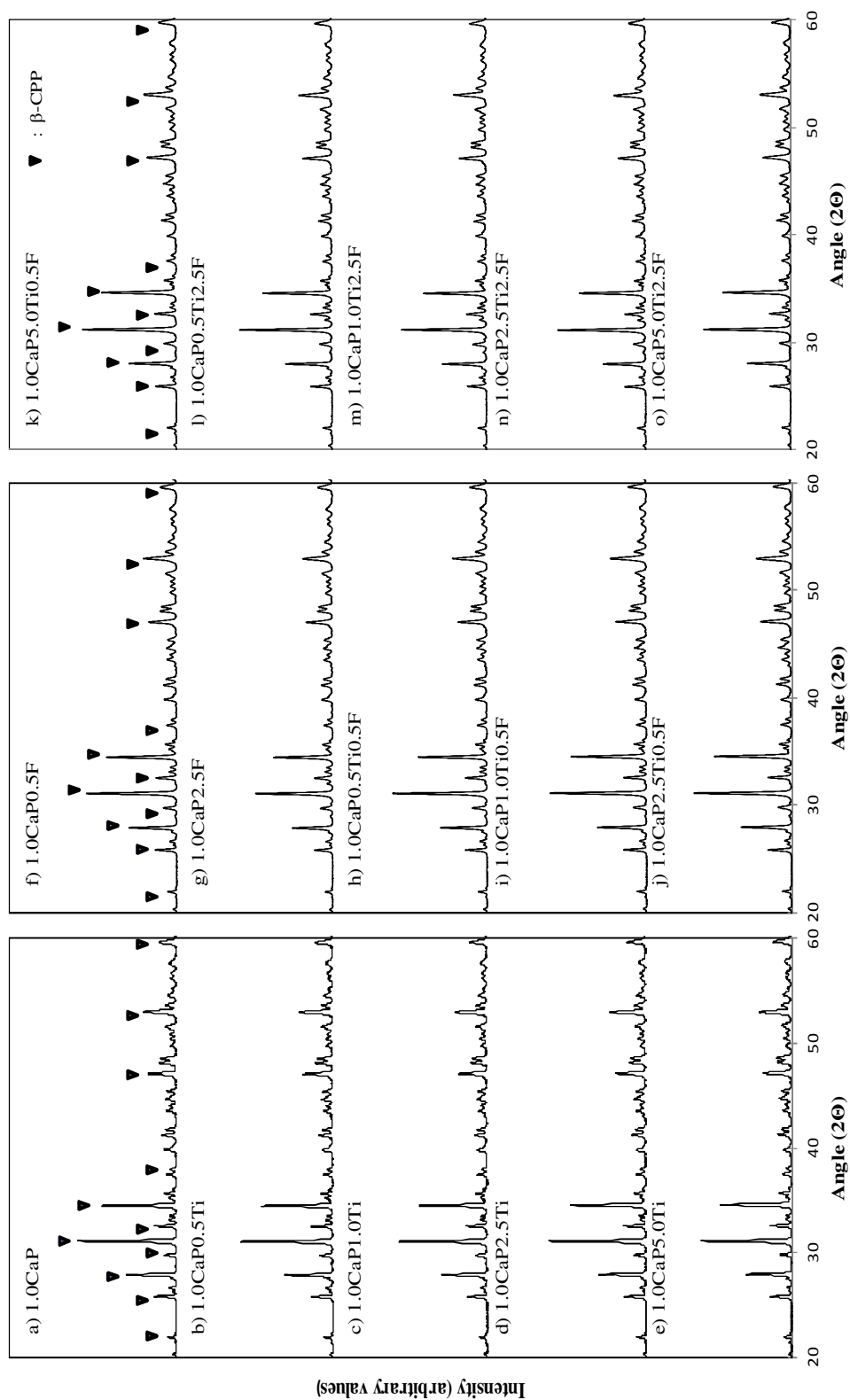


Figure 3.1: XRD patterns of CaPs with Ca to P ratio of 1.0 sintered at 1100°C.

According to Figure 3.2, when sintering temperature was increased to 1300°C, for most of the doped and undoped samples, all the observed reflection peaks corresponded to those of the β -CPP phase (ICDD file # 11-0177). The patterns demonstrated that α -TCP (ICDD file # 9-348) was also observed in for some of the materials as a second phase. Similarly, as Wu et al. stated high sintering temperature lead to phase changes which resulted in biphasic or triphasic calcium phosphate [115].

The characteristic peaks of β -CPP appear in the range of the 2θ (27.59°- 34.3°) and the patterns of β -CPP have three main peaks at d-spacing equal to 2.61, 2.90 and 3.23 proving the formation of β -CPP compound. Above 700°C, when Ca/P ratio is equal to 0.75, HA transformed totally to TCP and $\text{Ca}_2\text{P}_2\text{O}_7$ phase [106]. These results exhibited a consistency with our investigation, at 1300°C, α -TCP and β -CPP phase observed. For example, samples: 1.0CaP, 1.0CaP0.5Ti, 1.0CaP1.0Ti, 1.0CaP0.5F, 1.0CaP2.5F, 1.0CaP0.5Ti0.5F, 1.0CaP1.0Ti0.5F, 1.0CaP0.5Ti2.5F, 1.0CaP1.0Ti2.5F, respectively, had β -CPP phase with the presence of α -TCP phase. Furthermore, same samples had a dominant phase of α -TCP with small amount of untransformed β -CPP phase. These samples could be listed as 1.0CaP0.5F, 1.0CaP2.5F, 1.0CaP0.5Ti0.5F, respectively.

Doping with Ti^{4+} ions at 1300°C modified the XRD patterns, with additional peaks for 1CaP2.5Ti, 1CaP5.0Ti, and 1.0CaP5.0Ti0.5F, respectively, and alterations in increased peak intensity when Ti^{4+} amount increased. For example, for the samples 1.0CaP2.5Ti and 1.0CaP5.0Ti, an additional peak at 43.56 in 2θ was observed, Figure 3.2 shows that the patterns of Ti^{4+} doped samples have some shift to higher angle compared to original β -CPP (ICDD file # 11-0177) proving chemical interaction between titanium and CaP.

The XRD patterns obtained for the samples doped with 0.5 mol.% and 2.5 mol.% F^- sintered at 1300°C are given in Figure 3.2. For the undoped 1CaP, both peaks of β -CPP and α -TCP were observed. After doping of F^- ions, a similar trend was observed. With increasing the F^- amount from 0.5 to 2.5 mol %, peak intensities increased and peaks get narrower in higher amount of F^- ions, so it can be concluded that the grain size of the samples increased. Qu et al. demonstrated that addition of F^- ions improves the structural stability of calcium phosphates [93].

The influence of Ti^{4+} and 0.5 mol.% F and 2.5 mol.% F ions content was studied on the CaPs. As a result of oxidization titanium dioxide formed. When Ti^{4+} and F^- amount increased, additional peaks of TiO_2 (at 25.8° in 2θ) was observed which overlaps with β -CPP. Co-doped samples revealed that the intensity of the peaks of the samples increased by increasing Ti^{4+} amounts. Moreover, other peaks at 43.62° and 53.04° in 2θ was observed for the sample 1.0CaP5.0Ti0.5F.

There were no obvious difference in position and relative intensity of each reflection for β -CPP sintered at 1100°C and 1300°C this phenomena is in correlation with the study of Linghong et al. [94].

XRD patterns of the CaPs with molar ratio of 1.25 sintered at 1100°C are given in Figure 3.3. As seen from the XRD patterns for undoped and doped samples, the peaks are attributed to the phases of β -TCP (ICDD file #9-169) and/or β -CPP (ICDD file 11-0177) because peaks of β -TCP and β -CPP are overlapping each other above the 2θ of 20° . As Ergun et al. mentioned the only stable phase was TCP [106]. Moreover, all precipitated HA totally disappeared [106]. Narrow peaks of the samples illustrate that they were highly crystalline when Ti^{4+} addition from 0.5 mol.% to 5 mol.%. Increasing the Ti^{4+} amount raised peak intensities.

As the F^- amount increased, the characteristic peaks of β -TCP and/or β -CPP appear in the range of 2θ (25° - 35°). According to results, F^- addition increased the crystallinity. Due to F^- ion doping into peak apatite lattice, peak shift to higher 2θ values in the positions of (211), (300) and (112) planes in an increasing manner with an increase in F^- ions content [75].

Increasing the Ti^{4+} and F^- ion amounts didn't influence the peak intensities. According to the results, increasing F^- ion amount from 0.5 mol.% to 2.5 mol.%, no fluctuations observed in the peak intensities. As seen from the XRD patterns for the samples with Ca to P molar ratio of 1.25 at 1100°C , the peaks are attributed to phases of β -TCP and/or β -CPP.

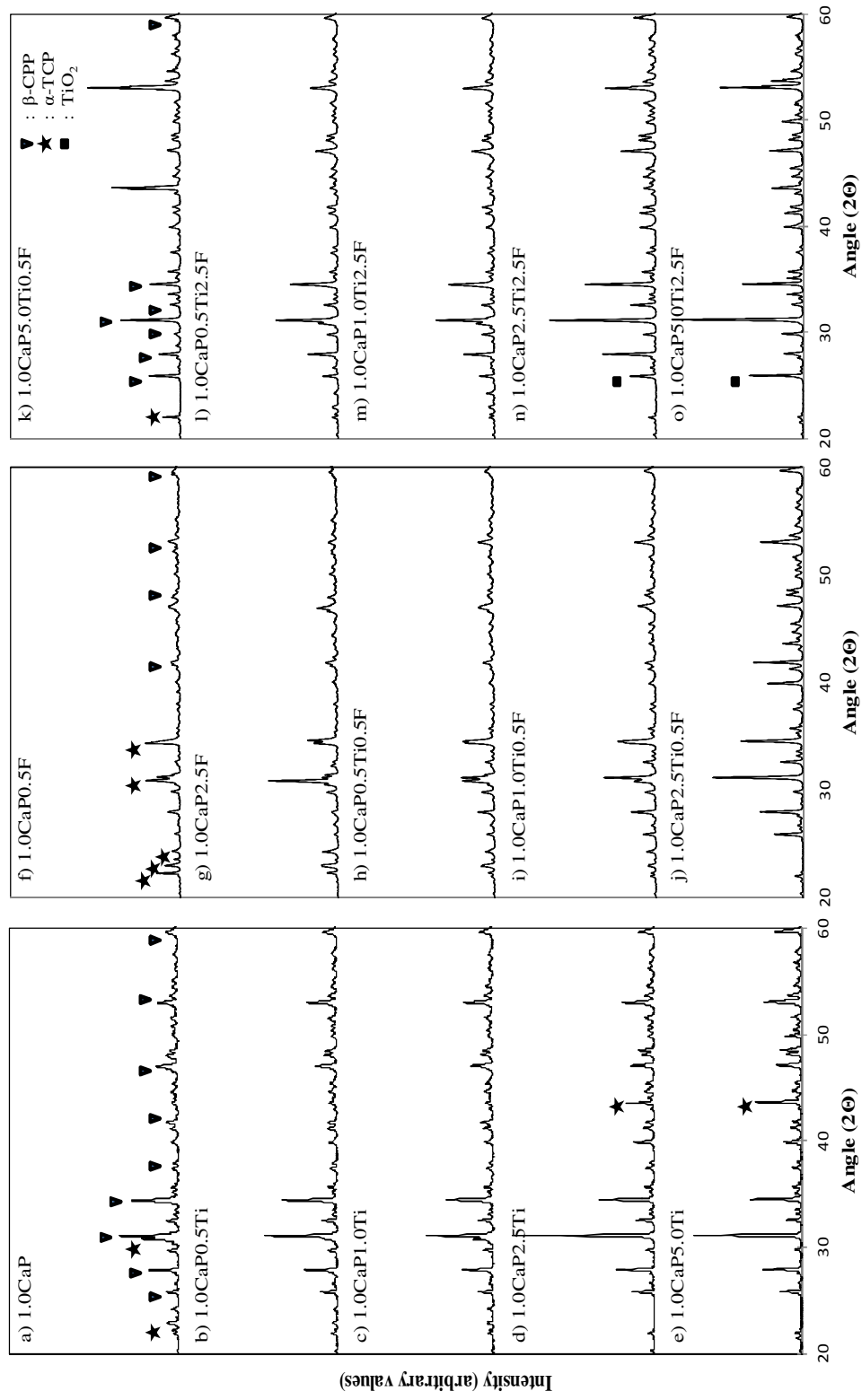


Figure 3.2: XRD patterns of CaPs with Ca to P ratio of 1.0 sintered at 1300°C.

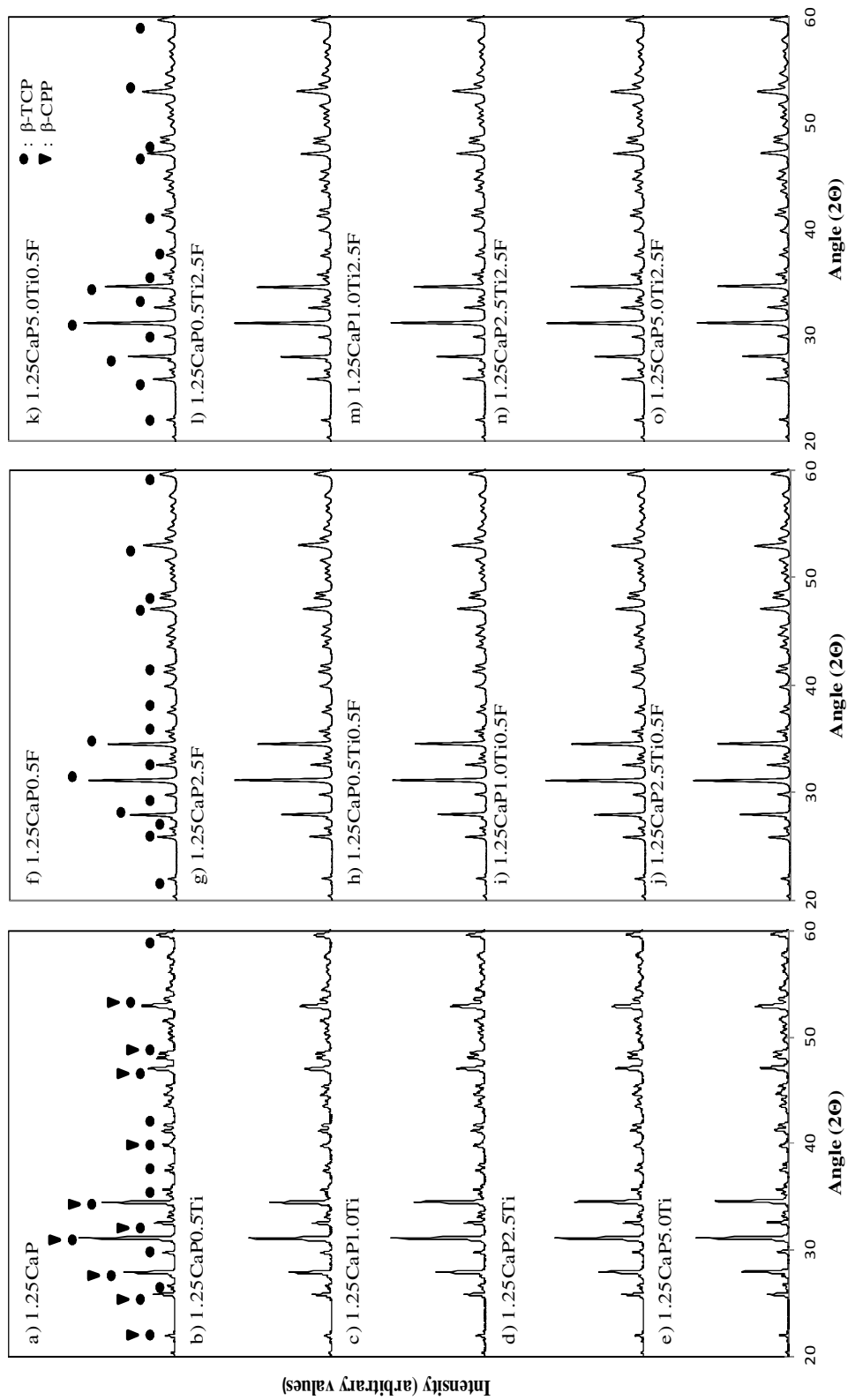


Figure 3.3: XRD patterns of CaPs with Ca to P ratio of 1.25 sintered at 1100°C.

XRD spectrums of CaPs with a Ca/P molar ratio of 1.25, sintered at 1300°C are given in Figure 3.4. As seen from the XRD patterns of the doped and undoped samples peaks are attributed to β -TCP (ICDD file #9-169) and/or β -CPP (ICDD file # 11-0177). As a third phase α -TCP (ICDD file #9-348) was also observed in for some of the samples. These results exhibited a consistency with the study by Ergun et al.,[106] when Ca/P ratio was between 1.0 and 1.3, the only stable phase was TCP [106].

Doping the CaPs with Ti^{4+} ions modified the XRD patterns and resulted in alterations in the intensity of some β -TCP peaks. Addition of Ti^{4+} ions improves the structural stability of the samples 1.25CaP2.5Ti which might indicate an increase in crystallinity. Additional peaks of TiO_2 (at 54.58 in 2θ) (ICDD file #21-1276) was observed in the samples 1.25CaP0.5Ti, 1.25CaP1.0Ti, 1.25CaP2.5Ti and 1.25CaP5.0Ti.

In the sample doped with 0.5 mol.%F ions, most of the β -TCP and/or β -CPP transformed into α -TCP phase. However, in the sample doped with 2.5 mol.%F ions had β -TCP and/or β -CPP was the main phase with the secondary phase of α -TCP. This showed that increasing the F^- amount stabilized the phases present at low temperature. However, as a result of the substitution of F^- ions, a slight shift to the left was observed.

Increasing Ti^{4+} and F^- ions together, revealed increase in peak intensities. For example, the broad peak pattern of sample 1.25CaP1.0Ti0.5F demonstrated lower crystallinity level. According to the co-doped samples, increasing the F^- ion amount from 0.5 to 2.5 mol.% increased peak intensities. This might demonstrate an improvement in the crystallinity of the samples, which was expected since F^- ion incorporation results in an increase in crystallinity [66]. As seen from the XRD patterns of CaPs with molar ratio of 1.25, the peaks are attributed to the phase of β -TCP and/or β -CPP and secondary phase of α -TCP especially in the samples with 1.25CaP1.0Ti0.5F, 1.25CaP2.5Ti2.5F. Additional peaks of TiO_2 (at 54.52 in 2θ) (ICDD file #21-1276) in 2θ was detected in the samples 1.25CaP0.5Ti0.5F, 1.25CaP1.0Ti0.5F, 1.25CaP2.5Ti0.5F, 1.25CaP5.0Ti0.5F 1.25CaP0.5Ti2.5F, 1.25CaP1.0Ti2.5F, 1.25CaP2.5Ti2.5F, and 1.25CaP5.0Ti2.5F.

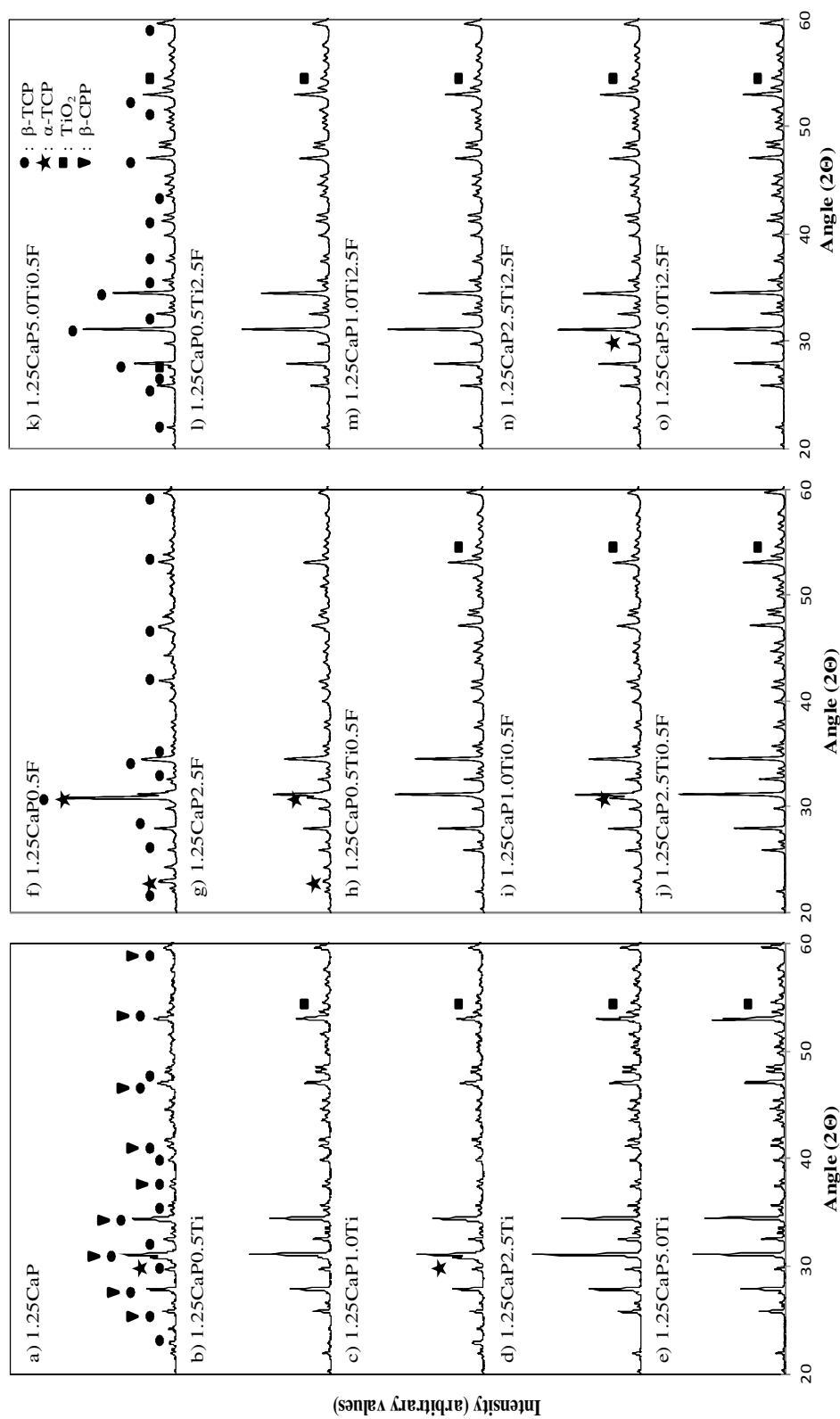


Figure 3.4: XRD patterns of CaPs with Ca to P ratio of 1.25 sintered at 1300°C.

XRD spectra of pure and co-doped CaPs with Ca/P molar ratio of 1.50, and sintered at 1100°C for 1h are shown in Figure 3.5. As seen from the XRD patterns of the samples with a Ca/P of 1.50, the peaks are attributed to secondary phase β -TCP (ICDD file #9-169) and also α -TCP (ICDD file # 9-348).

However, when Ca/P ratio was 1.50, the only stable phase was TCP after the study by Ergun et al. [106]. These result not consistent with Ergun et al. study [106] when stoichiometric ratio was 1.55 due to the nature of precipitation method used to synthesize CaPs in this study, it is very difficult to synthesize pure TCP even if Ca/P is adjusted to 1.5 in the beginning of the synthesis by precipitation method [101]. Moreover, heat treatments above 750°C lead to Ca deficient apatite to decompose to β -TCP [101]. In another study, they demonstrated that below 1120°C, β -TCP phase observed when Ca/P ratio were 1.47 to 1.56 [110].

Narrow peaks of the samples illustrate that they were highly crystalline when Ti^{4+} ion addition was changed from 0.5 to 5 mol.%. Increasing the Ti^{4+} amount from 0.5 to 5 mol.% increased the peak intensities of β -TCP and decreased the peaks of α -TCP in the samples of 1.50CaP0.5Ti, 1.50CaP1.0Ti, 1.50CaP2.5Ti and 1.50CaP5.0Ti. Presence of high amount of Ti^{4+} ions almost resulted in disappearance some of the α -TCP peaks. Increasing the F^- ion amount from 0.5 to 2.5 mol.% resulted in presence of both phases of β -TCP and HA. When F^- amount changed from 0.5 to 2.5 mol.%, presence of α -TCP phase increased when compared to β -TCP phase. Qu et al. illustrated that F^- ion addition to calcium phosphates enhanced the structural stability [93]. Moreover, when there were 0.5%F present in the Ti^{4+} doped CaPs, changing the Ti^{4+} amount from 0.5 to 2.5 mol.% decreased the presence of HA phase and increased the presence of β -TCP phase, respectively, in the samples 1.50CaP0.5Ti0.5F, 1.50CaP1.0Ti0.5F and 1.50CaP2.5Ti0.5F and 1.50CaP5.0Ti0.5F. For the 2.5%F and 0.5 to 5 mol.% Ti^{4+} doped CaPs, a similar trend was observed regarding to presence of β -TCP and HA. With the Ti^{4+} ion addition β -TCP phase in 1.50CaP5.0Ti, 1.50CaP5.0Ti0.5F and 1.50CaP5.0Ti2.5F totally disappeared.

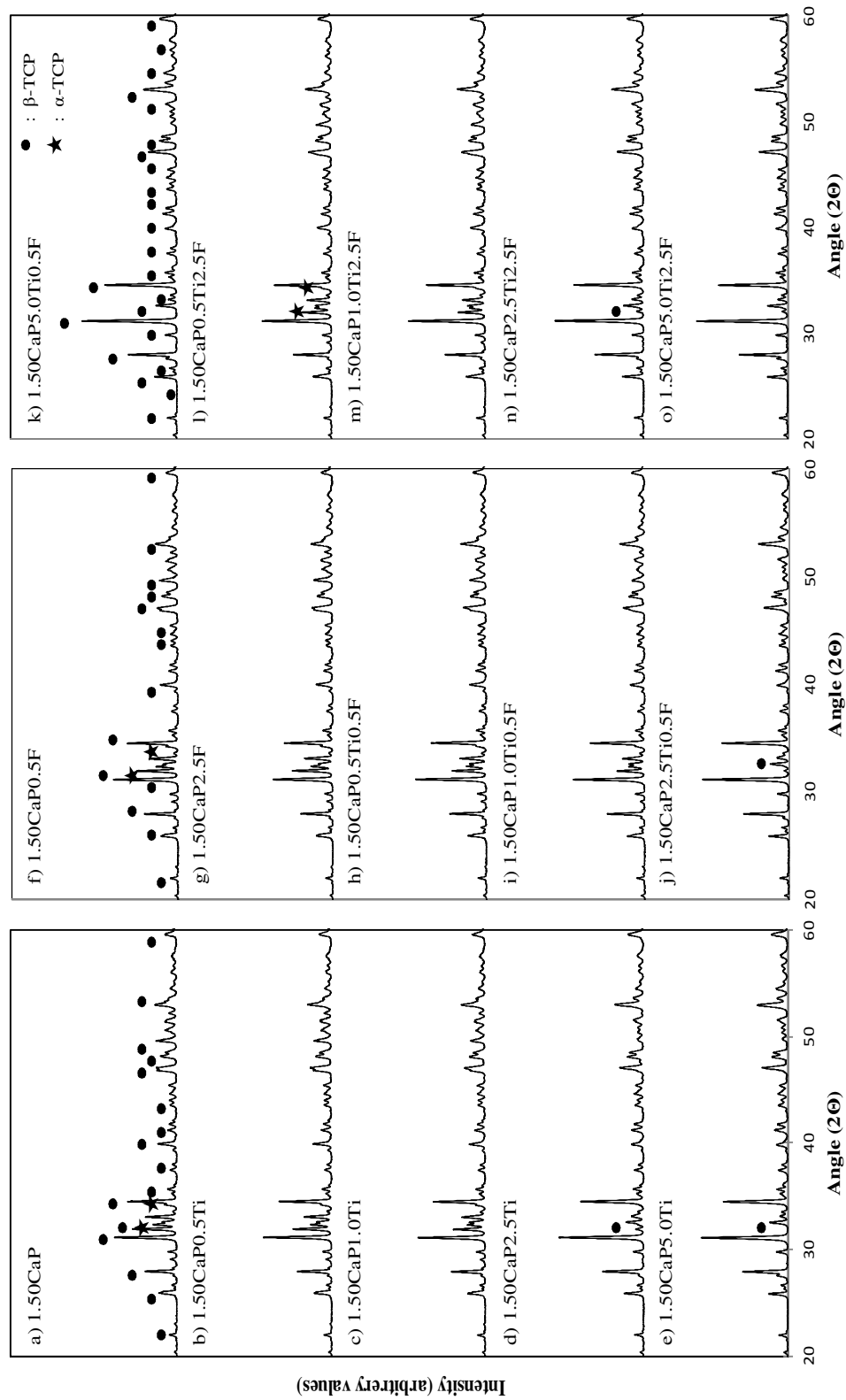


Figure 3.5: XRD patterns of CaPs with Ca to P ratio of 1.50 sintered at 1100°C.

In Figure 3.6, XRD spectrums of CaPs with molar ratio of 1.50, sintered at 1300°C given. As seen from the XRD pattern for the undoped sample, the peaks are attributed to α -TCP (ICDD file # 9-348), β -TCP (ICDD file # 9-169) and TiO_2 (ICDD file # 21-1276). As Wu stated high sintering temperature lead to phase changes which resulted in biphasic or triphasic calcium phosphate [115]. In the previous studies, when Ca/P ratio was 1.55, a biphasic HA/TCP structure were observed [106]. Kannan et al. showed that biphasic HA/TCP ceramics demonstrated modified properties than the single phase of HA or TCP [107].

Doping with Ti^{4+} modified the XRD patterns and alterations in intensity of some TCP peaks. As noted previously, additional phase β -TCP appeared next to α -TCP. After increasing of Ti^{4+} ions additional low-intensity peaks of HA observed and peak intensities increased. XRD pattern shows that some of the peaks of α -TCP has disappeared, the main crystalline phases of α -TCP remained after Ti^{4+} ion addition. No severe fluctuations in the XRD peak positions due to addition of fluoride ions into α -TCP were determined in the XRD patterns of 1.50CaP0.5F and 1.50CaP2.5F, except that the peak intensities decreased when compared to pure 1.50CaP. Additional peaks of TiO_2 (at 27.28 in 2θ) was observed in the samples with high amount of Ti^{4+} ions (1.50CaP5.0Ti, 1.50CaP5.0Ti0.5F and 1.50CaP5.0Ti2.5F).

Increased Ti^{4+} and F^- amount increased peak intensities, three of the sharper peak correspond to β -TCP, disappeared completely at 1.50CaP2.5Ti0.5F. The broader peak pattern of 1.50CaP5Ti0.5F demonstrated the smaller crystal sizes and lower crystallinity degree. According to the results, increasing F^- ion amount from 0.5 mol.% to 2.5 mol.%, increased the peak intensities. This might demonstrate an improvement in the crystallinity of the samples, which was expected since F^- ion incorporation results in an increase in crystallinity [66]. As noted previously, addition of Ti^{4+} ions to the samples increased peak intensities and crystallinity.

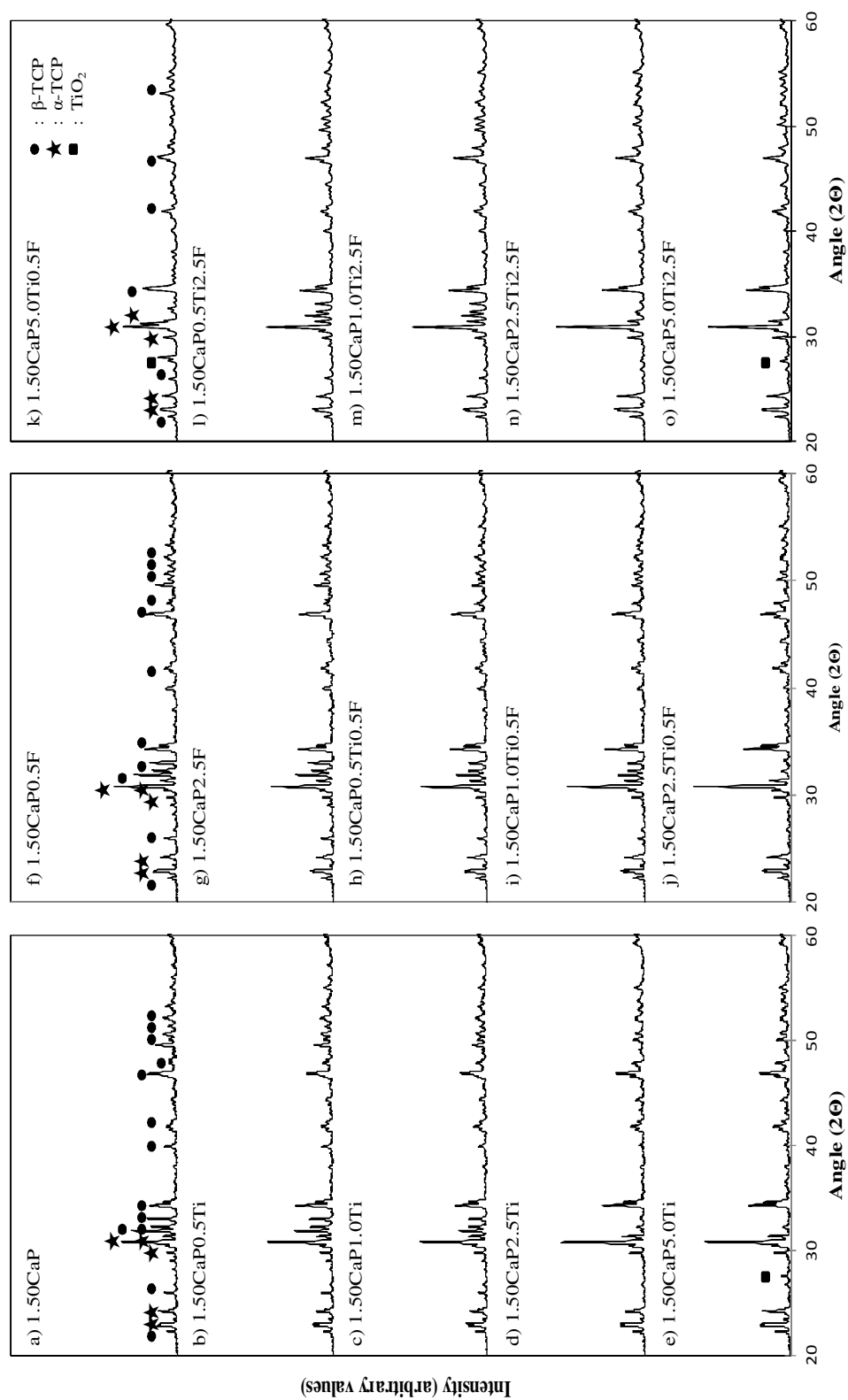
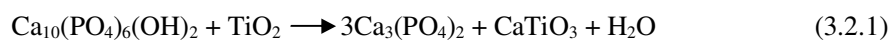


Figure 3.6: XRD patterns of CaPs with Ca to P ratio of 1.50 sintered at 1300°C.

XRD patterns of the different compounds with Ca/P molar ratio of 1.67 and sintered at 1100°C are given in Figure 3.7. For the undoped sample, the peaks of HA (ICDD file # 9-432) and β -TCP (ICDD file # 9-169) were observed due to sample had the optimum Ca/P ratio of 1.667 to produce pure HA [106]. In these study, result is in correlation with Basar et al. [86].

According to the results, the peaks are attributed to β -TCP, HA and CaO phases for Ti^{4+} doped samples. When Ti^{4+} amount increased from 0.5 to 5 mol.% resulted in increase of the peak intensities of β -TCP, CaO phase and decrease of the peaks of HA. Doping with Ti^{4+} ions modified the XRD patterns, with additional reflections, and alterations in intensity of some HA peaks. A low-intensity peaks were detected at 27.96° , 29.24° , 29.82° and 33.90° . This result consistent with Ergun study [70]. He mentioned about at 1100°C decomposition of the HA to TCP observed [70]. After increasing of Ti^{4+} ion amount peak intensities decreased, it indicates that crystallinity degree of the powders is low. In the Ti^{4+} doped samples as a second phase β -TCP was observed. Because of high sintering temperature and Ti^{4+} trigger the decomposition of HA into TCP [107]. With increasing Ti^{4+} amount, additional peaks of TiO_2 was observed overlapping with β -TCP at $27.8 (2\theta)$ in the samples of 1.67CaP1.0Ti, 1.67CaP2.5Ti, 1.67CaP5.0Ti, 1.67CaP1.0Ti0.5F, 1.67CaP2.5Ti0.5F, 1.67CaP5.0Ti0.5F, 1.67CaP1.0Ti2.5F, 1.67CaP2.5Ti2.5F and 1.67CaP5.0Ti2.5F.

The results of the XRD pattern for the Ti^{4+} doped samples showed that HA and Ti^{4+} reaction products were rutile (TiO_2) and $\beta\text{-Ca}_3(\text{PO}_4)_2$ as given in equation 3.2.1 [71]. As Ergun et al. stated anatase TiO_2 converts to rutile and catalyze the decomposition of the HA to $\beta\text{-Ca}_3(\text{PO}_4)_2$ [71].



The most intense $\beta\text{-Ca}_3(\text{PO}_4)_2$ and rutile peaks were at 2θ (25.80, 27.77, 29.66, 31.03) and (41.23, 54.32), respectively and HA decompose to $\text{Ca}_3(\text{PO}_4)_2$ and H_2O at 960°C [112].

In doped samples 1.67CaP2.5Ti, 1.67CaP2.5Ti, 1.67CaP5.0Ti, 1.67CaP1.0Ti0.5F, 1.67CaP2.5Ti0.5F, 1.67CaP5.0Ti0.5F, 1.67CaP1.0Ti2.5F, 1.67CaP2.5Ti2.5F and 1.67CaP5.0Ti2.5F, CaTiO_3 (at 47.54, 58.78 in 2θ) (ICDD file # 42-0423) was found at 1100°C. Meaning that doped samples were thermally unstable at high sintering temperature

[69]. According to Ergun et al., at 960°C HA decomposed to $\text{Ca}_3(\text{PO}_4)_3$ and H_2O and with reaction of titania, CaTiO_3 formed [112]. There was no direct reaction between HA and titanium but reaction between titanium oxide layer detected [112].

XRD patterns of F^- doped samples are presented in Figure 3.7 which assigned the peaks relative to HA, β -TCP and CaO (ICDD file # 37-1497) phase. According to the results, F^- ion amount at 0.5 mol.% increased the peak intensities of β -TCP and decreased the HA for the sample of 1.67CaP0.5F. As the F^- ion amount increased to 2.5 mol.% F^- addition increased the HA phase and decreased β -TCP and CaO peak intensity in the sample of 1.67CaP2.5F. Qu et al. demonstrated that addition of F^- ions improves the structural stability of HA [93]. Due to F^- ion doping into peak apatite lattice, peak shift to higher 2θ values in the position of (211), (300) and (112) planes in an increasing manner with an increase in F^- ions content [75].

Although, the XRD pattern of the samples 1.67CaP0.5Ti0.5F and 1.67CaP0.5Ti2.5F are matched with HA with minute amount of β -TCP, addition of Ti^{4+} ions to the samples 1.67CaP1.0Ti0.5F, 1.67CaP2.5Ti0.5F, 1.67CaP5.0Ti0.5F, 1.67CaP1.0Ti2.5F, 1.67CaP2.5Ti2.5F and 1.67CaP5.0Ti2.5F showed HA, β -TCP and CaO phases. According to XRD pattern for the Ti^{4+} and F^- doped samples TiO_2 (ICDD file # 21-1276) β -TCP and CaO (ICDD file # 37-1497) peaks observed with increasing Ti^{4+} ions. The most intense TiO_2 and β -TCP peaks were at 2θ (41.23, 54.32) and (27.77, 31.03, 34.37), respectively.

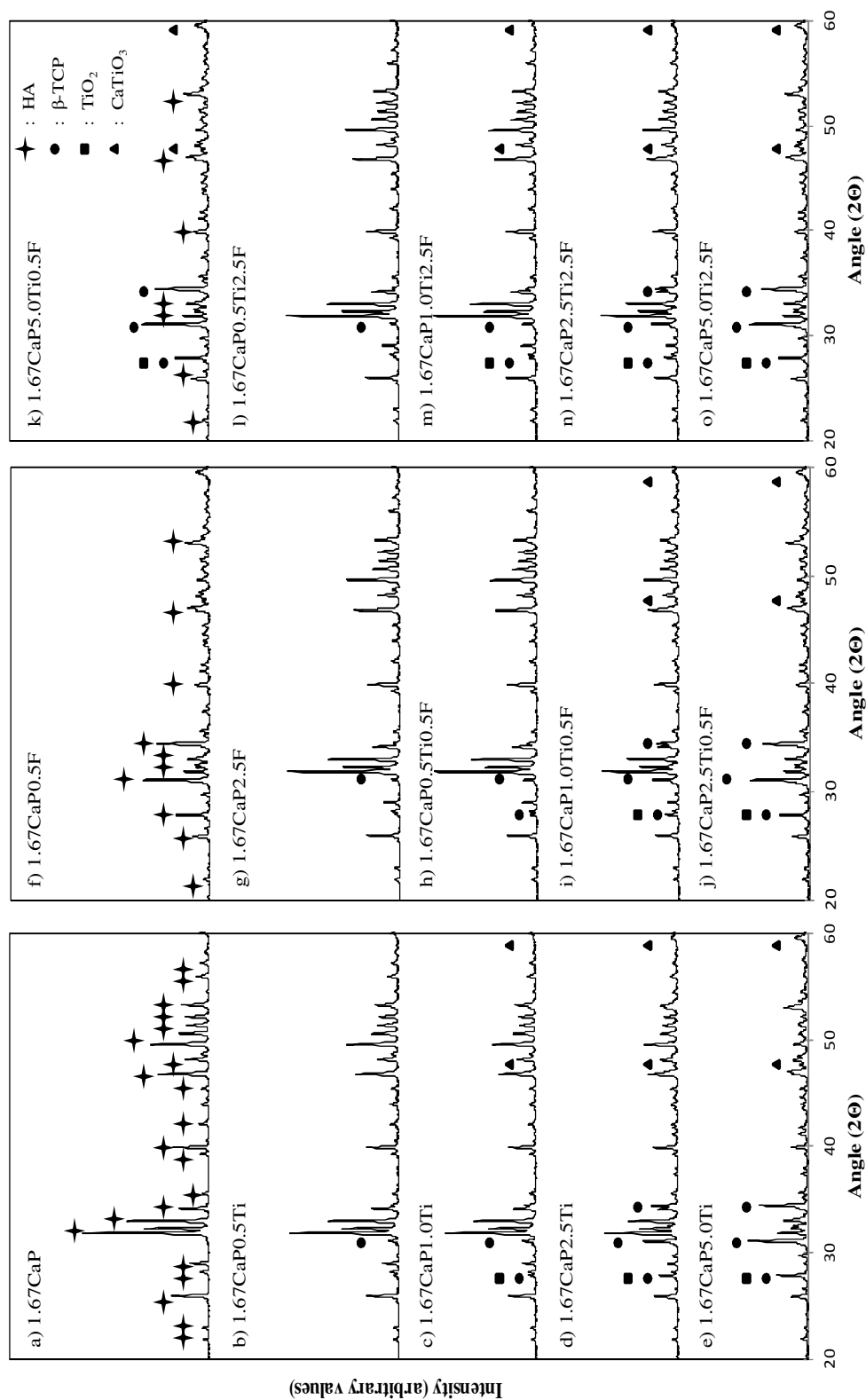


Figure 3.7: XRD patterns of CaPs with Ca to P ratio of 1.67 sintered at 1100°C.

The XRD pattern of the samples with Ca/P molar ratio of 1.67, sintered at 1300°C, are given in Figure 3.8. For undoped sample, XRD pattern coincide with the HA (ICDD file # 9-432). Moreover, there were very small amount of α -TCP, CaTiO_3 (ICDD file # 42-0423) and CaO (ICDD file # 37-1497) phases in the XRD pattern of the sample.

Doping with Ti^{4+} ions modified the XRD patterns. The characteristic peaks of HA (ICDD file # 9-432), α -TCP (ICDD file # 9-348) and CaO (ICDD file # 37-1497) appeared. According to Elliot et al. when HA was sintered between 700°C and 1125°C, it decomposed to β -TCP or a biphasic system of β -TCP and HA [16]. This transformation varied with respect to substituted ions and sintering temperatures. In these study doping the samples with Ti^{4+} ions trigger the decomposition of HA into α -TCP phase.

XRD pattern showed that the characteristic peaks of HA almost disappeared when Ti^{4+} ion amount was 5.0 mol.%. As a second phase α -TCP was observed in HA after Ti^{4+} addition at 1300°C. These results indicate that the stability of HA decreased as the sintering temperature and Ti^{4+} amount increased. High sintering temperature and Ti^{4+} trigger the decomposition of HA into TCP [107]. As a Ergun stated Ti^{4+} ion can be regarded as an α -TCP stabilizing agent in HA [70]. In doped samples 1.67CaP0.5Ti, 1.67CaP1.0Ti 1.67CaP2.5Ti, 1.67CaP5.0Ti, 1.67CaP0.5Ti0.5F, 1.67CaP1.0Ti0.5F, 1.67CaP2.5Ti0.5F, 1.67CaP5.0Ti0.5F, 1.67CaP0.5Ti2.5F, 1.67CaP1.0Ti2.5F, 1.67CaP2.5Ti2.5F and 1.67CaP5.0Ti2.5F, CaTiO_3 (at 47.54, 58.78 in 2θ) (ICDD file #42-0423) was found at 1300°C. Meaning that doped samples were thermally unstable at high sintering temperature [69]. Different from 1100°C, with increasing sintering temperature to 1300°C additional peaks of α -TCP observed.

According to XRD patterns, addition of F^- ions demonstrated peaks of HA (ICDD file # 9-432) and small amount of α -TCP. The main crystalline phase of HA remained. No severe fluctuations in the XRD peak positions due to addition of fluoride ions determined. The reason for improved stability was mainly due to the structural stability provided by precipitation method [48] and addition of F^- ions for the doped samples [93]. Due to Ca/P ratio of HA, the material becomes more stable after sintering [24]. This explains the structural stability in this study.

After addition of Ti^{4+} and F^- ions (0.5 mol.% to 5.0 mol.% Ti and 0.5 mol.%, 2.5 mol.% F ions), HA (ICDD file # 9-432) and α -TCP (ICDD file #9-348) phases were observed. As reported previously, with increasing the Ti^{4+} amount, HA peaks almost disappeared and only α -TCP characteristic peaks remained. The positions of the peaks were slightly shifted to the right with respect to the positions of pure α -TCP.

XRD pattern for the Ti^{4+} and F^- doped samples when sintering temperature increased to 1300°C only two peaks of α -TCP observed with increasing Ti^{4+} ions.

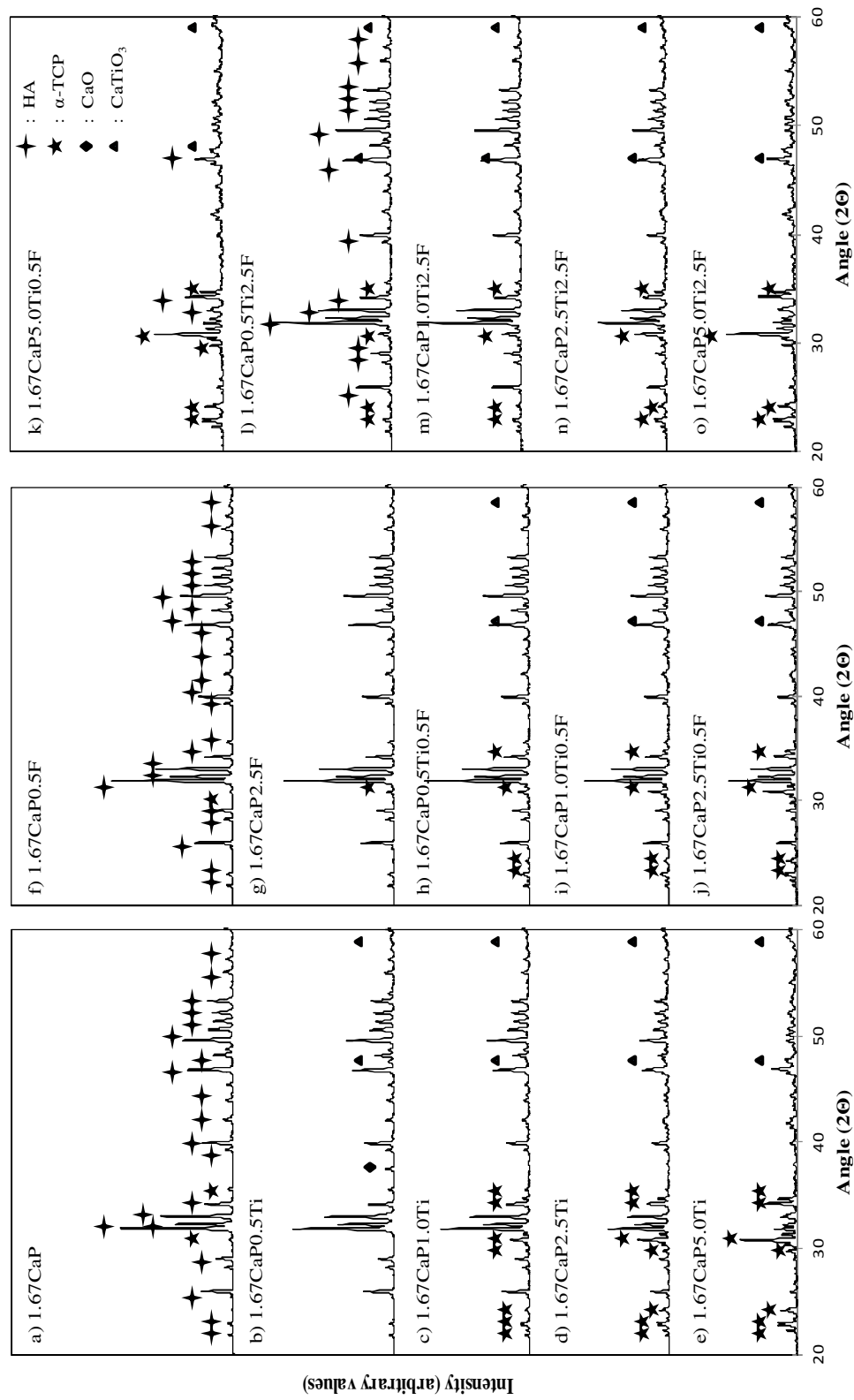


Figure 3.8: XRD patterns of CaPs with Ca to P ratio of 1.67 sintered at 1300°C.

In Figure 3.9, XRD spectrums of CaPs with molar ratio of 2.0, sintered at 1100°C given. As seen from the XRD pattern for the undoped sample, the peaks are attributed to HA (ICDD file # 9-432) and as a second phase of small amount of CaO detected. Due to presence of too much Ca^{2+} ions in the system [106], Chou et al. revealed that CaO exhibits cytotoxicity due to it increase the pH in a cellular environment [117].

Doping with Ti^{4+} ion modified the XRD patterns and alterations in intensity of some peaks of CaO. Increased Ti^{4+} ion amount decreased the peak intensities of CaO due to CaTiO_3 (at 47.6, 59.2 in 2θ) (ICDD file #42-0423) was formed at 1100°C. No severe fluctuations in the XRD peak positions due to addition of titanium ions into HA were determined.

According to XRD patterns, addition of Ti^{4+} and F^- ions demonstrated only peaks of HA (ICDD file # 9-432) and CaO appear in the 2θ (37.3°). No severe fluctuations in the XRD peak positions and peak intensities due to addition of Ti^{4+} and F^- ions into samples were determined. Narrow peaks of the samples illustrate that they were highly crystalline when Ti^{4+} and F^- ions addition. The maximum peaks of the CaO appeared in the samples of 2.0CaP2.5F and 2.0CaP0.5Ti2.5F.

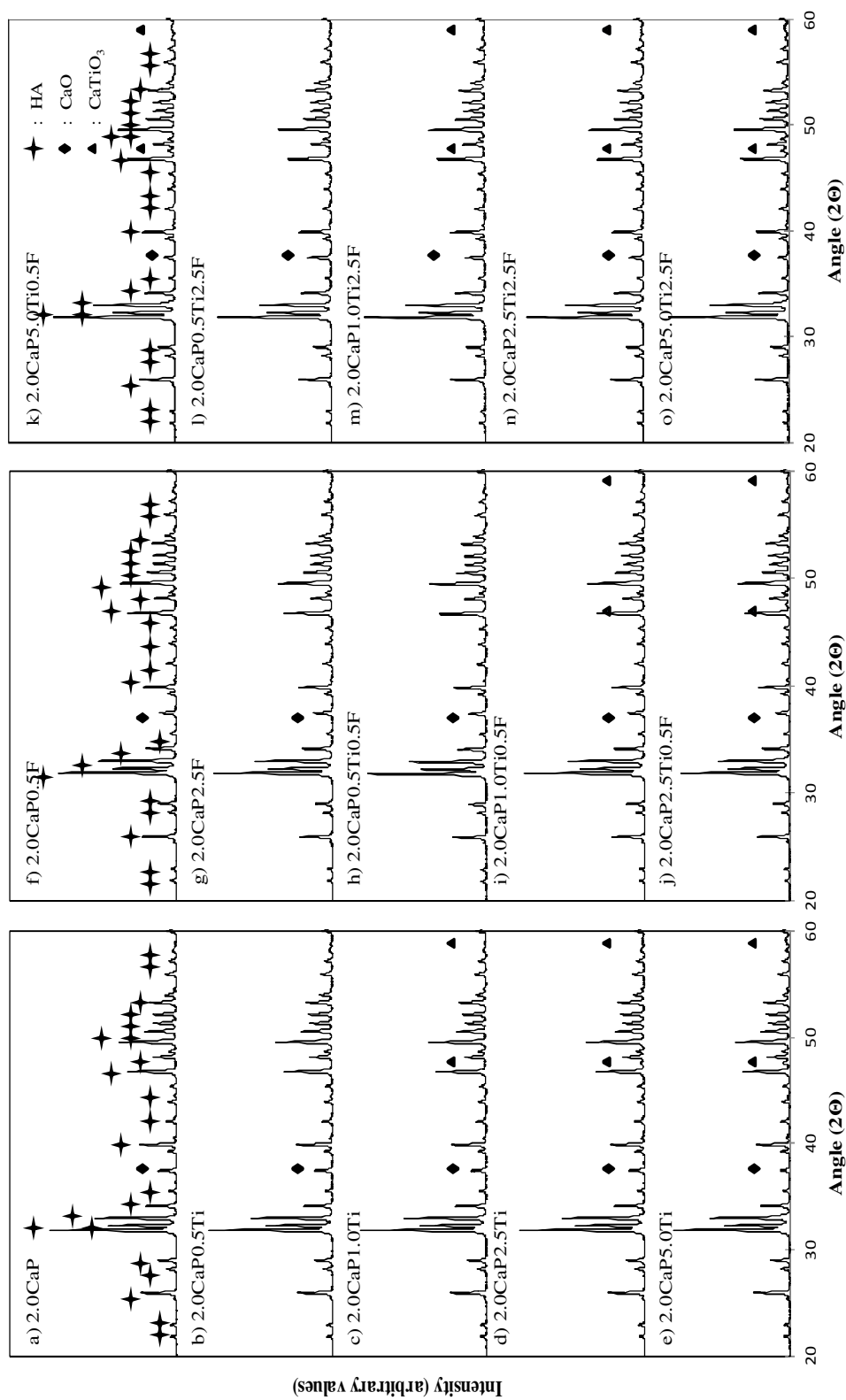


Figure 3.9: XRD patterns of CaPs with Ca to P ratio of 2.0 sintered at 1100°C.

The XRD patterns of the different compounds with molar ratio of 2.0 sintered at 1300°C given in Figure 3.10. For the undoped and doped samples, the peaks of HA (ICDD file # 9-432), α -TCP and small amount of CaO were observed. CaTiO_3 (at 47.58, 58.92 in 2θ) (ICDD file #42-0423) was formed at 1300°C. No severe fluctuations in the XRD peak positions due to addition of titanium and fluoride ions into HA were determined.

There was not a considerable difference in the intensity of the undoped and doped samples at 1300°C for samples with Ca/P ratio 2.0. Narrow peaks for both sintering temperature indicate that they were highly crystalline. With increasing sintering temperature from 1100°C to 1300°C, CaO peak at 2θ angle of 37.3° almost disappeared in the Ti^{4+} added samples. When comparing the ratios of CaO, the amount of CaO at 1100°C higher than that at 1300°C. The peak intensity of the CaO at 1300°C decreased because of CaTiO_3 (at 47.6, 59.2 in 2θ) (ICDD file #42-0423) was formed.

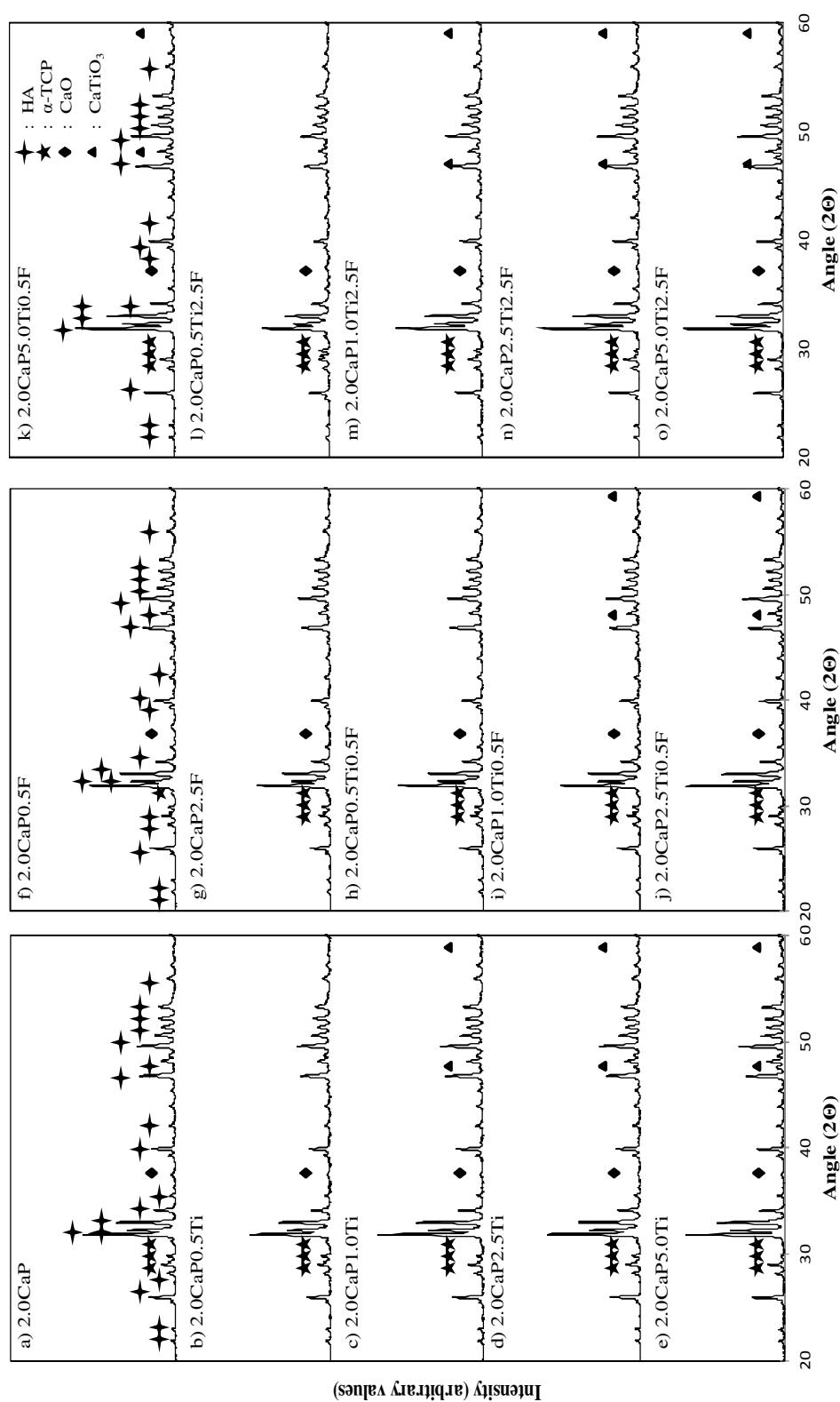


Figure 3.10: XRD patterns of CaPs with Ca to P ratio of 2.0 sintered at 1300°C.

3.2.1.1 Lattice Parameter Measurements of Pure and Doped Hydroxyapatite

Hexagonal lattice parameters, unit cell volume and change in the unit cell volume of the samples of HA are given in Table 3.3.

As seen in Table 3.3, it was observed for pure HA, both of the lattice parameters and its unit cell volume were decreased by increasing the sintering temperature. According to results, addition of Ti^{4+} ion increased the lattice parameter “a” and “c” except for sample 1.67CaP1.0Ti. Huang et al. revealed that incorporation of Ti^{4+} into the HA lattice structure led to an increase in the cell volume in both a and c axis [69]. We expect to see an increase in the lattice parameters because of differences of the ionic size of Ti^{4+} ions.

When sintering temperature increased, the lattice parameters of co-doped samples were not in correlation with amount of with Ti^{4+} ion concentration. There was a decrease in ‘a’ and ‘c’ lattice parameters except for the sample with 1.67CaP2.5Ti. According to Ribeiro et al. substitution of Ti^{4+} ions for calcium ions expected to lead a decrease in the lattice parameters because ionic radius of calcium (0.99Å) is greater than Ti^{4+} (0.68Å) [9]. Ergun et al. demonstrated that Ti^{4+} incorporation into the apatite structure caused lattice shrinkage because of the ionic radii of Ti^{4+} is smaller than that of all components of HA: Ca, O, and P [70].

Lattice parameters of co-doped samples with F^- ions in Table 3.4 demonstrated that increasing the sintering temperature causes an increase in the lattice parameters of HAs. At two different sintering temperature, when F^- ion content was increased, both of the lattice parameters were increased. It was previously mentioned that F^- addition made very small changes in the crystal lattice of HA [96].

Table 3.3: Hexagonal lattice parameters of pure and doped CaPs with a Ca/P ratio of 1.67 sintered at 1100°C

Sample ID	Sintered at 1100 °C					Sintered at 1300 °C				
	a(Å)	c(Å)	V(Å ³)	$\Delta V(\text{Å}^3)$		a(Å)	c(Å)	V(Å ³)	$\Delta V(\text{Å}^3)$	
1.67CaP	9.4054	6.8683	1573.03	-7.82		9.3965	6.8639	1569.04	-11.80	
1.67CaP0.5Ti	9.4067	6.8694	1573.71	-7.14		9.4086	6.8687	1574.19	-6.66	
1.67CaP1.0Ti	9.4053	6.8677	1572.85	-7.99		9.3969	6.915	1580.86	0.01	
1.67CaP2.5Ti	9.4082	6.8664	1567.90	-12.95		9.8659	6.9329	1567.70	-13.15	
1.67CaP5.0Ti	9.6240	6.716	1610.47	29.63		9.3328	6.9375	1564.44	-16.41	
1.67CaP0.5F	9.3961	6.8632	1568.75	-12.10		9.4012	6.8667	1571.26	-9.59	
1.67CaP2.5F	9.3994	6.8663	1570.56	-10.29		9.4030	6.8708	1572.80	-8.05	
1.67CaP0.5Ti0.5F	9.4115	6.8742	1576.42	-4.43		9.4037	6.8715	1573.19	-7.66	
1.67CaP1.0Ti0.5F	9.4073	6.8725	1574.62	-6.22		9.4050	6.8685	1572.94	-7.91	
1.67CaP2.5Ti0.5F	9.4044	6.8408	1566.39	-14.45		9.4267	6.8743	1578.19	-2.66	
1.67CaP5.0Ti0.5F	9.4956	6.7687	1546.99	-33.86		9.5848	6.6177	1574.00	-6.85	
1.67CaP0.5Ti2.5F	9.4039	6.8686	1572.59	-8.26		9.3997	6.8693	1571.35	-9.50	
1.67CaP1.0Ti2.5F	9.4087	6.8722	1575.02	-5.82		9.4014	6.8714	1572.40	-8.45	
1.67CaP2.5Ti2.5F	9.4369	6.8695	1580.50	-0.35		9.4127	6.9286	1580.13	-0.72	
1.67CaP5.0Ti2.5F	9.4997	6.8122	1591.62	10.77		9.7641	6.3946	1578.37	-2.47	

Due to F^- addition into HA, parameter “a” was decreased and parameter “c” was increased. Because of increase in parameter “c” was bigger than increase in parameter “a”, these changes resulted in very small increase in unit cell volumes when compared with pure HA. Amount of F^- doping was related with the changes in lattice parameters which result is correlation with c except a in this study. Samples which were doped with F^- ions showed a significant decrease in both ‘a’ and ‘c’ lattice parameters at 1100°C. It is expected that doping of HA with F^- ions causes shrinkage in unit cell volumes because ion size of F^- ion is smaller than that of OH ion. The effective ionic radius of F^- is 1.33 Å while the ionic radius for OH is 1.37 Å [97]. Jha et al. revealed that both of the lattice parameters were decreased with increasing the fluoride ion concentration and also, the reaction temperature had a significant effect on ‘a’ and ‘c’ lattice parameters [98]. Atom positions of OH, F^- and Ti^{4+} ions along c-axis are given in Table 3.4. According to the Table 3.3, no change in c-axis was expected due to F^- ion positions are very close to the “O” ion position in OH ion

Table 3.4: Z positions of the ions of OH and F [66].

Ion	Atoms	Z
OH	O	0.2 or 0.3, 0.7 or 0.8
	H	0.06 or 0.44, 0.56 or 0.94
F	F	0.25, 0.75

F^- and Ti^{4+} ions co-doping at 1100°C led to a decrease in lattice parameters of samples in 1.67CaP1.0Ti0.5F, 1.67CaP5.0Ti0.5F and increase in 1.67CaP0.5Ti0.5F, 1.67CaP5.0Ti0.5F. When sintering temperature was increased to 1300°C and Ti^{4+} amount increased from 0.5 mol.% to 5 mol.%, an increase in the parameter “a” and in the parameter “c” was observed except in 1.67CaP1.0Ti0.5F. Due to Ti^{4+} and 2.5%F addition into HA increased the parameter “a” and increased the parameter “c” except for the samples 1.67CaP2.5Ti2.5F and 1.67CaP5.0Ti2.5F.

3.2.2 Fourier Transform Infrared Spectroscopy

FTIR was applied to identify the presence of the bonds related to CaP and the presence of bands related to F^- and Ti^{4+} ions. FTIR results of the CaPs doped with Ti^{4+} and F^- ions are presented in Figures 3.11- 3.20.

The FTIR spectra of the synthesized pure and doped 1CaP after the sintering at $1100^{\circ}C$ for 1h is given in Figure 3.11. All of the doped and undoped samples sintered at $1100^{\circ}C$ demonstrated the characteristic bands for β -CPP. FTIR reference frequencies of β -CPP are given in Table 3.5. β -CPP peaks at $1130-945\text{ cm}^{-1}$ were attributed to phosphate stretching and bending mode of vibration as seen in Table 3.6. The bands at $630-518\text{ cm}^{-1}$ were due to the phosphate bending mode of vibrations. The bands at 3438 and 1612 cm^{-1} were corresponding to OH^- [102], indicating the minimum amount of absorbed water in the samples. The asymmetrical stretching and bending modes of PO_4^{3-} were observed at around 1091 , 1170 , 980 and 534 cm^{-1} , respectively [100]. The asymmetrical stretching and bending modes of PO_4^{3-} ions were declined by increasing the Ti^{4+} amount. After adding different Ti^{4+} ion concentration, a significant decrease was observed in the band peaks. Same peaks were detected for the samples of 1CaP0.5Ti, 1CaP1.0Ti, 1CaP2.5Ti and 1CaP5.0Ti. The intensity of the peaks at 696 cm^{-1} decreased with increasing F^- amount in the samples and also OH-F bonding were visible in this sample. This is due to the fact that F^- ion replaces OH^- ion in the CaP structure. When the F^- amount in the samples increased, this resulted in decreased OH^- ion concentration in the CaP structure because of the replacement of F^- ion which resulted in a decrease in the intensity of the peaks at 696 cm^{-1} [92]. This result revealed that F^- ion incorporated into the CaP structure successfully. Increased F^- and Ti^{4+} ions amount resulted in decreased peak intensities. The asymmetrical stretching and bending modes of PO_4^{3-} decreased with increasing ion concentrations.

Table 3.5: Frequencies and assignment and frequencies of CPP.

Assignment	Infrared Frequency (cm ⁻¹)	Ref. #
OH and/or adsorbed water	3432 and 1644 cm ⁻¹	[102]
$\nu_4\text{PO}_4^{3-}$ bend	726 and 613-494 cm ⁻¹	[102]
$\nu_3\text{PO}_4^{3-}$ stretch	1186-941 cm ⁻¹	[102]
OH-F band	720 and 3544.6	[89]

Table 3.6: FTIR band locations in the samples with Ca/P molar ratio 1.0 at 1100°C.

Sample ID	OH ⁻ Adsorbed Water	$\nu_4\text{PO}_4^{3-}$	$\nu_3\text{PO}_4^{3-}$	OH-F
1CaP	3425/1600	536	1128/-	-
1CaP0.5Ti	3427/1595	543	1126/831	746
1CaP1.0Ti	3433/1600	545	1126/837	750
1CaP2.5Ti	3450/1591	557	1124/900	842
1CaP5.0Ti	3462/1583	590	1107/914	844
1CaP0.5F	3423/1595	547	1137/-	750
1CaP2.5F	3431/1593	543	1134/-	752
1CaP0.5Ti0.5F	3787/1591	543	1128/829	752
1CaP1.0Ti0.5F	3782/1593	551	-/837	-
1CaP2.5Ti0.5F	3787/1589	541	1120/842	746
1CaP5.0Ti0.5F	3791/1598	555	1166/900	840
1CaP0.5Ti2.5F	3801/1596	555	1145/883	829
1CaP1.0Ti2.5F	3795/1596	545	1141/879	829
1CaP2.5Ti2.5F	3780/1610	555	1141/896	840
1CaP5.0Ti2.5F	3786/1602	543	1180/906	835

By Ti^{4+} addition, OH⁻ band shifted to 3462 cm⁻¹ (Table 3.6). Furthermore, F⁻ ion addition demonstrated a shift to 3431 cm⁻¹ and with increasing F⁻ ion amount the bands shifted to the higher wavenumbers. This indicates that there are changes occurred in the sample structure [120]. Only in the samples doped with F⁻ ions, another band of OH...F was observed. High amount of shifts was detected for the samples with Ti^{4+} and 2.5F ions. Ozek et al. demonstrated that when F⁻ ion amount increased, shift to the smaller wavenumbers was detected because of hydrogen bonds between F⁻ and H⁺ ions [92]. As expected, in the F⁻

undoped samples no band was observed at 3543 cm^{-1} , which is the evidence of the F^- ion integration into the β -CPP.

According to Figure 3.12, when sintering temperature was increased to 1300°C characteristic bands for β -CPP & α -TCP (samples of 1CaP, 1CaP0.5Ti and 1CaP5.0Ti), the bands for PO_4^{3-} groups and OH^- groups were detected (Table 3.7). In the 0.5 mol.%-2.5 mol.% F^- and 0.5 mol.%-5.0 mol.% Ti^{4+} doped samples the characteristic peaks of β -CPP and β -TCP were observed. β -TCP peaks were observed at around the infrared frequencies 1126 cm^{-1} and 971 cm^{-1} [103]. Band at $3500\text{-}3300\text{ cm}^{-1}$ relating to vibration of the absorbed water (OH^- libration band) in sample structure detected except for the samples with Ti^{4+} and 0.5F^- ions it is almost disappeared. The asymmetrical stretching and bending modes of PO_4^{3-} ions were increased by increasing Ti^{4+} amount. Different from the samples sintered at 1100°C , when the F^- amount in the samples increased, resulted in increased OH^- ion concentration in the CaP structure, which is in conflict with the result of Ozek [92]. Addition of Ti^{4+} and F^- ion increased the peak intensities. OH^- libration band decreased in the samples with increased Ti^{4+} and 2.5 mol.% F^- ions. Maximum stretching bands (ν_3) were observed in the samples doped with 5.0 mol.% Ti ions.

Table 3.7: FTIR band locations in the samples with Ca/P molar ratio 1.0 at 1300°C.

Sample ID	OH ⁻ Adsorbed Water	$\nu_4\text{PO}_4^{3-}$	$\nu_3\text{PO}_4^{3-}$	OH-F
1CaP	3435	545	1109	-
1CaP0.5Ti	3436	547	1105	819
1CaP1.0Ti	3448	547	1091	833
1CaP2.5Ti	3425	543	1099	831
1CaP5.0Ti	3469	543	1093	827
1CaP0.5F	3450	545	1110	769
1CaP2.5F	3448	549	1087	748
1CaP0.5Ti0.5F	3475	553	1101	746
1CaP1.0Ti0.5F	3450	545	1095	740
1CaP2.5Ti0.5F	3494	545	1093	833
1CaP5.0Ti0.5F	3462	543	1097	833
1CaP0.5Ti2.5F	3483	545	1093	831
1CaP1.0Ti2.5F	3456	540	1095	817
1CaP2.5Ti2.5F	3462	541	1091	837
1CaP5.0Ti2.5F	3469	540	1095	831

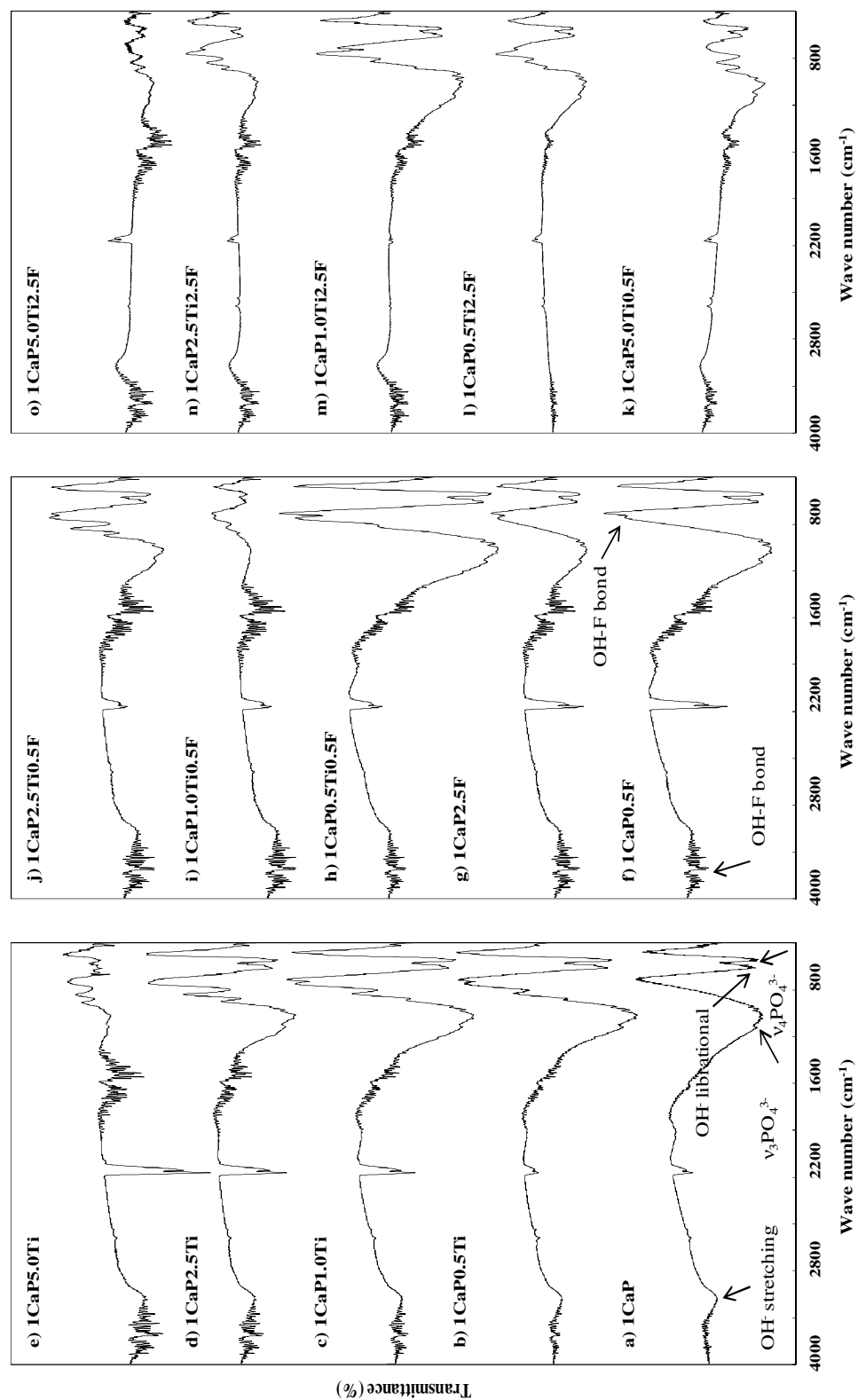


Figure 3.11: FTIR patterns of CaPs with Ca to P ratio of 1 sintered at 1100°C.

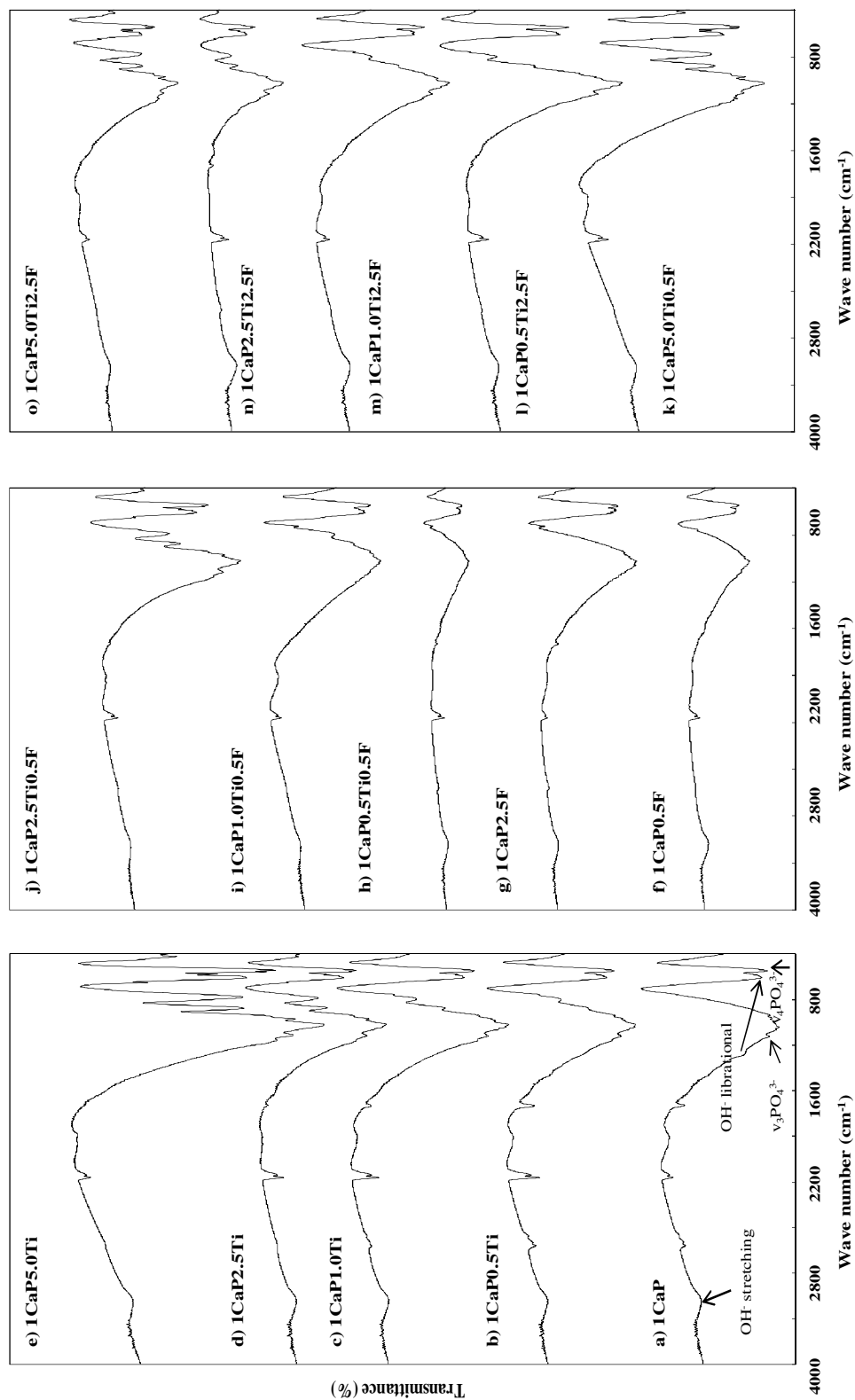


Figure 3.12: FTIR patterns of CaPs with Ca to P ratio of 1 sintered at 1300°C.

According to Figure 3.13 at 1100°C, corresponding bands given in Table 3.8 showed that at 611 and 538 cm^{-1} , components of the ν_4 O-P-O bending mode of β -TCP were observed [88]. The bands in the range of 1558-1398 cm^{-1} indicated that samples of OCP contain large quantities of carbonate ions [88]. The characteristic P-O bands of OCP appear at 1126, 1083, 1043 cm^{-1} and HPO_4^{2-} bands at 968 and 941 cm^{-1} . P-O bands appearing at 549 and 611 cm^{-1} implies that the samples have an OCP structure. Band at 3960-3400 cm^{-1} and 2000-1300 relating to vibration of the absorbed water in sample structure was observed. Among the entire samples, OH^- librational bands are not visible. Increasing the Ti^{4+} amount decreased the peak intensities of asymmetrical stretching (ν_3) and bending (ν_4) modes of PO_4^{3-} . When the F^- amount in the samples increased, this resulted in decrease of OH^- ion concentration in the CaP structure because of the replacement of F^- ion which resulted in decrease in the intensity of the peaks [92]. Increasing the Ti^{4+} and 0.5 mol.% F ion amount decreased the peak intensities of stretching (ν_3) and bending (ν_4) modes of PO_4^{3-} .

Table 3.8: FTIR band locations in the samples with Ca/P molar ratio 1.25 at 1100°C.

Sample ID	OH^- Stretching	$\nu_4\text{PO}_4^{3-}$	HPO_4^{2-}	OH-F
1.25CaP	3546	611	1128	-
1.25CaP0.5Ti	3546	615	1139	-
1.25CaP1.0Ti	3546	613	1124	-
1.25CaP2.5Ti	3544	605	1145	-
1.25CaP5.0Ti	3544	615	1130	-
1.25CaP0.5F	3479	615	1134	3649-779
1.25CaP2.5F	3479	615	1130	3649-775
1.25CaP0.5Ti0.5F	3460	-	997	3649-783
1.25CaP1.0Ti0.5F	3481	-	991	3649-781
1.25CaP2.5Ti0.5F	3487	617	1047	3649-765
1.25CaP5.0Ti0.5F	3504	505	-	3649-883
1.25CaP0.5Ti2.5F	3483	607	1132	3649-877
1.25CaP1.0Ti2.5F	3483	592	1134	3649-877
1.25CaP2.5Ti2.5F	3483	617	1136	3649-841
1.25CaP5.0Ti2.5F	3483	615	1126	3649-896

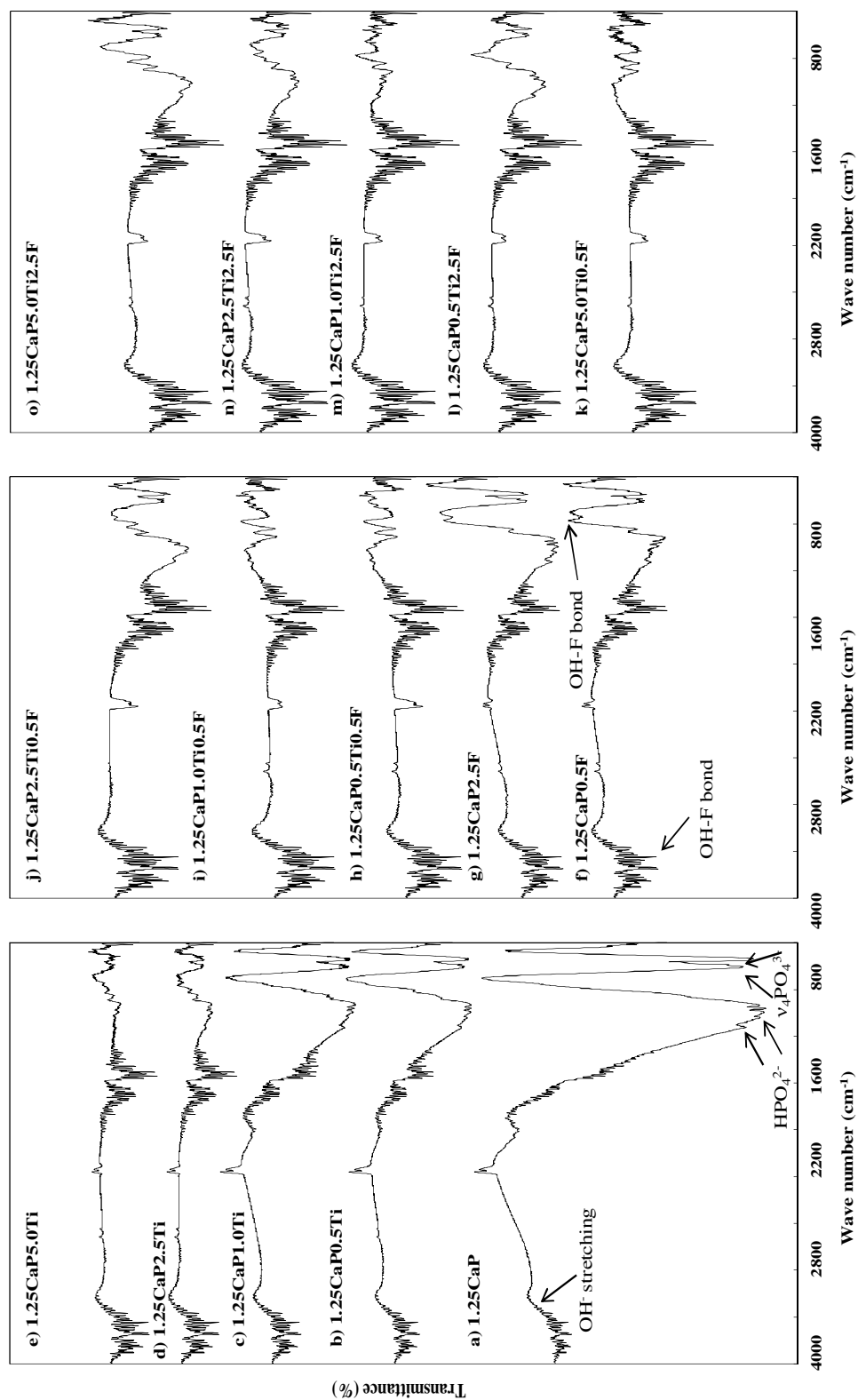


Figure 3.13 : FTIR patterns of CaPs with Ca to P ratio of 1.25 sintered at 1100°C.

Characteristic bands of the samples given in Figure 3.14 are represented in Table 3.9. ν_4 O-P-O bending modes of β -TCP are positioned at 613 and 543 cm^{-1} as seen in Figure 3.14 [88]. When sintering temperature increased to 1300°C, the intensity of peaks around the PO_4^{3-} groups increased with increasing of Ti^{4+} ions. OH^- libration band which came from HA disappeared and OH^- stretching band decreased in the samples with increasing the Ti^{4+} ions. Maximum stretching bands (ν_3) were increased in the samples doped with Ti^{4+} ions. Peak intensities were increased by increasing the Ti^{4+} amount. There is an increase in the peak intensities and increased stretching (ν_3) and bending (ν_4) modes of PO_4^{3-} ion when the Ti^{4+} and F^- amount was increased.

Table 3.9: FTIR band locations in the samples with Ca/P molar ratio 1.25 at 1300°C.

Sample ID	OH^- Stretching	$\nu_4\text{PO}_4^{3-}$	HPO_4^{2-}	OH-F
1.25CaP	3456	613	1124	-
1.25CaP0.5Ti	3483	611	1124	-
1.25CaP1.0Ti	3483	613	1122	-
1.25CaP2.5Ti	3462	615	1118	-
1.25CaP5.0Ti	3475	611	1114	-
1.25CaP0.5F	3450	615	1114	765
1.25CaP2.5F	3467	609	1089	783
1.25CaP0.5Ti0.5F	3456	607	1095	742
1.25CaP1.0Ti0.5F	3489	611	-	736
1.25CaP2.5Ti0.5F	3506	613	1122	835
1.25CaP5.0Ti0.5F	3462	613	1109	833
1.25CaP0.5Ti2.5F	3475	613	1122	827
1.25CaP1.0Ti2.5F	3463	613	1122	821
1.25CaP2.5Ti2.5F	3456	611	1122	835
1.25CaP5.0Ti2.5F	3475	617	1110	829

According to Figure 3.15, bands of HA and β -TCP were observed for pure 1.50CaP sintered at 1100°C as seen in Table 3.10. Bands assigned to $\nu_4\text{PO}_4^{3-}$ groups were around from 580 to 572 cm^{-1} . O-P-O bending modes assigned to ν_3 were around 1100 - 940 cm^{-1} . The OH^- stretching is apparent at 3572 cm^{-1} which is a characteristic of HA. Between the range from 4000 to 3500 cm^{-1} , broad band of low intensity peaks was observed which revealed trace amount of water joined into the structure of the sample [88]. With increasing Ti^{4+} ion amount, the OH^- stretching and libration band, which is characteristic of HA,

disappeared. Consequently, the transmittance intensities of OH⁻ bands decreased when Ti⁴⁺ ion content increased due to the acceleration in the decomposition of HA to β -TCP in the presence Ti⁴⁺ ions. Because of this, in Ti⁴⁺ doped samples, transformation from CaO to Ca(OH)₂ was not observed. Addition and rising of F⁻ ion amount to the samples with Ti⁴⁺ resulted in an increase in the intensity of peaks of OH⁻ stretching and libration bands so intensity of hydroxyl band was increased by increasing F⁻ ion content. The intensity of the $\nu_4\text{PO}_4^{3-}$ and $\nu_3\text{PO}_4^{3-}$ bending decreased with increasing Ti⁴⁺ and F⁻ ion concentration. Azami et al. revealed that the intensity of the $\nu_4\text{PO}_4^{3-}$ (O-P-O) bend at 605 cm⁻¹ increased, while at 565 cm⁻¹ decreased with addition of fluorination [91]. When the results compared with Azamis study [87] addition of Ti ion amounts decreased the intensity of the $\nu_4\text{PO}_4^{3-}$ (O-P-O) bend.

Table 3.10: FTIR band locations in the samples with Ca/P molar ratio 1.50 at 1100°C.

Sample ID	OH ⁻ Stretching	$\nu_3\text{PO}_4^{3-}$	$\nu_4\text{PO}_4^{3-}$	OH-F
1.50CaP	3749	939	609	-
1.50CaP0.5Ti	3749	927	613	-
1.50CaP1.0Ti	3751	933	613	-
1.50CaP2.5Ti	3751	925	613	-
1.50CaP5.0Ti	3751	925	615	-
1.50CaP0.5F	3749	921	607	777
1.50CaP2.5F	3749	937	611	777
1.50CaP0.5Ti0.5F	3751	904	503	779
1.50CaP1.0Ti0.5F	3749	908	503	781
1.50CaP2.5Ti0.5F	3751	943	615	615
1.50CaP5.0Ti0.5F	3751	-	738	786
1.50CaP0.5Ti2.5F	3749	941	607	887
1.50CaP1.0Ti2.5F	3749	912	740	879
1.50CaP2.5Ti2.5F	3751	919	601	773
1.50CaP5.0Ti2.5F	3751	970	611	833

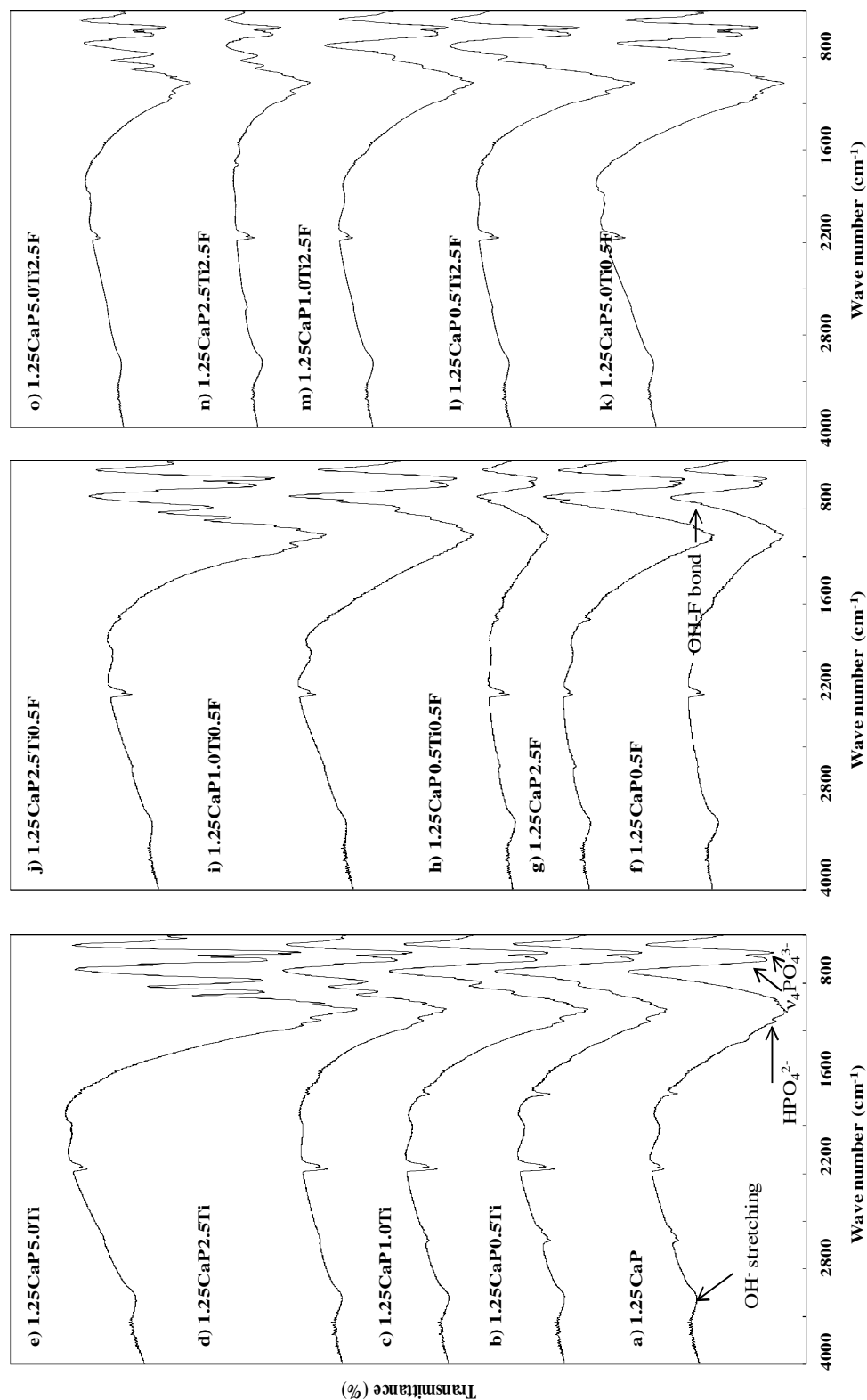


Figure 3.14: FTIR patterns of CaPs with Ca to P ratio of 1.25 sintered at 1300°C.

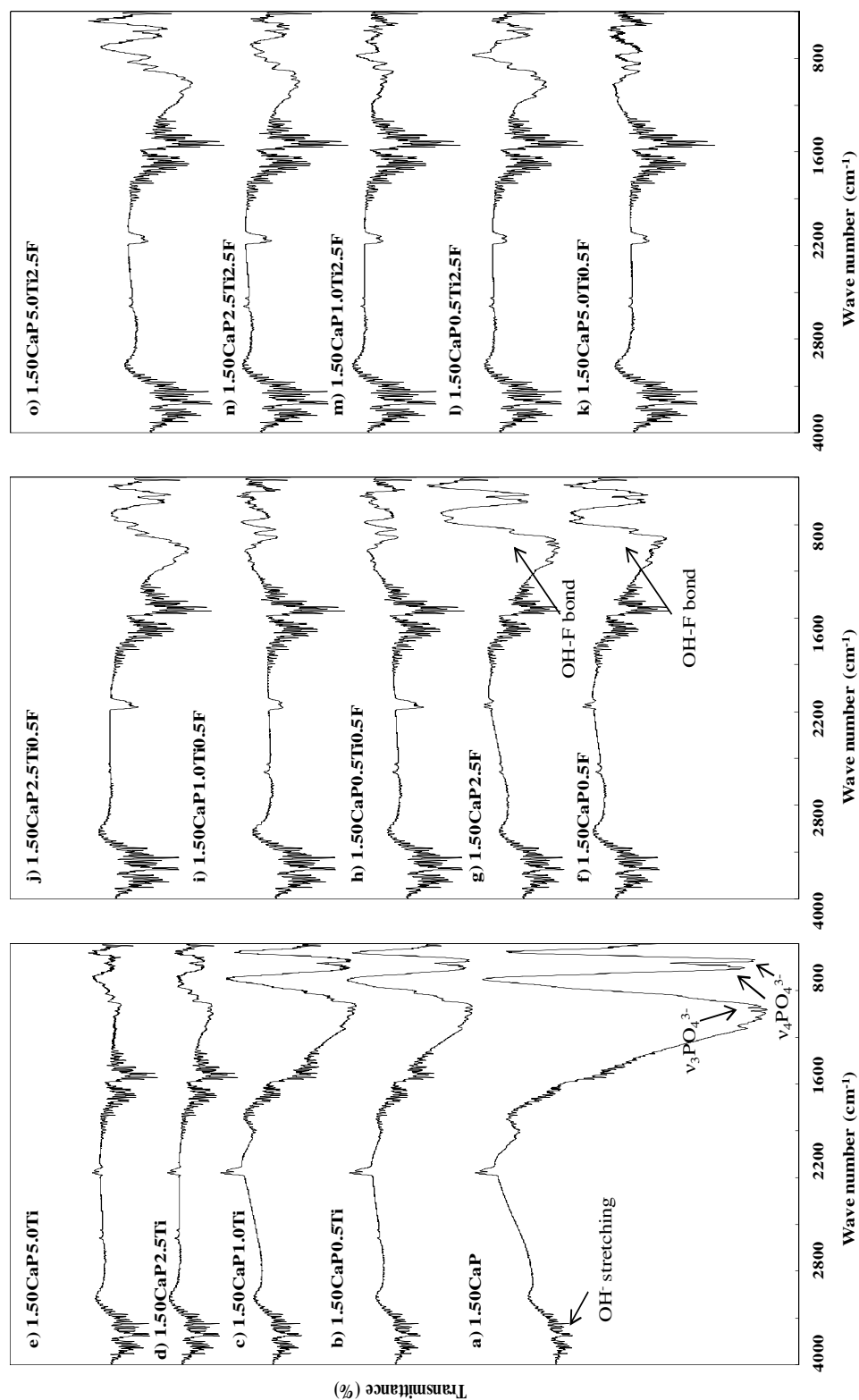


Figure 3.15: FTIR patterns of CaPs with Ca to P ratio of 1.50 sintered at 1100°C.

According to Figure 3.16, bands given in Table 3.11, doped and undoped samples revealed the characteristic bands of β -TCP and also a few bands of HA. The bands at 3905-3593 cm^{-1} assigned to absorbed water in the samples. The bands at 615-553 cm^{-1} and 1118-1035 cm^{-1} were attributed to the $\nu_4\text{PO}_4^{3-}$ O-P-O bending mode and $\nu_3\text{PO}_4^{3-}$ antisymmetric P-O stretching mode, respectively. The intensity of peaks around the $\nu_1\text{PO}_4^{3-}$ P-O symmetric stretching increased with increasing Ti^{4+} ions.

In the samples doped with F^- ions, the spectrum obtained was characteristic of β -TCP/HA. Increasing the F^- ion addition triggered the peak intensities. The intensity of the peak at 796 cm^{-1} raised up with increasing F^- amount in the samples and also OH-F bonding was visible in this sample. This is due to the fact that F^- ion replaces with OH^- ion in the CaP structure.

The characteristic bands of β -TCP and HA were observed in the doped samples. The intensity of the $\nu_4\text{PO}_4^{3-}$ and $\nu_3\text{PO}_4^{3-}$ bending raised with increasing Ti^{4+} and 0.5 F^- doped samples. However, increasing the Ti^{4+} ions and F^- amount to 2.5 mol.% resulted in decreasing the peak intensities. Thus, it can be said that increasing the degree of fluorination in the samples with 0.5 mol.% to 5.0 mol.% Ti^{4+} amounts resulted in a decrease in the intensity of the peaks.

Table 3.11: FTIR band locations in the samples with Ca/P molar ratio 1.50 at 1300°C.

Sample ID	OH ⁻ Stretching	$\nu_1\text{PO}_4^{3-}$	$\nu_3\text{PO}_4^{3-}$	$\nu_4\text{PO}_4^{3-}$	OH-F
1.50CaP	3448	-	1109	611	-
1.50CaP0.5Ti	3462	952	1099	607	-
1.50CaP1.0Ti	3448	894	1101	613	-
1.50CaP2.5Ti	3456	829	1095	609	-
1.50CaP5.0Ti	3469	833	1093	611	-
1.50CaP0.5F	3442	950	1107	601	765
1.50CaP2.5F	3462	964	-	609	738
1.50CaP0.5Ti0.5F	3462	-	-	615	740
1.50CaP1.0Ti0.5F	3475	883	-	615	736
1.50CaP2.5Ti0.5F	3456	977	1091	613	833
1.50CaP5.0Ti0.5F	3442	989	1095	613	831
1.50CaP0.5Ti2.5F	3469	975	1101	613	825
1.50CaP1.0Ti2.5F	3469	950	1095	613	811
1.50CaP2.5Ti2.5F	3450	979	1095	615	833
1.50CaP5.0Ti2.5F	3483	985	1089	617	827

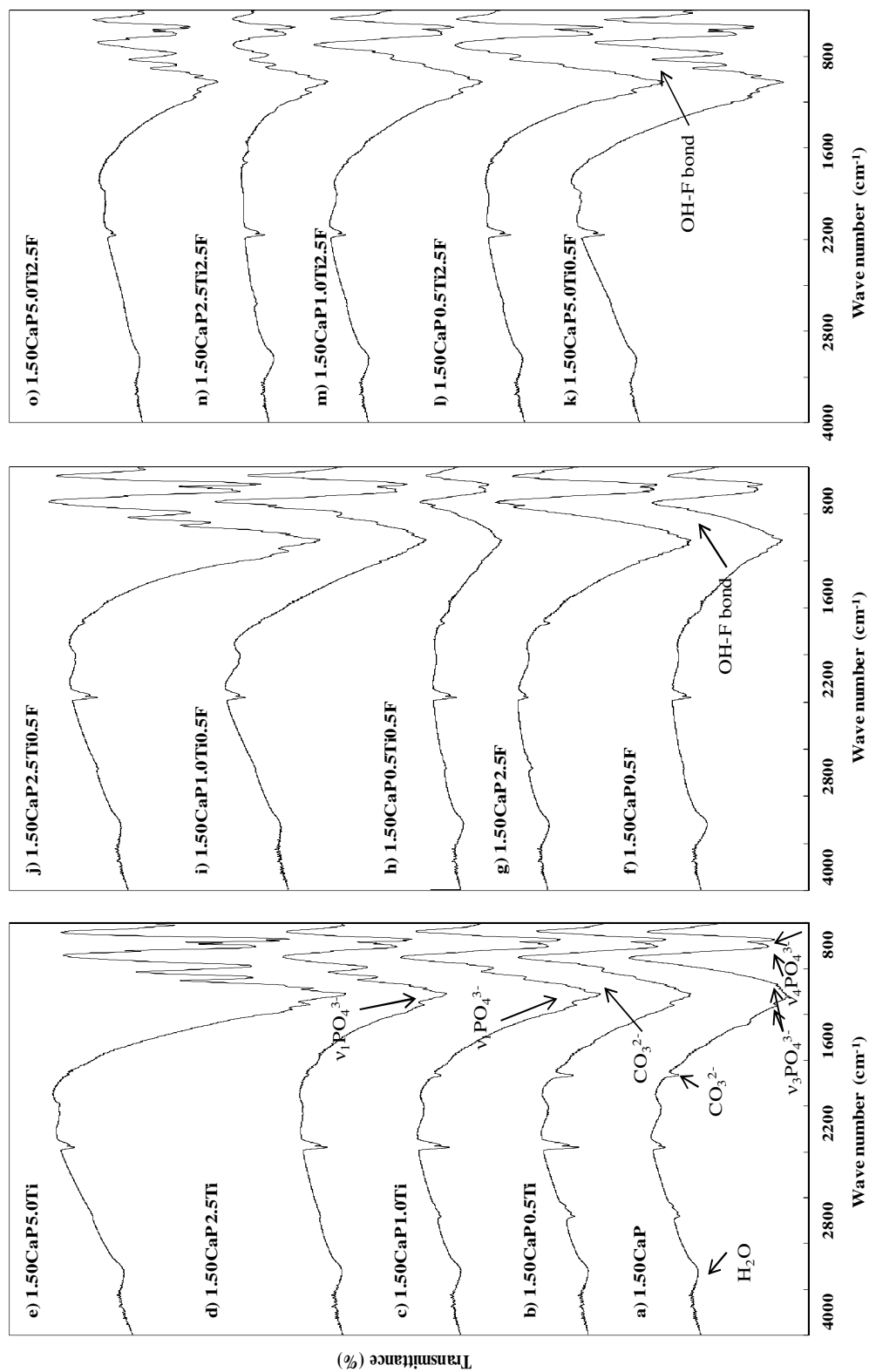


Figure 3.16: FTIR patterns of CaPs with Ca to P ratio of 1.50 sintered at 1300°C.

FTIR spectra of the pure and doped HA samples sintered at 1100°C and 1300°C for 1h are given in Figures 3.17-3.18.

As shown in Figure 3.17, bands given in Table 3.12, for all samples sintered at 1100°C, the FTIR spectra of the characteristic absorption bands of HA are observed. The two bands at 3571 and 634 cm^{-1} belong to the OH⁻ libration vibration mode. OH⁻ absorption bands appear at 2200-1600 cm^{-1} showed high amount of dehydroxylation. The asymmetrical stretching (ν_3), bending (ν_4) and (ν_1) modes of PO_4^{3-} ion are detected at around 1047 and 1091 cm^{-1} , 572 and 601 cm^{-1} , and 966 cm^{-1} , respectively. The bands at 1541-1508 cm^{-1} and 956 cm^{-1} correspond to the ν_3 and ν_2 stretching vibrations of the carbonate groups, respectively. These peaks demonstrate that the HA encloses some CO_3^{2-} groups in PO_4^{3-} sites of apatite lattice [104]. Because of the presence of carbonates in the constituents of hard tissues, existence of low amount of CO_3^{2-} can enhance the bioactivity of HA [104].

Table 3.12: Frequencies and assignments of CaPs.

Assignment	Infrared Frequency (cm^{-1})	Ref. #
OH ⁻ (stretching)	3571.6	[88]
OH ⁻ (libration)	631.7	[88]
Adsorbed water	~3300-3600	[88]
$\nu_4\text{PO}_4^{3-}$ (O-P-O) bend	571,611	[88]
$\nu_3\text{PO}_4^{3-}$ (P-O) stretch	1092 and 1040	[88]
$\nu_2\text{PO}_4^{3-}$ (O-P-O) bend	~462-474	[88]
$\nu_1\text{PO}_4^{3-}$ (P-O) bend	961	[88]
OH- F bond	~ 720 and 3570	[89][90]

OH⁻ stretching and libration band which are characteristics of HA were disappeared by increasing the Ti^{4+} amount. Increasing the Ti^{4+} amount decreased the peak intensities of asymmetrical stretching (ν_3) and bending (ν_4) modes of PO_4^{3-} . Samples doped with F⁻ ions revealed no difference in the intensity of the peaks of OH stretching. When the F⁻ amount in the samples increased, this resulted in increased peak intensities. Addition of Ti^{4+} and F⁻ ion decreased the peak intensities. OH⁻ libration and stretching band decreased in the

samples with increasing the Ti^{4+} and 0.5 mol.% F^- ions. Maximum stretching bands (ν_3) were observed in the samples doped with 0.5 mol.% Ti^{4+} ions. Different trend was observed when F^- ion concentration changed from 0.5 to 2.5 mol.%. Peak intensities increased with increasing Ti^{4+} amount until 1.67CaP1.0Ti2.5F. FTIR bands of HA and HA- TiO_2 are given in Table 3.14. As a consequence, there was a reduction in the OH^- peak heights and a decrease in stretching (ν_3) and bending (ν_4) modes of PO_4^{3-} ion when the Ti^{4+} amount was 5 mol.%

Table 3.13: FTIR band locations in the samples with Ca/P molar ratio 1.67 at 1100°C.

Sample ID	OH^- Str./Lib.	$\nu_1\text{PO}_4^{3-}$	$\nu_2\text{PO}_4^{3-}$	$\nu_3\text{PO}_4^{3-}$	$\nu_4\text{PO}_4^{3-}$
1.67CaP	3571/634	968	474	1091	601
1.67CaP0.5Ti	3573/636	970	474	1095	601
1.67CaP1.0Ti	3571/634	970	474	1093	601
1.67CaP2.5Ti	3568/636	973	476	1097	601
1.67CaP5.0Ti	3649/605	977	470	1118	605
1.67CaP0.5F	3749/634	966	472	1095	599
1.67CaP2.5F	3749/630	968	472	1093	601
1.67CaP0.5Ti0.5F	3747/636	970	474	1091	601
1.67CaP1.0Ti0.5F	3749/636	970	470	1091	603
1.67CaP2.5Ti0.5F	3751/630	970	470	1091	599
1.67CaP5.0Ti0.5F	3749/605	975	-	1126	597
1.67CaP0.5Ti2.5F	3782/638	970	474	1093	601
1.67CaP1.0Ti2.5F	3786/634	972	476	1091	601
1.67CaP2.5Ti2.5F	3776/638	968	474	1091	603
1.67CaP5.0Ti2.5F	3782/607	977	-	1122	607

Table 3.14: FTIR bands of HA and HA-TiO₂ [105].

Assignment	HA (Inf. Freq.(cm ⁻¹))	HA-TiO ₂ (Inf. Freq.(cm ⁻¹))
OH ⁻	1629	1629
O-H	3455	3421
O-H	3633	3566
$\nu_1\text{PO}_4^{3-}$	-	961
$\nu_2\text{CO}_3^{2-}$	872	884
$\nu_3\text{PO}_4^{3-}$	1039	1039
$\nu_4\text{PO}_4^{3-}$	572	605
ν_1 (O-H)	627	636
$\nu_3\text{CO}_3^{2-}$	1418	-
$\nu_3\text{CO}_3^{2-}$	1478	1476

According to the FTIR spectra given in Figure 3.18, bands given in Table 3.14, sintered at 1300°C, main characteristic peaks of HA are observed. OH⁻ libration band at 626 cm⁻¹ almost disappeared in the doped HAs. OH stretching band detected in all samples except for 1.67CaP5.0Ti and the magnitude decreased with the addition of Ti⁴⁺ and F⁻ ions. Stretching (ν_3) and bending (ν_4) modes of PO₄³⁻ ion were observed in the samples. The broad band of low intensity peaks was visible in the range of 3940-3490 and 1955-1300 in the doped samples with Ti⁴⁺ and 0.5, 2.5F%. Thus, it is possible to say that trace amount of water was incorporated into the structure of the samples.

Table 3.15: FTIR band locations in the samples with Ca/P molar ratio 1.67 at 1300°C.

Sample ID	OH ⁻ Str./Lib.	$\nu_1\text{PO}_4^{3-}$	$\nu_2\text{PO}_4^{3-}$	$\nu_3\text{PO}_4^{3-}$	$\nu_4\text{PO}_4^{3-}$
1.67CaP	3571/628	968	462	1089	603
1.67CaP0.5Ti	3571/636	970	453	1089	599
1.67CaP1.0Ti	3570/626	964	457	1097	601
1.67CaP2.5Ti	3570/632	962	-	1091	601
1.67CaP5.0Ti	3568/601	960	437	-	-
1.67CaP0.5F	3570/634	968	459	1091	601
1.67CaP2.5F	3571/634	962	464	1093	603
1.67CaP0.5Ti0.5F	3571/634	968	460	1095	601
1.67CaP1.0Ti0.5F	3570/634	962	468	1091	603
1.67CaP2.5Ti0.5F	3568/632	968	472	1091	603
1.67CaP5.0Ti0.5F	3570/607	977	-	1128	-
1.67CaP0.5Ti2.5F	3571/638	968	476	1095	603
1.67CaP1.0Ti2.5F	3573/636	972	474	1093	601
1.67CaP2.5Ti2.5F	3571/638	970	474	1095	599
1.67CaP5.0Ti2.5F	3649/605	979	-	1124	-

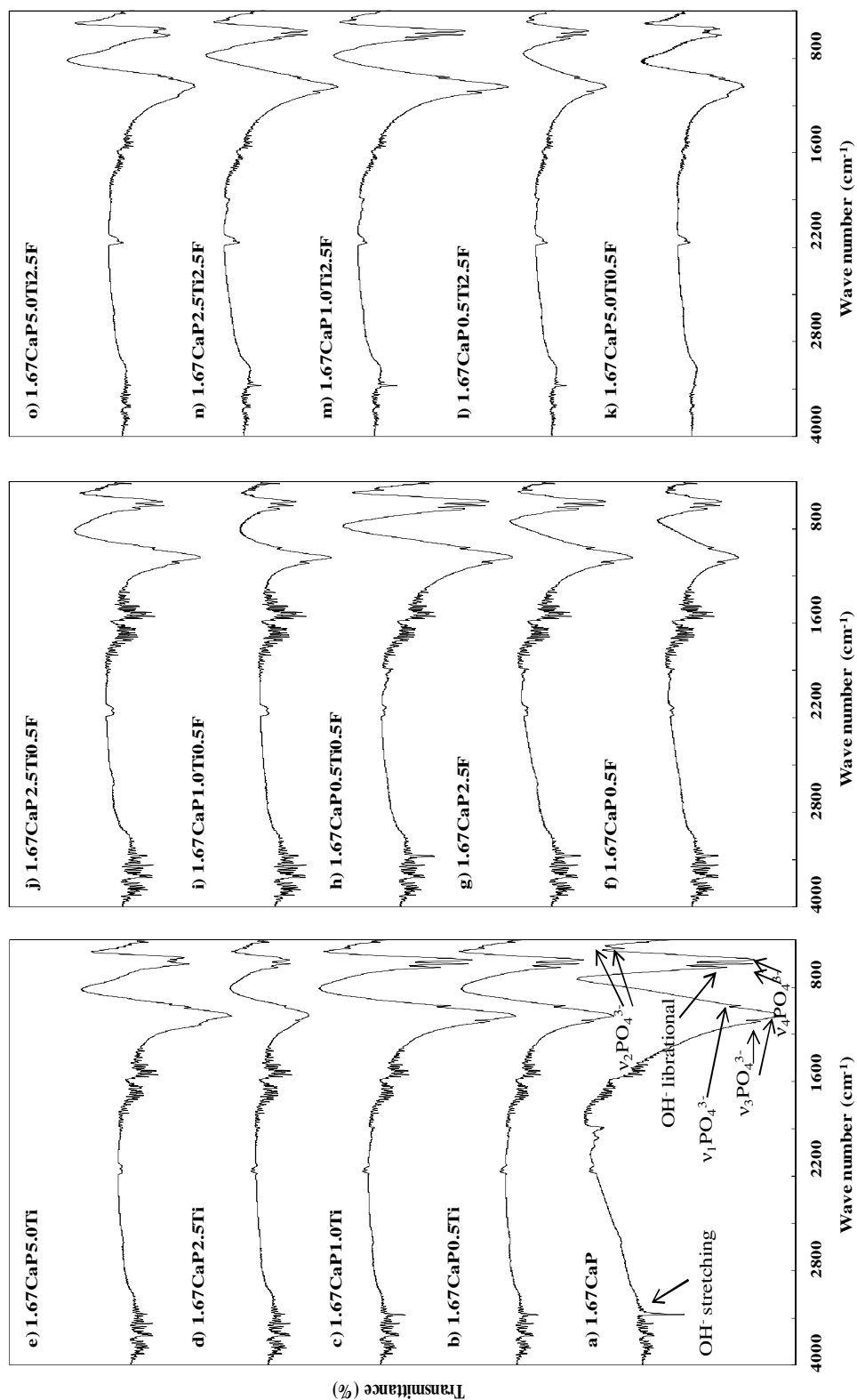


Figure 3.17: FTIR patterns of CaPs with Ca to P ratio of 1.67 sintered at 1100°C.

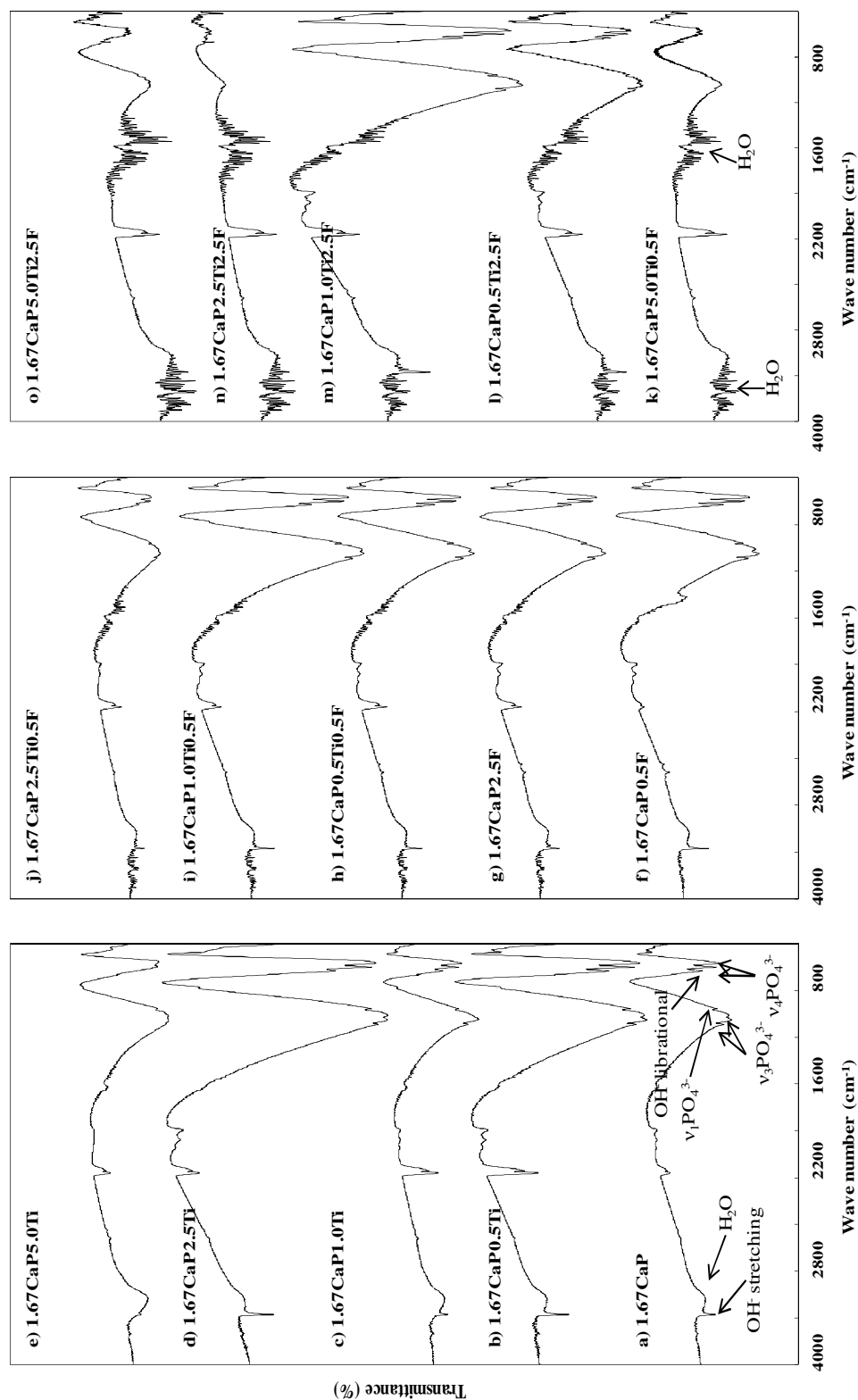


Figure 3.18: FTIR patterns of CaPs with Ca to P ratio of 1.67 sintered at 1300°C.

In Figure 3.19, the bands (Table 3.16) for OH⁻ libration and stretching, which came from HA, are visible at 3570-636 cm⁻¹. The broad band of low intensity peaks was demonstrated in the range of 3900-3400 cm⁻¹ and 1934-1307 cm⁻¹, in all samples because a trace amount of water was incorporated into the structure of the samples. The smallest stretching (ν_3) and bending (ν_4) modes of PO₄³⁻ ion were observed at the sample 2CaP2.5Ti. Those bands at 948, 1031 and 1087 cm⁻¹ are the characteristic bands of phosphate stretching while the bands at 563 and 599 cm⁻¹ are due to phosphate bending vibration. When the F⁻ amount in the samples increased, peak intensities, stretching (ν_3) and bending (ν_4) modes of PO₄³⁻ ion raised. Addition of Ti⁴⁺ and 0.5F⁻ and 2.5 mol.% F⁻ ion dropped the peak intensities. Maximum peak was observed for the sample of 2CaP0.5Ti2.5F. The intensity of peaks around the ν_1 PO₄³⁻ P-O symmetric stretching was visible at 970 cm⁻¹.

Table 3.16: FTIR band locations in the samples with Ca/P molar ratio 2.0 at 1100°C.

Sample ID	OH ⁻ Str./Lib.	ν_1 PO ₄ ³⁻	ν_2 PO ₄ ³⁻	ν_3 PO ₄ ³⁻	ν_4 PO ₄ ³⁻
2.0CaP	3570/630	964	459	1087	599
2.0CaP0.5Ti	3570/632	970	462	1093	601
2.0CaP1.0Ti	3570/628	972	462	1093	599
2.0CaP2.5Ti	3566/632	970	462	1093	599
2.0CaP5.0Ti	3570/630	962	466	1095	599
2.0CaP0.5F	3568/636	973	462	1093	601
2.0CaP2.5F	3568/634	958	462	1093	601
2.0CaP0.5Ti0.5F	3570/634	970	466	1095	599
2.0CaP1.0Ti0.5F	3570/634	970	468	1095	601
2.0CaP2.5Ti0.5F	3568/636	970	462	1093	599
2.0CaP5.0Ti0.5F	3568/630	970	462	1083	599
2.0CaP0.5Ti2.5F	3568/634	970	462	1083	599
2.0CaP1.0Ti2.5F	3570/634	970	462	1078	601
2.0CaP2.5Ti2.5F	3568/634	970	464	1083	599
2.0CaP5.0Ti2.5F	3566/636	970	462	1083	601

FTIR spectra of pure and doped CaPs with a molar ratio of 2 sintered at 1300°C are given in Figure 3.20. Doped and undoped samples bands given in Table 3.17 showed the characteristic spectra of HA. The OH⁻ libration was observed at 667 cm⁻¹. The broad band of low intensity peaks was visible in the range of 3926-3498 cm⁻¹ and 2025-1274 cm⁻¹ relating to vibration of the absorbed water in the sample structure. The asymmetrical

stretching (ν_3), bending (ν_4) and (ν_1) modes of PO_4^{3-} ion were detected at around 1101-1062 cm^{-1} , 603-567 cm^{-1} and 966 cm^{-1} , respectively. The peak intensities went down with raising the sintering temperature.

Table 3.17: FTIR band locations in the samples with Ca/P molar ratio 2.0 at 1300°C.

Sample ID	OH ⁻ Str./Lib.	$\nu_1\text{PO}_4^{3-}$	$\nu_2\text{PO}_4^{3-}$	$\nu_3\text{PO}_4^{3-}$	$\nu_4\text{PO}_4^{3-}$
2.0CaP	3568/640	972	472	1103	603
2.0CaP0.5Ti	3568/638	970	472	1095	603
2.0CaP1.0Ti	3566/638	973	470	1099	601
2.0CaP2.5Ti	3568/640	975	470	1085	603
2.0CaP5.0Ti	3568/638	977	472	1097	603
2.0CaP0.5F	3568/636	970	476	1078	607
2.0CaP2.5F	3575/649	975	474	1093	607
2.0CaP0.5Ti0.5F	3571/649	975	486	1093	611
2.0CaP1.0Ti0.5F	3573/644	975	486	1049	609
2.0CaP2.5Ti0.5F	3573/646	975	486	1097	609
2.0CaP5.0Ti0.5F	3573/646	975	476	1093	609
2.0CaP0.5Ti2.5F	3570/619	975	476	1091	615
2.0CaP1.0Ti2.5F	3579/611	975	476	1091	615
2.0CaP2.5Ti2.5F	3597/611	975	476	1091	615
2.0CaP5.0Ti2.5F	3585/609	975	476	1091	615

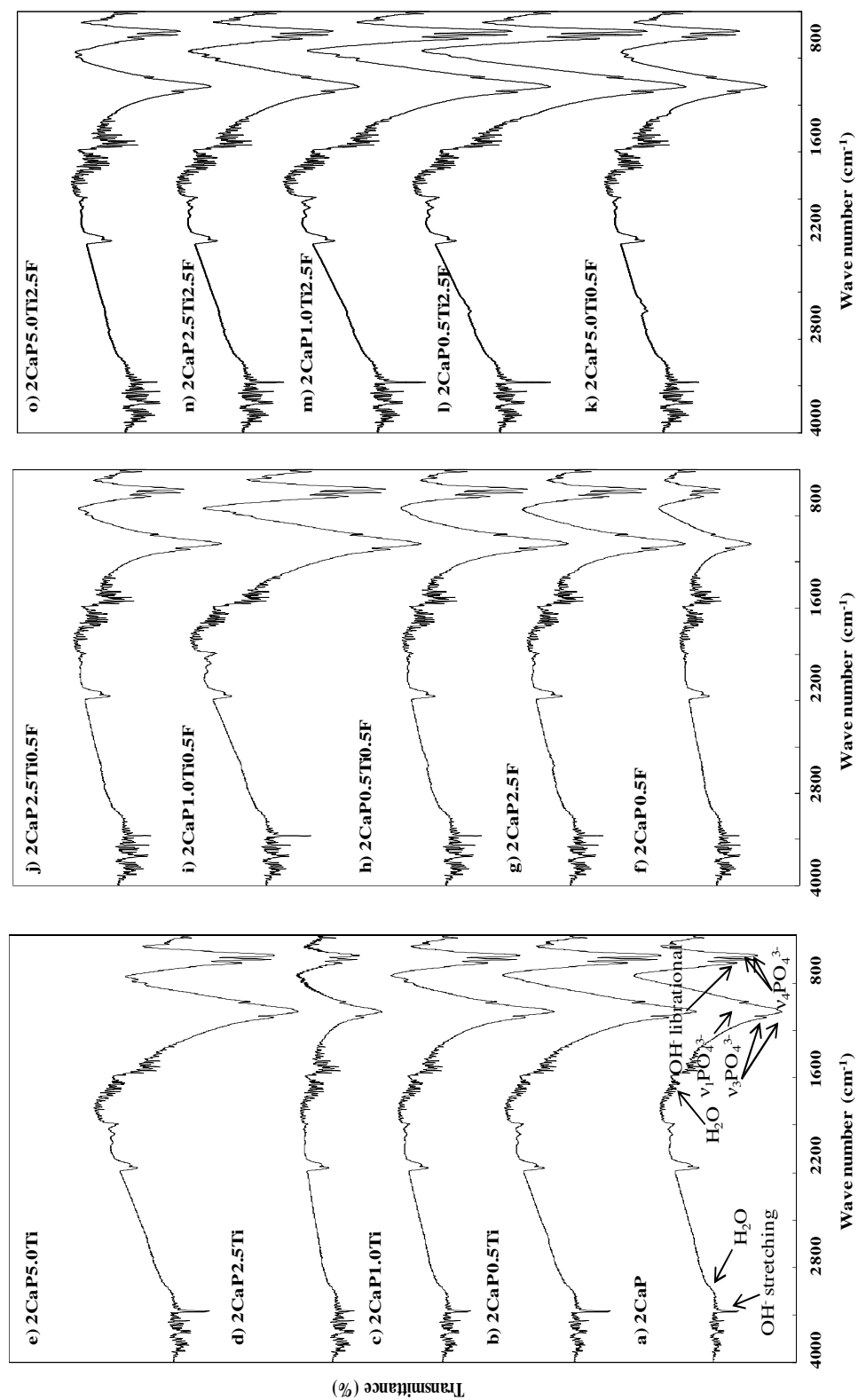


Figure 3.19: FTIR patterns of CaPs with Ca to P ratio of 2.0 sintered at 1100°C.

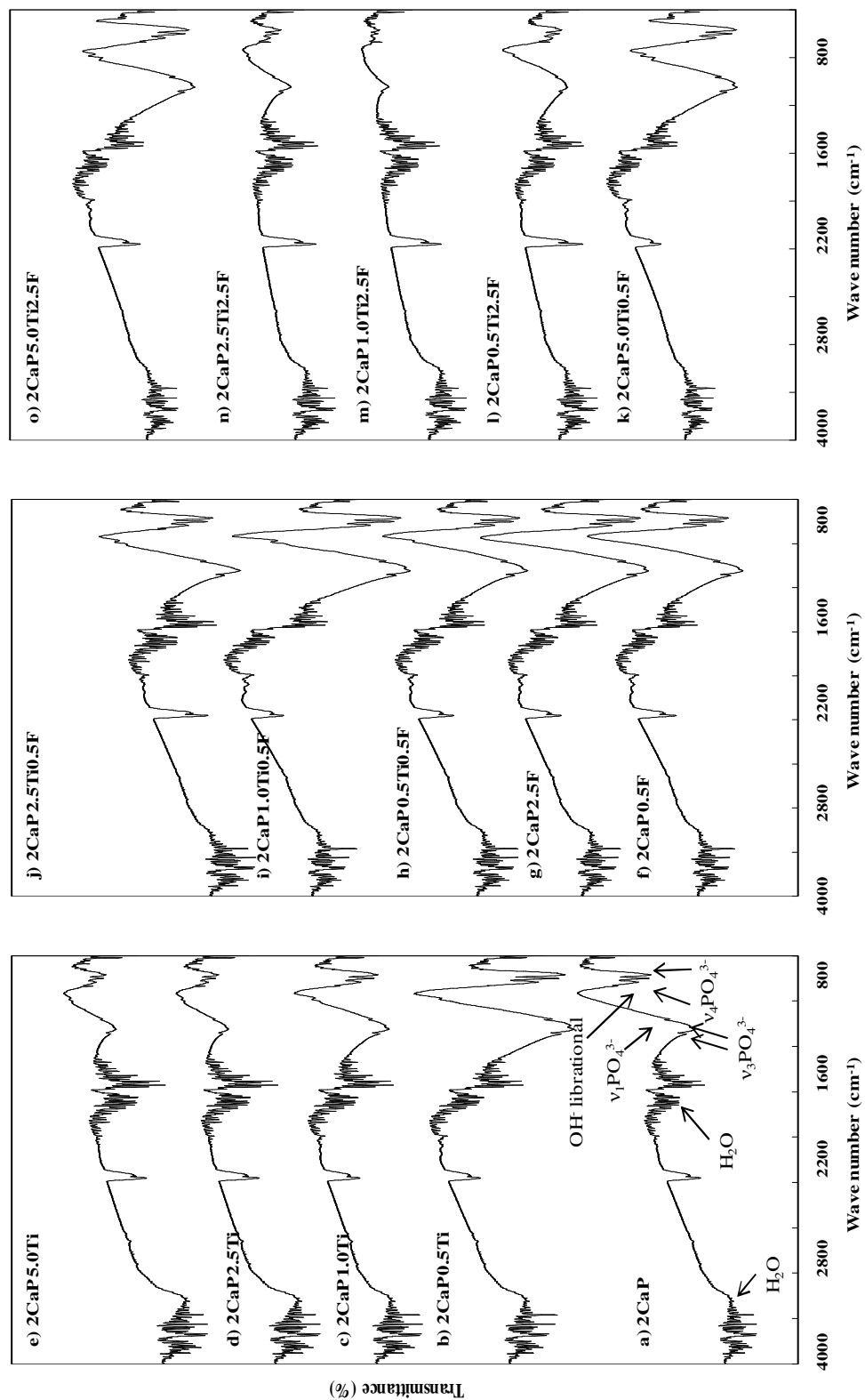


Figure 3.20: FTIR patterns of CaPs with Ca to P ratio of 2.0 sintered at 1300°C.

3.2.3 Scanning Electron Microscopy

SEM images of pure and doped CaPs sintered at 1100°C and 1300°C are given in Figures 3.21-3.30. The morphology of the doped and undoped samples were inspected.

SEM images revealed that temperature and ion amounts of dopants had significant effect on grain sizes of the samples. According to Wang et al. sintering has three stages: First stage, due to low-density of green body and lacking in physical integrity, little amount of adhesion among adjacent particles [113]. Second stage, at the connection points among the particles necks begins to appear. The last stage started when the pores closed [113].

It was seen from SEM images that the CaPs sintered at 1100°C had more uniform microstructures and fine grains. There is a relationship between amount of dopant and sintering temperature with grain sizes of apatites [86]. It was reported that HA had nanosize grains after sintering at 900°C and 1100°C, while there is a severe grain growth after the sintering at 1300°C [86].

After the sintering at 1100°C, pure CaPs with molar a ratio of 1 had the smallest grain size when compared to doped CaPs with the same molar ratio. Doping the samples with Ti^{4+} triggered the enlargement of the grain sizes and large pores at 1100°C. Sample with 1CaP5.0Ti had the porous structure which indicated in the literature that porous CPP ceramics have the better mechanical properties [94]. Increasing the Ti^{4+} amount from 0.5 to 5.0 mol.% resulted in an enlargement of grain sizes of the materials at 1100°C and 1300°C. Because high sintering temperature provides the activation energy for grain growth [34].

With the addition of F^- ions, the grain sizes of the samples were increased (Figure 3.22). According to SEM images, structure of the samples with F^- ions are denser. This result is in relevance with micro-hardness result which shows that doping of the samples with F^- ions causes an increase in hardness at 1300°C whereas a decrease at 1100°C.

Doped CaPs with Ti^{4+} and F^- ions, had grain sizes which represent mixed behavior after the sintering at 1100°C and 1300°C. It was clearly seen that average grain sizes of the doped samples were increased by Ti^{4+} and F^- ion addition.

According to Figure 3.22 it is obvious that grain size of the samples at 1300°C exhibited severe increases when compared to low sintering temperature. It could be concluded that increasing the sintering temperature has an important effect on the change in grain size of the samples. Samples of 1.0CaP, 1CaP5.0Ti, 1.0CaP0.5F and 1.0CaP1.0Ti2.5F melted at 1300°C due to eutectic appearance at melting temperatures of 1280°C, 1287°C and 1300°C [109] .

When sintering temperature was changed from 1100°C to 1300°C, the grain sizes were increased by a factor between 3 and 6 when Ti^{4+} added, factor of 3 when F^- added, of factor 8 when doped with Ti^{4+} and 0.5F and factors of 9, 11 and 29 when Ti^{4+} and 2.5F were added into the samples, respectively. Ramesh et al. revealed that when sintering temperature changed from 1150°C to 1300°C, the average grain size increased by a factor of more than 7 [54]. High sintering temperatures trigger the grain growth. Because increasing the sintering temperature raised the grain sizes through high temperature grain growth [108]. In the present study, it was seen that increasing sintering temperature caused an increase in the grain size of CaP with molar ratio of 1. Samples with 1CaP0.5Ti0.5F, 1CaP2.5Ti0.5F and 1CaP5.0Ti2.5F had porous structure at 1100°C. With increasing the sintering temperature to 1300°C, necks were observed in the samples (second stage of sintering) and grain shapes increased which led to isolated pores. According to the SEM images and average grain sizes, it can be concluded that increasing the sintering temperature had a significant effect on the grain sizes of the materials.

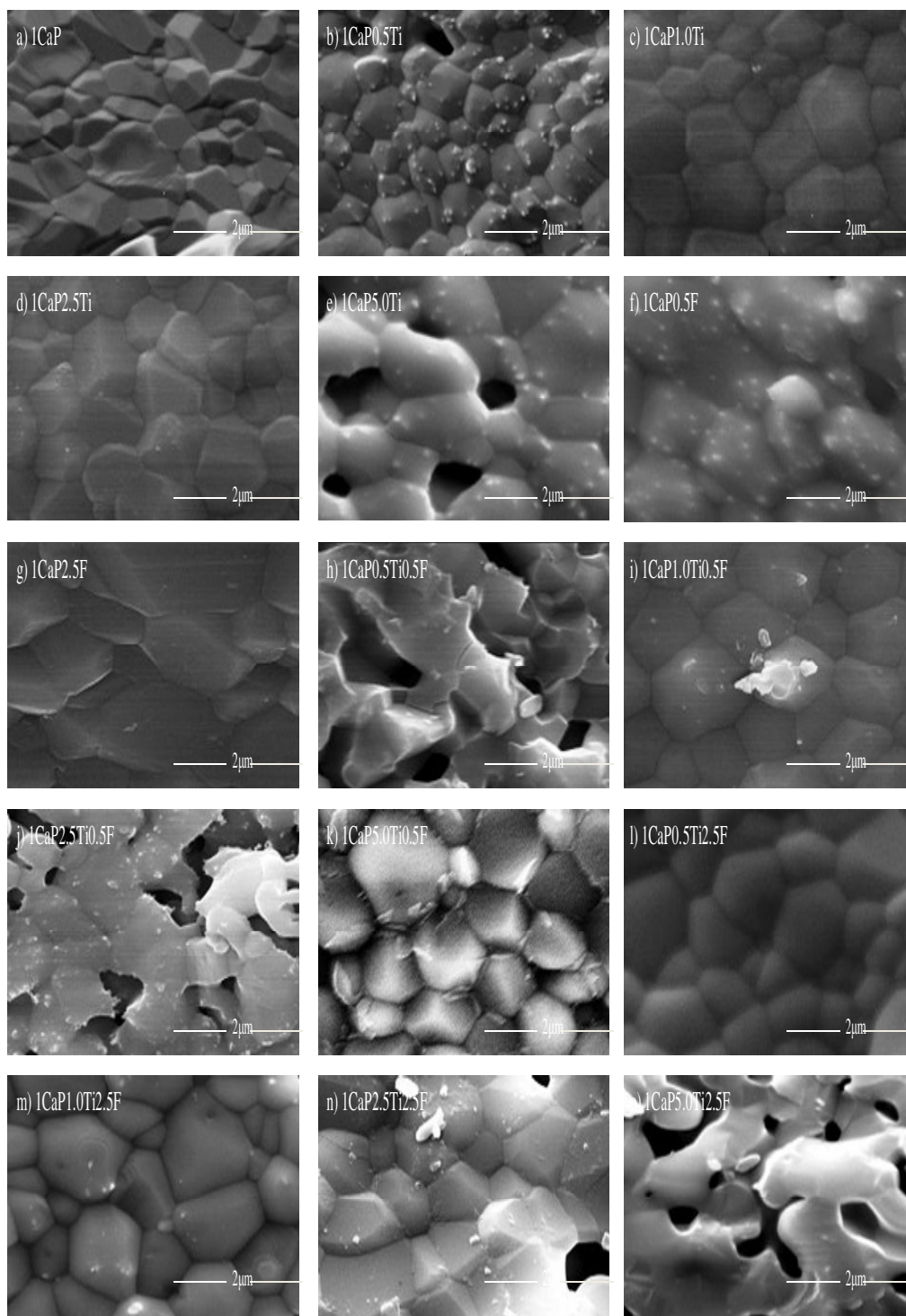


Figure 3.21: SEM images of CaPs with Ca to P ratio of 1.0 sintered at 1100°C.

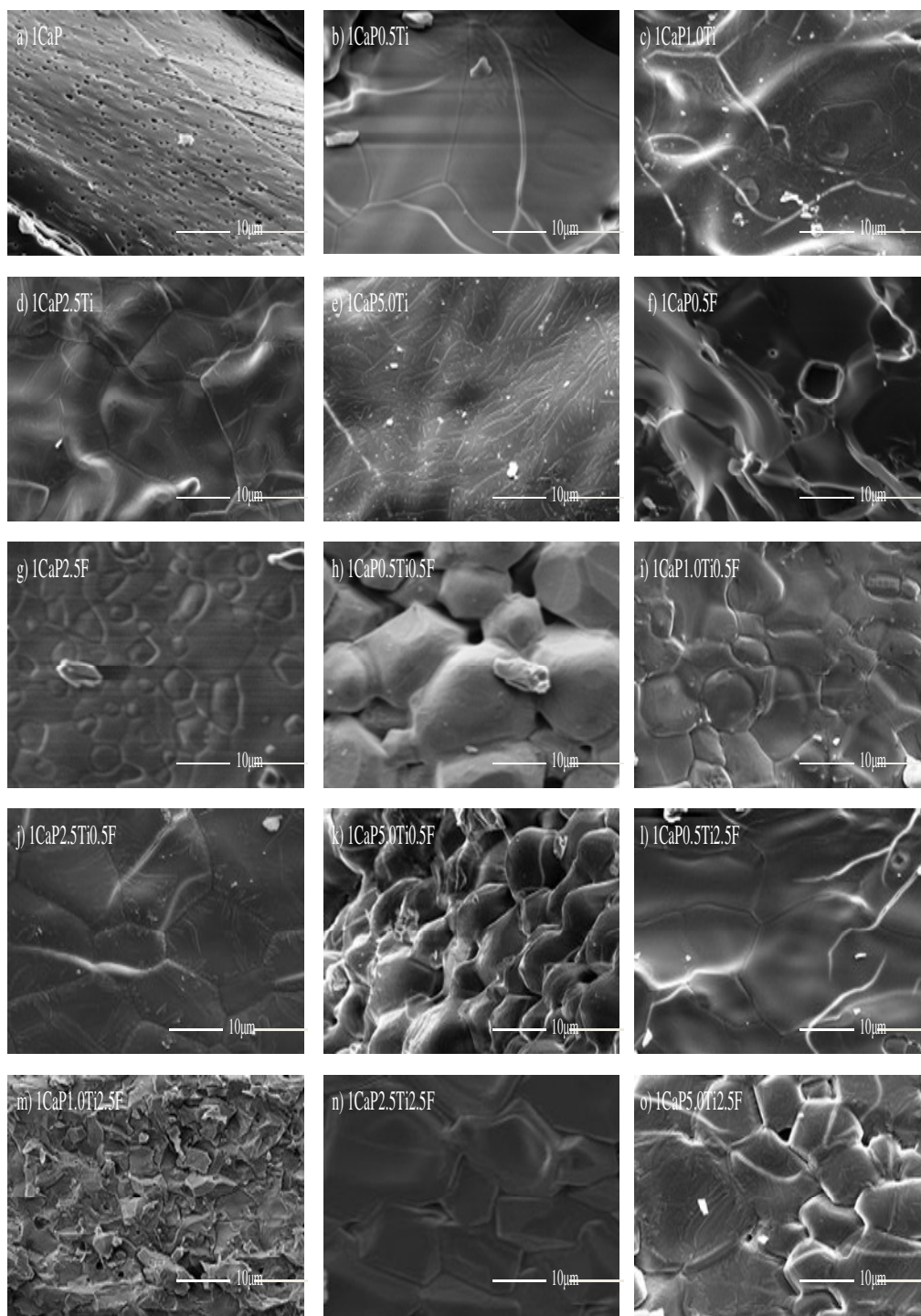


Figure 3.22: SEM images of CaPs with Ca to P ratio of 1.0 sintered at 1300°C.

When molar ratio increased to 1.25 (Figure 3.23), addition of Ti^{4+} ions amount from 0.5 to 5.0 mol.% at 1100°C resulted in a decrease in grain size when compared to pure 1.25CaP. With the addition of F^- ions, the grain size of the samples were decreased. It can be easily detected that fluoride had a significant effect on crystal size and stability of apatite structures since F^- ions decrease the crystal size and increase the stability [87]. It was presented that F^- ions substituted OH^- groups decreased the degree of disordered in HA structure and theoretically 50% of F^- ion concentration is enough to stabilize the HA structure by changing the arrangement of F^- ions with OH^- groups [87]. This concentration could be increased in experiments due to the random substitution of OH^- ions with F^- ions [87]. Grain sizes of samples with 0.5 mol.% F^- and Ti^{4+} amount from 0.5 to 5.0 mol.%, had mixed behaviours after the sintering at 1100°C. Increasing the F^- ions to 2.5 mol.% resulted in an increase in grain sizes when amount of Ti^{4+} was increased. It was found that average grain sizes of the samples with molar ratio of 1.25 decreased when doped with Ti^{4+} and F^- ions except the samples 1.25CaP0.5F and 1.25CaP5.0Ti0.5F.

According to Figure 3.24, high grain sizes were obtained for most of the samples after increasing the sintering temperature from 1100°C to 1300°C. By increasing the sintering temperature from 1100°C to 1300°C, samples with F^- ions resulted in an increase in their grain sizes. Increasing the Ti^{4+} amount from 0.5 to 5 mol.% resulted in an increase in the grain sizes. In 0.5 F^- co-doped samples, raising the amount of Ti^{4+} ions from 0.5 to 5 mol.%, samples had mixed behaviors after sintering at 1300°C. In 2.5 F^- co-doped samples, increasing the amount of Ti^{4+} ions from 0.5 to 5 mol.%, resulted in an increase in their grain sizes after the sintering at 1300°C. Acquired average grain sizes were ranged from 4 to 22 μm .

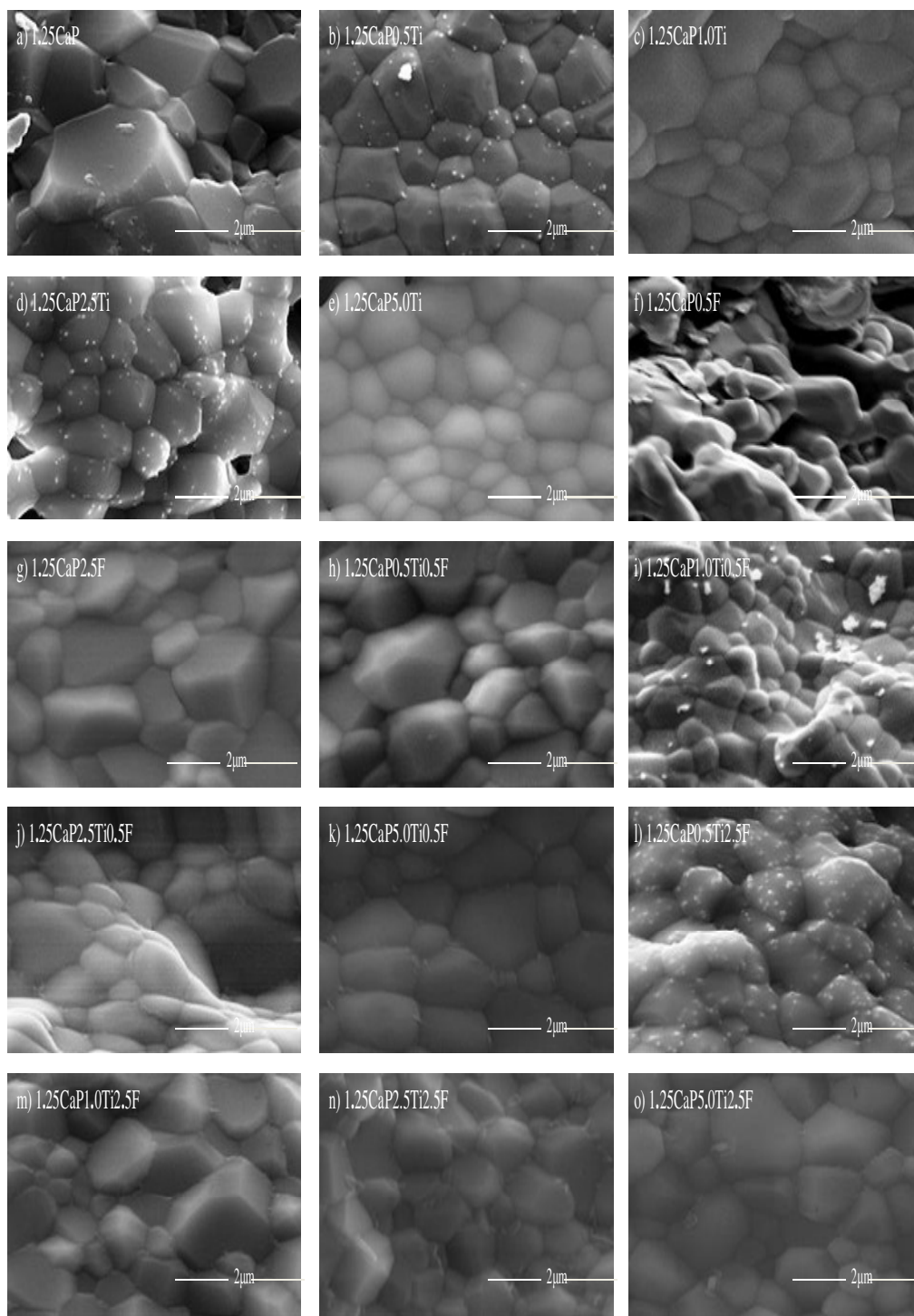


Figure 3.23: SEM images of CaPs with Ca to P ratio of 1.25 sintered at 1100°C.

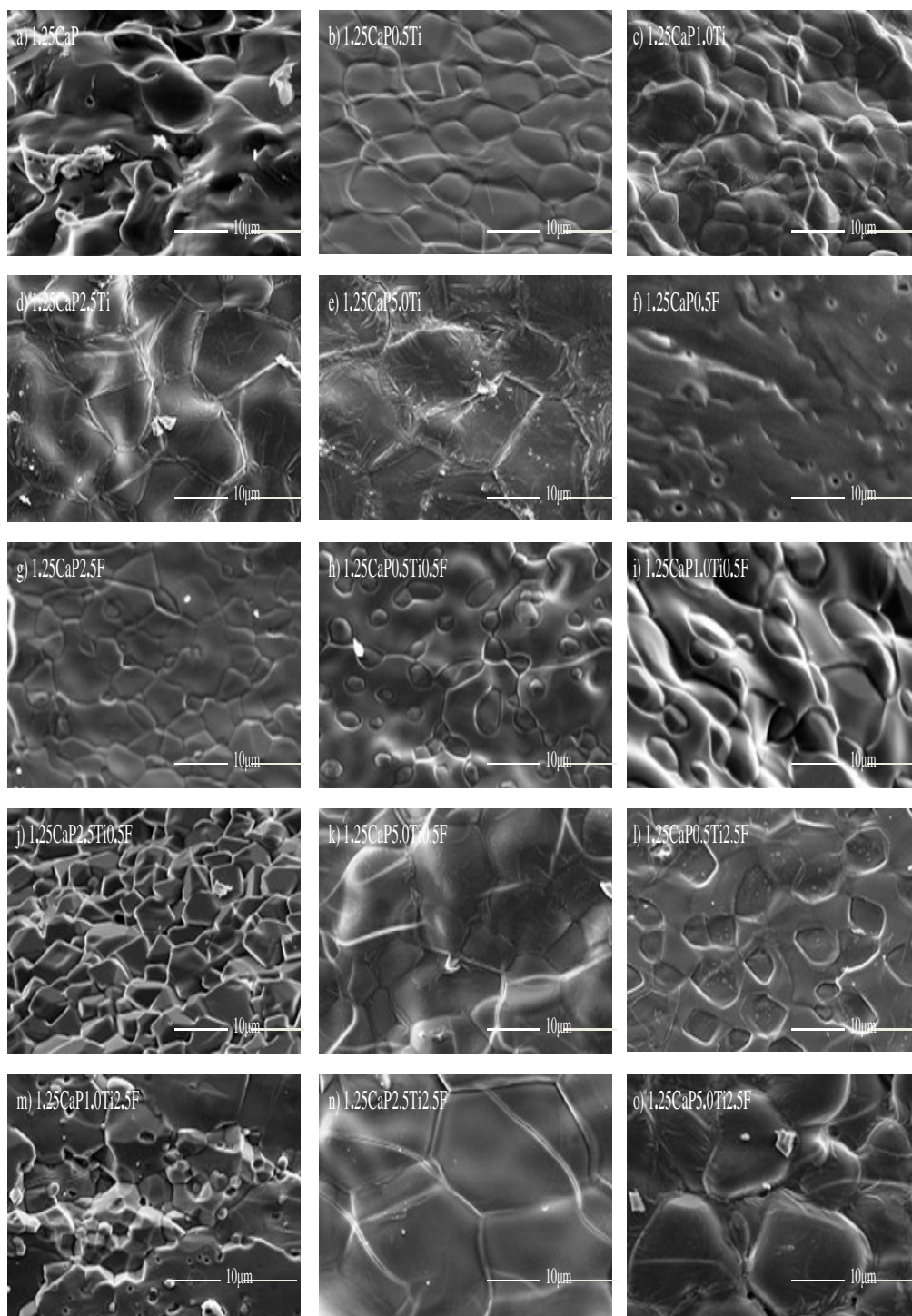


Figure 3.24: SEM images of CaPs with Ca to P ratio of 1.25 sintered at 1300°C.

When Ca/P ratio was 1.50 after the sintering at 1100°C, it was seen that increasing the Ti^{4+} amount from 0.5 to 5 mol.%, grain sizes were increased when compared to pure 1.50CaP as seen in Figure 3.25. It was determined that samples doped with Ti^{4+} had higher average grain size than pure 1.50CaP except for 1.50CaP0.5Ti. Because of this, it can alter the mechanical properties of the samples. According to SEM images, grain sizes of the samples increased when compared to pure β -TCP. Due to increasing in Ti^{4+} ion content grain sizes of the samples increased. It was observed that average grain sizes of co-doped samples with F^- ions increased by increasing the F^- ion amount. However, co-doped samples with F^- ions had no pores on their surfaces. Co-doped samples with F^- ions demonstrated that F^- ions decreased the grain size. In 0.5%F and 2.5%F co-doped samples, increasing the amount of Ti^{4+} ions from 0.5 to 5 mol.%, resulted in mixed behaviour after the sintering at 1100°C.

SEM images of the samples with Ca to P ratio of 1.50 sintered at at 1300°C are given in Figure 3.26. According to these results, co-doped samples with Ti^{4+} ions had smaller average grain size than pure 1.50CaP at 1300°C. Increasing the Ti^{4+} amount resulted in an increase in the grain size of the materials. When F^- ion concentration was increased, grain size of the samples increased. Co-doped samples with Ti^{4+} and 0.5 and 5 mol. % F^- ions had mixed behaviour. Grain sizes of the samples with 1.50CaP5.0Ti0.5F and 1.50CaP5.0Ti2.5F were reduced significantly with the addition of 5.0 mol.% Ti^{4+} ions.

According to Figure 3.27, for the samples with a molar ratio of 1.67 and sintered at 1100°C, large grain sizes were obtained for most of the compositions after increasing the Ti^{4+} amount from 0.5 to 5 mol.% than pure HA. Average grain sizes of the 1.67CaP0.5Ti-1.67CaP5.0Ti at 1100°C were higher but 1.67CaP0.5Ti-1.67CaP5.0Ti at 1300°C were smaller than that of pure 1.67CaP. SEM images of the average grain size of the Ti^{4+} added samples showed that grain size 254 nm increased to 916 nm at 1100°C and 9053 nm decreased to 2181 at 1300°C, thus demonstrating that incorporation of Ti^{4+} into the HA structure allows the grain growth during sintering at 1100°C but prevent the grain growth at 1300°C. All samples with 2.5 mol. Ti^{4+} had significant decrease in their grain sizes.

Increase in F^- ion amount in the samples from 0.5 to 2.5 mol.% led to decrease in their grain sizes at 1100°C. In another study, when the F ion amount increased to 5 mol.%, grain sizes of the co-doped samples increased and addition of F^- ion resulted in less dense materials because the bond that forms between F^- and OH^- groups reduces the rate of

diffusion regulating the densification [83]. Therefore, increasing the F^- ion substitution decreased the grain sizes [83]. In 0.5F and 2.5F co-doped samples, increasing the Ti^{4+} ions amount from 0.5 to 5% resulted in mixed behaviors after sintering at 1100°C.

Grain sizes of the samples doped with Ti^{4+} ions from 0.5 to 5 mol.% at 1300°C were smaller than that of pure 1.67CaP as seen in Figure 3.28. In 0.5F and 2.5F co-doped samples, increasing the amount of Ti^{4+} ions from 0.5 to 5 mol.% samples had inconsistent behaviors after the sintering at 1300°C. Samples with 1.67CaP1.0Ti and 1.67CaP0.5Ti0.5F melted at 1300°C due to appearance of eutectic at melting temperatures of 1280°C, 1287°C and 1300°C [109].

At 1100°C, samples with 1.67CaP1.0Ti, 1.67CaP2.5Ti, 1.67CaP5.0Ti and 1.67CaP5.0Ti0.5F characterized with porous structure. Klawitter et al. stated that presence of macropores precipitated resorption and bone ingrowth [116]. Due to Ti^{4+} and F^- ions additions, increasing the sintering temperature to 1300°C resulted in dense contacts between the grains and significant grain boundary zones.

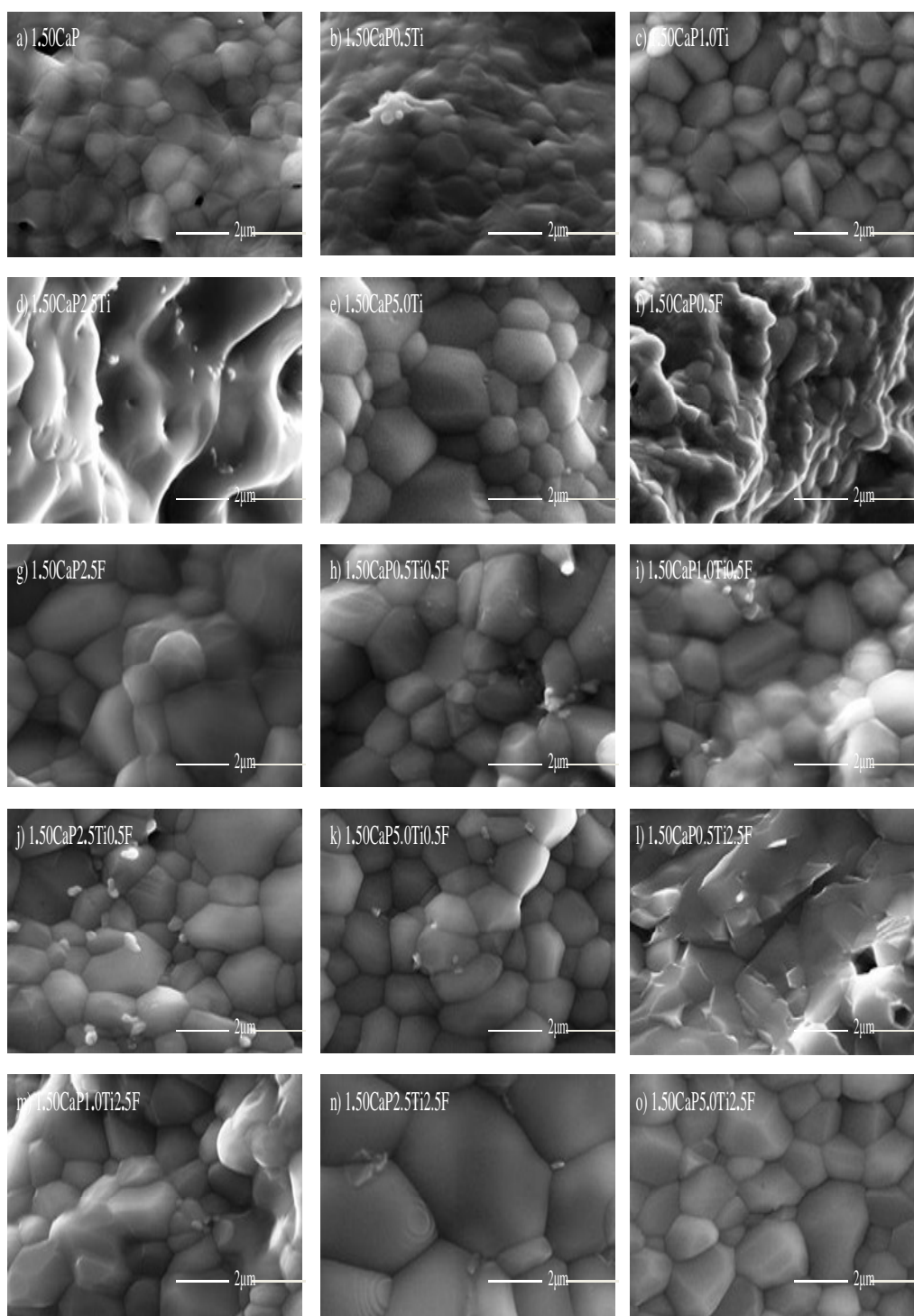


Figure 3.25: SEM images of CaPs with Ca to P ratio 1.50 sintered at 1100°C.

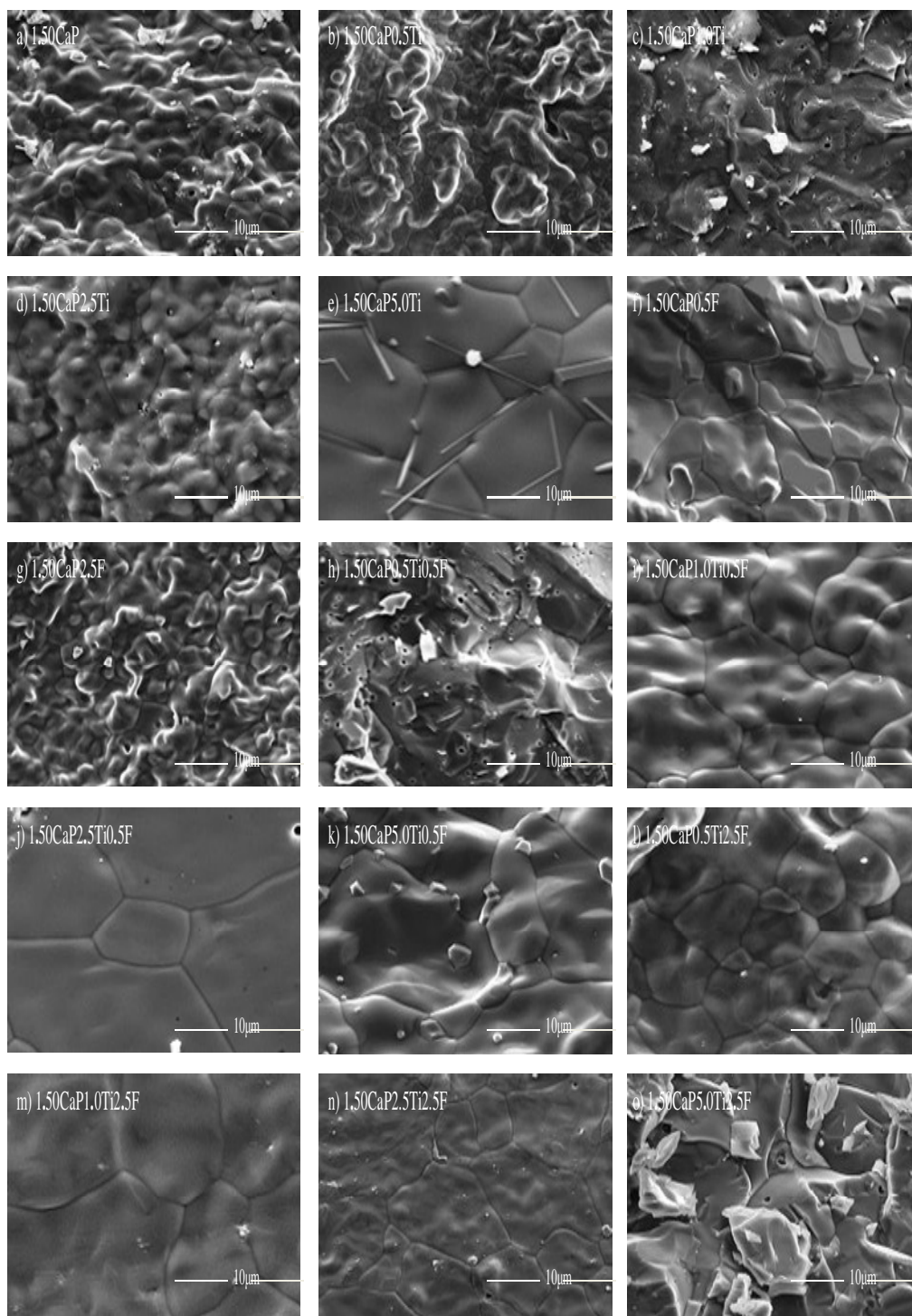


Figure 3.26: SEM images of CaPs with Ca to P ratio of 1.50 sintered at 1300°C.

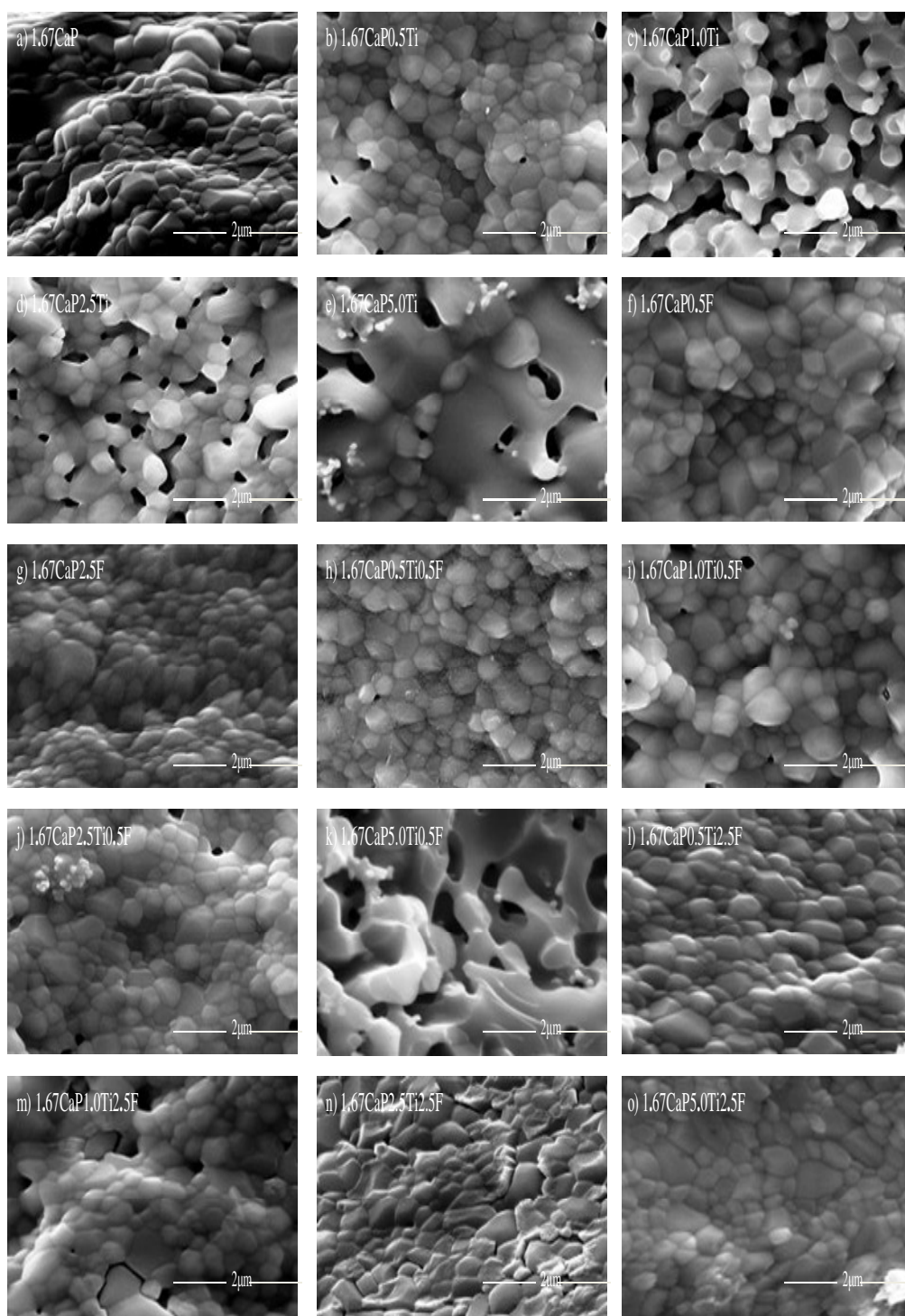


Figure 3.27: SEM images of CaPs with Ca to P ratio of 1.67 sintered at 1100°C.

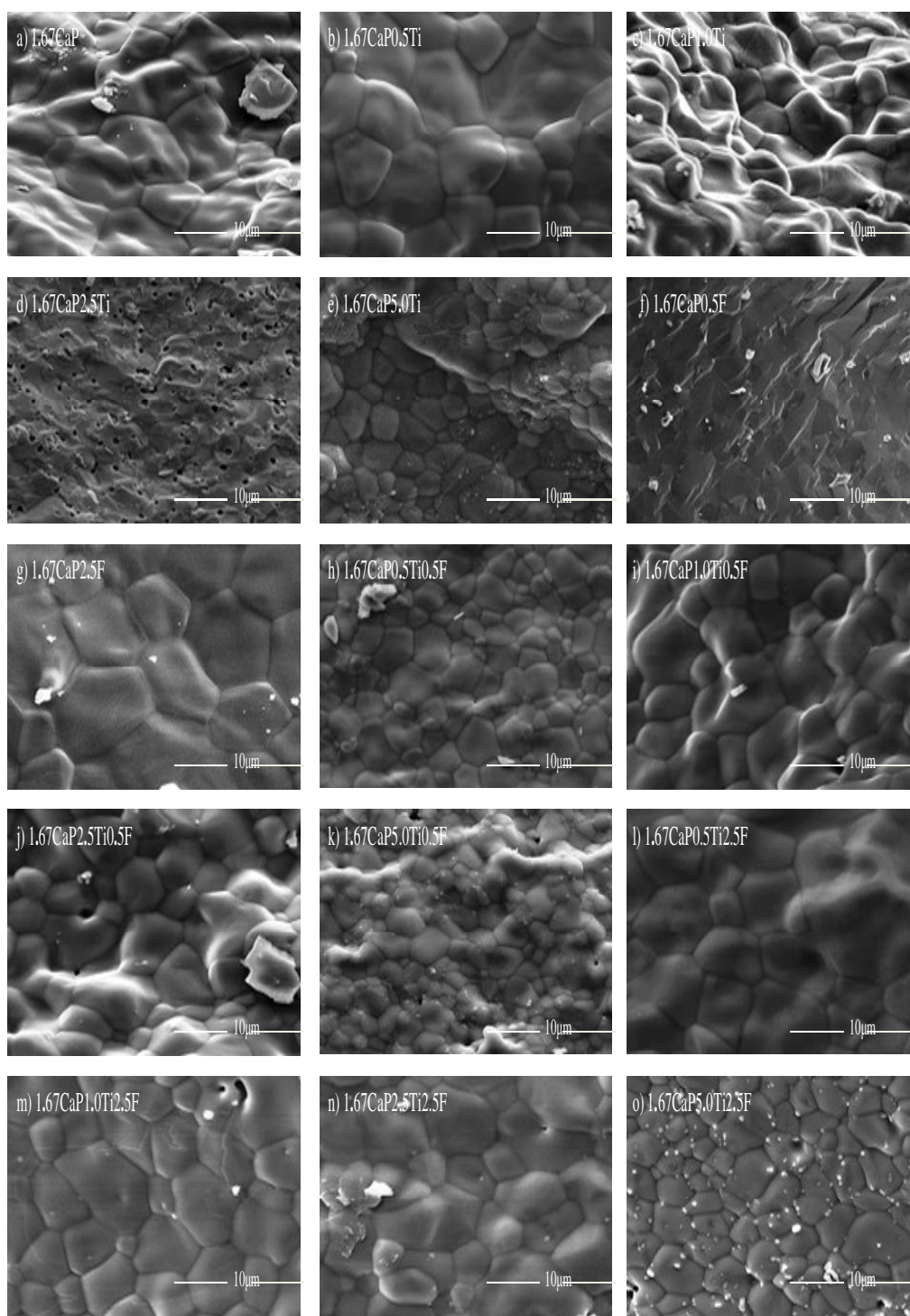


Figure 3.28: SEM images of CaPs with Ca to P ratio of 1.67 sintered at 1300°C.

Grain sizes of the samples with Ca to P ratio of 2.0 are presented in Table 3.18. When sintering temperature was increased from 1100°C to 1300°C, grain sizes of all ceramics were increased. As Raynaud stated, due to high calcination, samples with Ca/P ratio of 2.0, had more rounded particles and necks observed at 1100°C [111]. According to Bohner, change in grain size should affect resorption rate because resorption of ceramics occurred at the grain boundaries [114]. Enlightened regions in the Figure 3.29 suggested that Ti^{4+} and F^- ions were homogeneously distributed in the co-doped samples. However, increasing the sintering temperature to 1300°C, they were apparently penetrated in more domains than at 1100°C.

Increasing the amount of F^- ions in the samples resulted in an increase in their grain sizes at both sintering temperatures. At sintering temperatures of 1100 and 1300°C, samples co-doped with Ti^{4+} and 0.5 and 5 mol.% F^- ions had showed varieties in their behaviours.

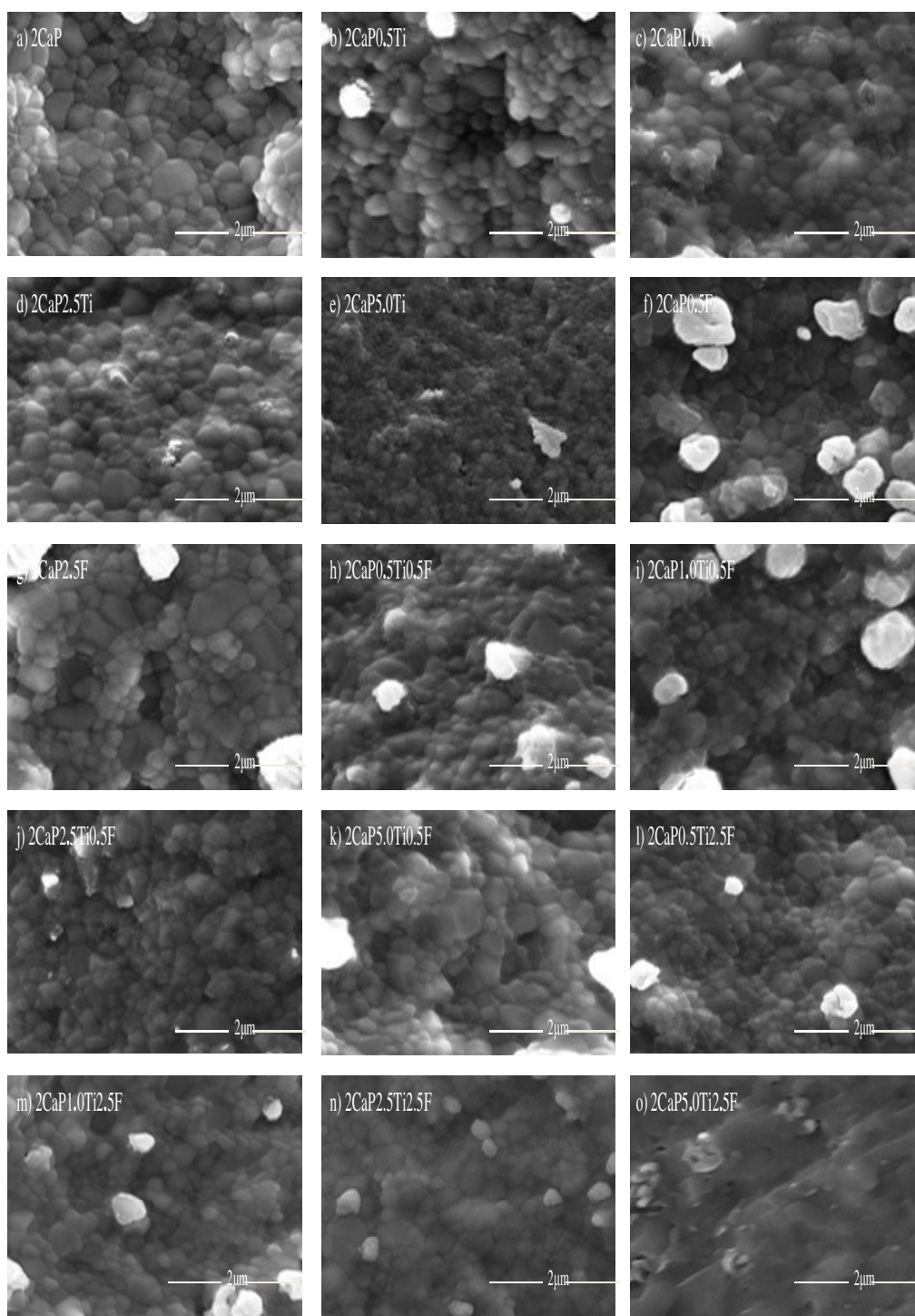


Figure 3.29: SEM images of CaPs with Ca to P ratio of 2.0 sintered at 1100°C.

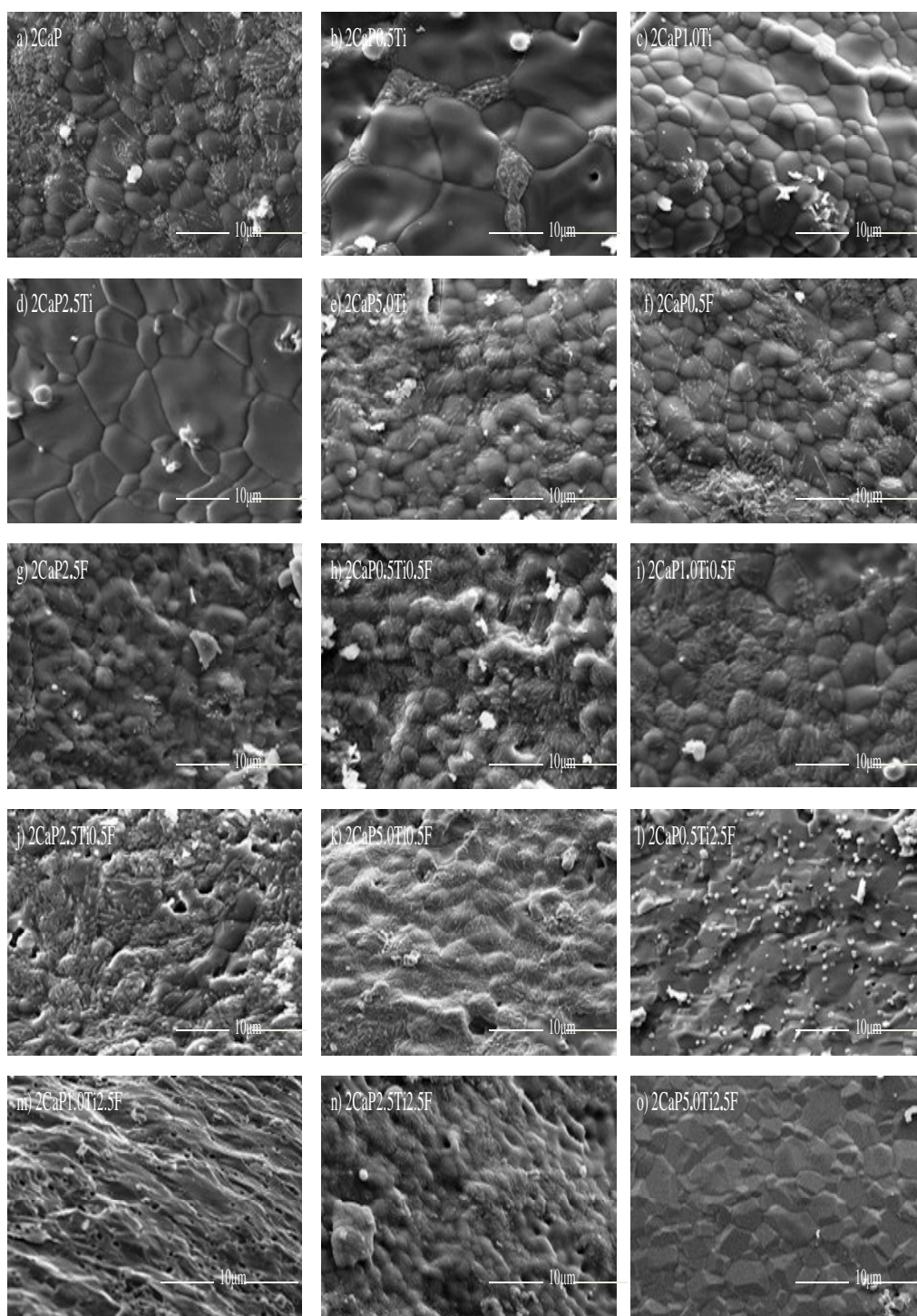


Figure 3.30: SEM images of CaPs with Ca to P ratio of 2.0 sintered at 1300°C.

Table 3.18: Average grain size of CaPs with molar ratios of 1,1.25, 1.50, 1.67, 2 sintered at 1100°C and 1300 °C.

Sample ID	n (Ca/P)= 1		n (Ca/P)= 1.25		n (Ca/P)= 1.50		n (Ca/P)= 1.67		n (Ca/P)= 2	
	Ave. Grain Size (nm)	Ave. Grain Size (nm)	Ave. Grain Size (nm)	Ave. Grain Size (nm)	Ave. Grain Size (nm)	Ave. Grain Size (nm)	Ave. Grain Size (nm)	Ave. Grain Size (nm)	Ave. Grain Size (nm)	Ave. Grain Size (nm)
	1100°C	1300°C	1100°C	1300°C	1100°C	1300°C	1100°C	1300°C	1100°C	1300°C
nCaP	489	Melted	897	Melted	406	15795	254	9053	265	1959
nCaP0.5Ti	618	36111	773	4764	308	4834	317	5014	285	6354
nCaP1.0Ti	907	19981	817	7623	718	Melted	507	8109	251	1095
nCaP2.5Ti	986	25926	612	11678	Melted	6245	441	Melted	262	2757
nCaP5.0Ti	913	Melted	572	13587	611	13027	916	2181	Melted	1280
nCaP0.5F	850	Melted	898	Melted	Melted	6566	412	Melted	273	1166
nCaP2.5F	1243	3871	731	5034	814	16468	229	5912	438	1173
nCaP0.5Ti0.5F	Melted	18871	677	9444	593	Melted	260	3396	164	2436
nCaP1.0Ti0.5F	1232	8598	854	3990	622	7800	368	3563	221	2273
nCaP2.5Ti0.5F	993	8662	608	4406	464	16296	266	2507	199	2633
nCaP5.0Ti0.5F	1098	8069	959	11389	513	15545	Melted	Melted	241	2940
nCaP0.5Ti2.5F	965	29167	562	7545	523	4679	303	3587	217	Melted
nCaP1.0Ti2.5F	1253	Melted	738	7744	494	11111	387	3162	234	Melted
nCaP2.5Ti2.5F	1129	11170	792	21256	1882	22457	240	3412	215	2032
nCaP5.0Ti2.5F	Melted	9336	854	13167	594	8160	342	2508	Melted	2350

3.3 Mechanical Investigation of the Samples

3.3.1 Micro-hardness Measurements

Micro-hardness test was used to investigate the effect of the sintering temperature on the mechanical properties of doped and undoped CaP samples. Micro-hardness test was applied to the samples sintered at 1100°C and 1300°C. Average μ -hardness values of samples are given in Table 3.19.

With regard to Table 3.19, when Ca to P molar ratio is 1.0, the lowest micro-hardness value of 1.21 GPa was measured for 1CaP5.0Ti sintered at 1100°C whereas the maximum micro-hardness value of 6.07 GPa was acquired for 1CaP2.5Ti2.5F sintered at 1300°C. According to the results after the sintering at 1100°C, increasing the amount of the Ti^{4+} ion led to a slight decrease in the micro-hardness values. Pure 1CaP had the highest magnitude when compared to Ti^{4+} ion added samples. Increasing the sintering temperature to 1300°C affected the magnitude of the micro-hardness in the increasing direction until the sample of 1CaP2.5Ti. The tendency differs by raising Ti^{4+} ion in the increasing direction. In other samples, micro-hardness magnitude of pure 1CaP increased by raising the sintering temperature. Micro-hardness values of the samples increased with increasing the sintering temperature and Ti^{4+} ion amount of the samples. This result indicated that increasing the sintering temperature positively affected the mechanical properties of the samples with molar ratio of 1.0. The hardness of CaP increased with increasing the sintering temperature however a decrease was observed with increasing degree of Ti^{4+} ion amount for the sample of 1CaP5.0Ti. It can be concluded that the hardness of the samples with higher amount of Ti^{4+} ion indicate an increase with increasing of sintering temperature.

When the amount of the F^- ion increased, a decrease in the micro-hardness values was observed at 1100°C. This outcome showed consistency with the study of Gross et al., which revealed that F^- ion incorporation improved the mechanical properties only up to a certain limit [70]. Afterwards when the limit exceeded, a decrease in the mechanical properties was detected as in this study. Co-doped sample with 2.5F had the lowest μ -hardness value. F^- ion addition increased the μ -hardness of the samples. Therefore, due to a decrease in the porosity of the samples, more compact and hard structures were obtained [121]. Increased

compatibility between F^- and H^+ atoms resulted in compact structure. When sintering temperature was increased to 1300°C and the amount of F^- ions raised from 0.5 to 2.5 mol.% F^- increase in the microhardness values was observed. It is possible to say that increasing the sintering temperature positively affected the mechanical properties of the samples. This result is in relevance with SEM result which shows that doping of the samples with F^- ions cause an increase in grain sizes at 1300°C but decrease at 1100°C. 1CaP0.5Ti0.5F had the highest micro-hardness, while 1CaP5.0Ti0.5F demonstrated the smallest micro-hardness at 1100°C when doped with Ti^{4+} and F^- ions. Nevertheless, there was a sharp decrease in μ -hardness. With increasing the Ti^{4+} amount, mechanical properties of the calcium phosphates deteriorated at 1100°C. According to the results, with increasing sintering temperature to 1300°C, μ -hardness of the samples containing Ti^{4+} and 0.5F decreased except the 1CaP2.5Ti0.5F.

Changing the molar ratio to 1.25 at 1100°C resulted in a decrease in the μ -hardness value except 1.25CaP2.5Ti. Increasing the Ti^{4+} ion amount decreased the μ -hardness value. Pure 1.25CaP had the one of the maximum microhardness value when compared to other samples. With increasing F^- ion amount, μ -hardness value decreased from 4.74 to 3.85 GPa. Changing the sintering temperature to 1300°C gave the same tendency as at 1100°C except for the F^- added samples. Kim et al. demonstrated that insertion of F^- ions increased μ -hardness values significantly. This reason explained the decrease in porosity of fluoridated samples [121]. Micro-hardness values of the samples with 2.5 mol.% F^- had higher values than the samples with 0.5 mol.% F^- at both sintering temperature. Micro-hardness value of 1.25CaP5.0Ti was higher than that of pure 1.25CaP and micro-hardness of the pure 1.25CaP decreased with increasing the sintering temperature.

When increasing the Ti^{4+} ion amount in the samples with molar ratio of 1.50 at 1100°C, initially the μ -hardness value increased and as the Ti^{4+} ion amount increased then decreased. Micro-hardness of the samples with Ti^{4+} ions increased when compared to pure 1.50CaP. According to the results, F^- addition increased the μ -hardness values from 4.44 to 4.80 GPa. Increasing the sintering temperature to 1300°C revealed a decrease in the value until 1.50CaP5.0Ti when Ti^{4+} ion added. Micro-hardness for pure 1.50CaP was higher than Ti^{4+} and F^- ion added samples. The hardness of CaP was decreased with increasing the sintering temperature. However, an increase was observed with increasing the degree of Ti^{4+} ion amount for the sample 1.50CaP5.0Ti. At 1100°C, all samples that contain Ti^{4+} and

F⁻ ions had higher μ -hardness values than at 1300°C. Consequently, the hardness of the samples with higher amount of Ti⁴⁺ ion indicate a decrease with an increase in sintering temperature.

Altering molar ratio to 1.67 revealed decrease in the μ -hardness and then slightly increase at 1100°C and 1300°C. At the same sintering temperature the maximum value was obtained at pure 1.67CaP. Consistent with this result, study of Chenglin et al. showed that that pure HA ceramics had a micro-hardness value of 4.72 GPa [84]. The hardness of 1.67CaP increased with increasing the sintering temperature. Increasing the Ti⁴⁺ ion addition worsened the μ -hardness of the co-doped samples at both sintering temperatures. The hardness of the samples with higher amount of Ti⁴⁺ ion indicated an increase with increasing the sintering temperature. However, F⁻ ion addition enhanced the μ -hardness values. At 1100°C, when the F⁻ ion addition increased, μ -hardness values increased [29] but with increasing the sintering temperature, a reduction observed. Samples doped with Ti⁴⁺ and F⁻ ions had smaller μ -hardness values than pure 1.67CaP after the sintering at both temperatures. With increasing Ti⁴⁺ and F⁻ ions amount the μ -hardness values decreased.

When molar ratio increased to 2.0 at 1100°C, micro-hardness values revealed various trend. Increasing the sintering temperature exposed more stabile values. Increasing the Ti⁴⁺ ion amount increased the micro-hardness values of the samples except for 2.0CaP2.5Ti. At 1100°C, micro-hardness value of pure 2.0CaP was higher than that at 1300°C.

As a result of this study, with increasing sintering temperature μ -hardness values of pure 1.0, 1.50 and 1.67 increased and 1.25, 2.0 decreased. It is obvious that at 1300°C higher μ -hardness values were obtained.

Table 3.19: Micro-hardness of CaPs with Ca/P ratios of 1,1.25, 1.50, 1.67 and 2 sintered at 1100°C and 1300°C.

Sample ID	Micro-Hardness (GPa), 1100°C					Micro-Hardness (GPa), 1300°C				
	n=1.0	n=1.25	n=1.50	n=1.67	n=2.0	n=1.0	n=1.25	n=1.50	n=1.67	n=2.0
nCaP	3.23 ± 0.18	4.17 ± 0.18	2.41 ± 0.19	3.69 ± 0.27	4.99 ± 0.40	3.42 ± 0.33	3.43 ± 0.31	4.46 ± 0.43	5.66 ± 0.79	4.29 ± 0.51
nCaP0.5Ti	3.20 ± 0.24	4.00 ± 0.32	4.15 ± 0.28	2.03 ± 0.40	4.56 ± 0.41	3.64 ± 0.35	4.16 ± 0.67	3.40 ± 0.21	3.74 ± 0.40	4.42 ± 0.39
nCaP1.0Ti	3.02 ± 0.55	3.9 ± 60.39	4.52 ± 0.10	1.31 ± 0.15	3.88 ± 0.37	3.71 ± 0.26	2.94 ± 0.31	3.33 ± 0.36	3.68 ± 0.49	4.77 ± 0.44
nCaP2.5Ti	2.03 ± 0.12	1.89 ± 0.21	3.95 ± 0.27	0.61 ± 0.03	4.79 ± 0.45	3.91 ± 0.37	2.80 ± 0.39	2.63 ± 0.25	3.25 ± 0.24	5.33 ± 0.17
nCaP5.0Ti	1.21 ± 0.33	3.58 ± 0.32	4.06 ± 0.18	0.80 ± 0.03	4.67 ± 0.88	3.35 ± 0.41	3.55 ± 0.55	3.18 ± 0.18	3.49 ± 0.28	3.88 ± 0.55
nCaP0.5F	3.78 ± 0.43	4.74 ± 0.26	4.44 ± 0.22	5.16 ± 0.37	4.68 ± 0.40	3.26 ± 0.41	2.64 ± 0.27	3.54 ± 0.18	4.80 ± 0.46	3.48 ± 0.26
nCaP2.5F	3.02 ± 0.50	3.85 ± 0.14	4.80 ± 0.62	5.49 ± 0.38	3.08 ± 1.49	3.30 ± 0.31	2.99 ± 0.21	3.87 ± 0.30	4.48 ± 0.22	4.54 ± 0.69
nCaP0.5Ti0.5F	3.57 ± 0.47	3.17 ± 0.40	4.42 ± 0.27	2.39 ± 0.12	5.95 ± 0.49	3.91 ± 0.83	3.43 ± 0.24	3.53 ± 0.17	4.73 ± 0.85	4.55 ± 0.24
nCaP1.0Ti0.5F	3.29 ± 0.51	4.43 ± 0.23	3.10 ± 0.15	2.26 ± 0.75	4.91 ± 0.38	3.46 ± 0.27	3.68 ± 0.41	3.50 ± 0.22	3.92 ± 0.45	4.07 ± 0.68
nCaP2.5Ti0.5F	1.82 ± 0.14	4.32 ± 0.30	4.52 ± 0.18	1.69 ± 0.12	5.82 ± 0.32	4.69 ± 0.63	2.82 ± 0.85	2.74 ± 0.25	3.86 ± 0.40	3.58 ± 0.16
nCaP5.0Ti0.5F	1.29 ± 0.17	3.47 ± 0.23	4.40 ± 0.26	1.10 ± 0.26	5.25 ± 0.60	2.82 ± 0.43	5.42 ± 0.64	2.65 ± 0.53	2.82 ± 0.24	4.67 ± 0.49
nCaP0.5Ti2.5F	2.42 ± 0.32	2.87 ± 0.57	4.27 ± 0.18	3.37 ± 0.49	5.32 ± 0.25	4.11 ± 0.48	4.02 ± 0.58	3.82 ± 0.54	4.41 ± 0.23	5.89 ± 0.62
nCaP1.0Ti2.5F	2.68 ± 0.21	3.23 ± 0.38	4.39 ± 0.27	1.33 ± 0.10	6.38 ± 0.77	3.61 ± 0.24	2.71 ± 0.18	3.61 ± 0.24	4.20 ± 0.30	4.91 ± 0.42
nCaP2.5Ti2.5F	1.74 ± 0.25	3.91 ± 0.30	3.65 ± 0.21	2.42 ± 0.09	3.88 ± 0.62	6.07 ± 1.67	4.01 ± 0.52	2.90 ± 0.18	3.47 ± 0.29	6.04 ± 0.63
nCaP5.0Ti2.5F	2.52 ± 0.26	2.24 ± 0.32	4.61 ± 0.32	1.14 ± 0.09	5.03 ± 0.48	3.02 ± 0.42	3.68 ± 0.73	3.01 ± 0.29	3.52 ± 0.11	5.27 ± 0.21

CHAPTER 4

CONCLUSION

In this study, CaPs doped with Ti^{4+} and F^- ions were synthesized by a precipitation method. Doping amount of F^- ions was kept at 0.5 and 2.5 mol.% whereas doping amount of Ti^{4+} ions was 0.5, 1.0, 2.5, and 5 mol.%. Synthesized CaPs had Ca/P molar ratios ranging from 1.00 to 2.00. All samples were sintered at 1100°C and 1300°C for 1h. Microstructural and mechanical properties of the sintered samples were investigated.

According to density measurements of doped and undoped samples, small densities were achieved when the sintering temperature was increased from 1100 to 1300°C. High amount of Ti^{4+} led to a decrease in densification when Ca/P ratio was 1.0, 1.25, 1.67 (at 1100°C) and 1.50, 2.0 (at 1300°C). However, increase in densities was observed when Ca/P molar ratio was 1.50, 2.0 (at 1100°C) and 1.0, 1.25, 1.67 (at 1300°C). Densities of the F^- addition revealed considerable decreases at 1100°C and 1300°C. Except for the densities of the doped samples with molar ratio of 1.0, densities for molar ratio of 1.50 at 1100 and 1300°C decreased. For Ti^{4+} and 0.5 F^- co-doped samples, as the Ti^{4+} amount raised, the density of the samples decreased at 1100°C and 1300°C, except for the samples with molar ratios of 1.0 and 1.25 at 1300°C. Although densities of Ti^{4+} and 2.5 F^- doped samples decreased with increasing the Ti^{4+} amount from 0.5 mol.% to 5.0 mol.% after the sintering at 1100 and 1300°C, densities of samples with Ca/P molar ratio of 1.50 and 1.67 increased at 1100°C. These results demonstrated that optimum amount of Ti^{4+} and F^- ions decreased the densification. Furthermore, the results revealed that increasing the sintering temperature decreased the densification. At high sintering temperature, decreased densities were most probably due to the removal of structural water from the system.

The XRD pattern demonstrated that for Ca to P ratio of 1 at 1100°C, β -CPP phase was observed. When sintering temperature was increased, β -CPP, α -TCP and TiO_2 were formed. Increasing the molar ratio to 1.25 and 1.50 resulted in phases of β -TCP and/or β -

CPP and β -TCP/ HA at 1100°C and β -TCP and/or β -CPP, α -TCP, TiO₂ and HA, α -TCP TiO₂ at 1300°C, respectively. In higher molar ratios of 1.67 and 2.0, HA, β -TCP, α -TCP, CaO, TiO₂, CaTiO₃ and HA, CaO, α -TCP, CaTiO₃ phases was observed. In the samples with molar ratio 1.50, α -TCP phase was identified besides HA at 1300°C, resulting in the formation of β -TCP/ α -TCP biphasic composites with different compositions. In XRD, small shifts in peak positions were observed, due to the incorporation of doping ions and increased crystallinity. In Ti⁴⁺ doped samples of 1.67 and 2.0, at sintering temperature of 1100°C and 1300°C, decomposition of TiHA and formation of CaTiO₃ occurred. Results demonstrated that HA with 0.5Ti and 1.0Ti may have appropriate potential for biomedical applications. XRD results for molar ratio 2.0 revealed that HA, α -TCP, CaTiO₃ and CaO phase detected. With increasing Ca²⁺ ions into the system, the intensity of CaO phase increased. The structural analysis showed that among the samples, β -TCP and α -TCP were the main phases. The phase compositions at higher sintering temperatures can be explained by the changes in stoichiometry of the samples and due to loss of ions and molecules.

In FTIR spectroscopy analysis, when molar ratio is 1, 1.25, 1.50, 1.67 and 2.0 and sintering temperature is 1100°C, the characteristic bands of β -CPP, β -CPP/ β -TCP, β -TCP/HA, HA and HA were observed, respectively. With increasing the sintering temperature to 1300°C, samples with molar ratio of 1.0 and 1.25 revealed additional secondary characteristic peaks of HA and β -TCP. In the samples of molar ratio 1.0 and 1.25, PO₄³⁻ (ν_1 , ν_2 , ν_3 , ν_4 vibrational modes) and OH⁻ (librational and stretching) bands associated β -CPP, TCP and HA were detected. Additional peaks were determined in F⁻ doped samples at 696 cm⁻¹, in the molar ratios of 1, 1.25 (at 1100°C and 1300°C) and 1.50 (only at 1100°C) indicating the successful incorporation of F⁻ ions.

SEM images confirmed that sintering temperature and amount of dopants had significant effect on grain sizes of the samples. According to the results, the average grain sizes of the doped and undoped samples decreased when Ca/P ratio increased. Grain sizes were generally increased when sintering temperature was raised from 1100°C to 1300°C. It can be concluded that increasing the sintering temperature activates the particle growth. With respect to grain size calculations, with Ti⁴⁺ ion addition, average grain sizes in CaPs with molar ratios of 1, 1.50 and 1.67 rised and 1.25, 2.0 decreased when sintering temperature was 1100°C. With increasing the sintering temperature to 1300°C, average grain sizes were increased in the samples with molar ratio of 1, 1.25 and decreased in 1.50, 1.67 and 2.0.

These findings demonstrate that with incorporation of Ti^{4+} ion decreasing average grain size prevented the grain growth and increasing the average grain size allowed the grain growth. However, Ti^{4+} ion above certain limit developed the decomposition of HA phases. At 1300 °C, the strongest coalescence was observed in the samples. In these samples, initial crystals totally changed and coalesced to form grains with bigger dimensions. F^- ion addition increased the grain sizes in 1, 1.50, 2.0, and decreased them in 1.25, 1.67 at 1100°C and 1300°C. The grain sizes of groups consisting of Ti^{4+} and F^- increased when sintering temperature rose to 1300°C and fluctuations in grain sizes were detected.

As a result of Vickers microhardness test, Ti^{4+} ion addition in large amounts decreased the μ -hardness of the samples at 1100°C and 1300°C, except samples with molar ratio 2.0 (at 1100°C) and 1.0, 2.0 (at 1300°C). This had a positive effect on the mechanical properties of the samples. Substitution of F^- ions decreased the μ -hardness values up to certain extent, however samples with 1.0 (at 1100°C) and 1.50 (at 1100°C and 1300°C) F^- incorporation increased the μ -hardness. For Ti^{4+} and 0.5 F^- co-doped samples, as the Ti^{4+} amount raised, the μ -hardness of the samples decreased at 1100°C and 1300°C, except for the samples with molar ratios 1.0 and 1.25 at 1300°C. Although μ -hardness of Ti^{4+} and 2.5 F^- doped samples increased with increasing the Ti^{4+} amount from 0.5 mol.% to 5.0 mol.% after the sintering at 1100°C, μ -hardness of samples with molar ratio of 1.0 and 2.0 at 1100°C and samples at 1300°C decreased.

High densities were obtained for 1.67CaP, 1.67CaP2.5Ti0.5F and 2CaP0.5Ti2.5F at 1100°C. Samples with 1.67CaP2.5F, 2CaP0.5Ti0.5F, 2CaP1.0Ti0.5F, 2CaP2.5Ti0.5F, 2CaP5.0Ti0.5F, 2CaP0.5Ti2.5F, 2CaP1.0Ti2.5F and 2CaP2.5Ti2.5F at 1100°C had smaller grain sizes than pure HA. Microhardness of the co-doped samples with molar ratio of 1.67 and 2.0 at 1100°C were increased when doped with Ti^{4+} and F^- ions. To conclude that when CaPs analyzed in terms of structural and mechanical properties. CaPs with molar ratio of 1.67 and 2.0 doped with 0.5 to 2.5 mol.% F^- and 0.5 to 5.0 mol.% Ti^{4+} sintered at 1100°C were found the most outstanding materials for future biomechanical applications because this doped samples gave the highest microhardness values, high densities and small grain sizes. Therefore, further investigations should be focused on this materials.

REFERENCES

- [1] http://www.ivy-rose.co.uk/HumanBody/Skeletal/Skeletal_System.php., last visited on September 2010.
- [2] Wang T., Feng Z., “Dynamic mechanical properties of cortical bone: The effect of mineral content”, *Materials Letters*, 59 (2005) 2277-2280.
- [3] http://commons.wikimedia.org/wiki/File:Composition_of_bone.png, last visited on October 2010.
- [4] Mow V.C., Hayes W.C., “Basic Orthopedic Biomechanics”, Raven Press, Ltd., NY, USA, (1991), 93-94.
- [5] <http://www.britannica.com/EBchecked/topic/434280/osteocyte>, last visited on November 2010.
- [6] <http://www.mananatomy.com/basic-anatomy/skeleton/classification-of-bones.htm>, last visited on November 2010.
- [7] Rho J.Y., Khun-Spearing L., Zioupos P., “Mechanical properties and the hierarchical structure of bone”, *Medical Engineering & Physics*, 20 (1998) 92-102.
- [8] Cullinane D.M., Einhorn T.A., “Biomechanics of Bone”, *Principles of Bone Biology*, Second Edition, 1 (2002) 17–32.
- [9] Ribeiro C.C., Gibson I.,Barbosa M. A., “The uptake of tianium ions by hydroxyapatite particles-structural changes and possible mechanism”, *Biomaterials*, 27 (2006) 1749-1761.

- [10] Bilezikian J.P., Raisz L.G., Rodan G.A. 'Principles of Bone Biology' Academic Press, San Diego, USA, (1996) 16-23.
- [11] Jee W.S.S., "Integrated Bone Tissue Physiology: Anatomy and Physiology; Bone Mechanics Handbook", 2nd edition, CRC Press, Utah, USA (2001) 42-51.
- [12] Currey J.D., "Bones: Structure and Mechanics", Princeton University Press, Princeton, NJ, USA, (2002) 63-81.
- [13] Fratzl P., Gupta H.S., Paschalis E.P., Roschger P., "Structure and mechanical quality of the collagen-mineral nano-composite in bone", Journal of Materials Chemistry, 14 (2004) 2115 -2123.
- [14] Liu H.S, Chin T.S., Lai L.S., Chiu S.Y., Chung K.H., Chang C.S., Lui M.T., "Hydroxyapatite synthesized by a simplified hydrothermal method", Ceramics International, 23 (1997) 19-25.
- [15] Fathi M.H., Hanifi A., "Evaluation and characterization of nanostructure hydroxyapatite powder prepared by simple sol-gel method", Materials Letters, 61 (2007) 3978-3983.
- [16] Elliot J.C., "Structure and Chemistry of the Apatites and Other Calcium Orthophosphates", Studies in Inorganic Chemistry, Elsevier (1994) 18-20.
- [17] Weatherell J.A., Robinson C., "The inorganic composition of teeth"; in Zipkin I. (ed): Biological Mineralization, John Wiley, NY, USA, (1973) 43-74.
- [18] Song Q., Wang C., Wen S., "Effects of doping on crystal and grain boundary in human enamel", Materials Science and Engineering A, 297 (2001) 272-280.
- [19] Yuan H., Kurashina K., de Bruijn J., Li Y., de Groot K., Zhang X., "A preliminary study on osteoinduction of two kinds of calcium phosphate ceramics", Biomaterials, 20 (1999) 1799-1806.

- [20] Toth J.M., Lynch K.L., Hackbarth D.A., "Ceramic-induced osteogenesis following subcutaneous implantation of calcium phosphates", *Bioceramics*, 6 (1993) 9-13.
- [21] Yang Z., Yuan H., Tong W., Zou P., Chen W., Zhang X., "Osteogenesis in extraskeletally implanted porous calcium phosphate ceramics: Variability among different kinds of animals", *Biomaterials*, 17 (1996) 2131-2137.
- [22] Yuan H., Li Y., Yang Z., Zhang X., "Osteoinduction of pure β -TCP ceramic in dogs", *Biomedical Materials Research in the Far East*, 3 (1997) 188-197.
- [23] Park E., Lee Y., Choi J., Oh S., Shin H., Kim K., Kim S.Y., Kim S., "Cellular biocompatibility and stimulatory effects of calcium metaphosphate on osteoblastic differentiation of human bone marrow-derived stromal cells", *Biomaterials*, 25 (2004) 3403-3411.
- [24] Besta S.M., Porterb A.E., Thiana E.S., Huang J., "Bioceramics: Past, present and for the future", *Journal of the European Ceramic Society*, 28 (2008) 1319-1327.
- [25] Ryu H., Youn H., Hong K., Chang B., Lee C., Chung S., "An improvement in sintering property of β -tricalcium phosphate by addition of calcium pyrophosphate", *Biomaterials*, 23 (2002) 909-914.
- [26] Moseke C., Gbureck U., "Tetracalcium phosphate: Synthesis, properties and biomedical applications", *Acta Biomaterialia*, 6 (2010) 3815-3823.
- [27] Chow L.C., Markovic M., Frukhtbeyn S.A., Takagi S., "Hydrolysis of tetracalcium phosphate under a near-constant-composition condition--effects of pH and particle size", *Biomaterials*, 26 (2005) 393-401.
- [28] Combes C., Rey C., "Amorphous calcium phosphates: Synthesis, properties and uses in biomaterials", *Acta Biomaterialia*, 6 (2010) 3362-3378.

- [29] Sun J., Chang W., Chen L., Huang Y., Juang L., Lin F., "The influence on gene expression profiling of osteoblasts behavior following treatment with the ionic products of sintered β -dicalcium pyrophosphate dissolution", *Biomaterials*, 25 (2004) 607-616.
- [30] Sekar C., Kanchana P., Nithyaselvi R., Girija E.K., "Effect of fluorides (KF and NaF) on the growth of dicalcium phosphate dehydrates (DCPD) crystal", *Materials Chemistry and Physics*, 115 (2009) 21-27.
- [31] Suzuki O., Kamakura S., Katagiri T., Nakamura M., Zhao B., Honda Y., Kamijo R., "Bone formation enhanced by implanted octacalcium phosphate involving conversion into Ca-deficient hydroxyapatite", *Biomaterials*, 27 (2006) 2671-2681.
- [32] Huan Z., Chang J., "Novel bioactive composite bone cements based on the β -tricalcium phosphate-monocalcium phosphate monohydrate composite cement system", *Acta Biomaterialia*, 5 (2009) 1253-1264.
- [33] Yingguang L., Zhuoru Y., Jiang C., "Preparation, characterization and antibacterial property of cerium substituted hydroxyapatite nanoparticles", *Journal of Rare Earths*, 25 (2007) 452-456.
- [34] Muralithran G., Ramesh S., "The effects of sintering temperature on the properties of hydroxyapatite", *Ceramics International*, 26 (2000) 221-230.
- [35] Rhee S.-H., "Synthesis of hydroxyapatite via mechanochemical treatment", *Biomaterials*, 23 (2002) 1147-1152.
- [36] Bett J.A.S., Christner L.G., Hall W.K., "Studies of the hydrogen held by solids. XII. hydroxyapatite catalysts", *Journal of the American Chemical Society*, 89 (1967) 5535-5541.

- [37] Pramanik S., Agarwal A.K., Rai K.N., Garg A., “Development of high strength hydroxyapatite by solid-state-sintering process”, *Ceramics International*, 33 (2007) 419-426.
- [38] Lim G.K., Wang J., Ng S.C., Chew C.H., Gan L.M., “Processing of hydroxyapatite via microemulsion and emulsion routes”, *Biomaterials*, 18 (1997) 1433-1439.
- [39] Jarudilokkul S., Tanthapanichakoon W., Boonamnuyvittaya V., “Synthesis of hydroxyapatite nanoparticles using an emulsion liquid membrane system”, *Colloids and Surfaces A: Physicochemical and Engineering Aspects*, 296 (2007) 149–153.
- [40] Koumoulidis G., Katsoulidis A., Ladavos A., Pomonis P., Trapalis C., Sdoukos A., Vaimakis T., “Preparation of hydroxyapatite via microemulsion route”, *Journal of Colloid and Interface Science*, 259 (2003) 254–260.
- [41] Yang J., Yang P., Wang W., Gai S., Wang J., Zhang M., Lin J., “Synthesis and characterization of Eu-doped hydroxyapatite through a microwave assisted microemulsion process”, *Solid State Sciences*, 11 (2009) 1923–1928.
- [42] Guo G., Sun Y., Wang Z., Guo H., “Preparation of hydroxyapatite nanoparticles by reverse microemulsion”, *Ceramics International*, 31 (2005) 869–872.
- [43] Shih W.J., Chen Y.H., Wang M.C., Hon , M.H. “Crystal growth and morphology of the nano-sized hydroxyapatite powders synthesized from $\text{CaHPO}_4 \cdot 2\text{H}_2\text{O}$ and CaCO_3 by hydrolysis method”, *Journal of Crystal Growth*, 270 (2004) 211–218.
- [44] Zhang X., Vecchio K., “Hydrothermal synthesis of hydroxyapatite rods”, *Journal of Crystal Growth*, 308 (2007) 133–140.
- [45] Feng W., Mu-Sen L., Yu-Peng L., Yong-Xin Q., “A simple sol–gel technique for preparing hydroxyapatite nanopowders”, *Materials Letters*, 59 (2005) 916–919.

- [46] Padmanabhan S., Balakrishnan A., Chu M., Lee Y., Kim T., Cho S., "Sol-gel synthesis and characterization of hydroxyapatite nanorods", *Particuology*, 7 (2009) 466-470.
- [47] Liu D., Troczynski T., Tseng W., "Water-based sol-gel synthesis of hydroxyapatite: Process development", *Biomaterials*, 22 (2001) 1721-1730.
- [48] Mobasherpour I., Heshajin M.S., Kazemzadeh A., Zakeri M., "Synthesis of nanocrystalline hydroxyapatite by using precipitation method", *Journal of Alloys and Compounds*, 430 (2007) 330-333.
- [49] Cengiz B., Gokce Y., Yildiz N., Aktas Z., Calimli A., "Synthesis and characterization of hydroxyapatite nanoparticles", *Colloids and Surfaces A: Physicochemical and Engineering Aspects*, 322 (2008) 29-33.
- [50] LeGeros R.Z., Lin S., Rohanizadeh R., Mijares D., LeGeros J.P., "Biphasic calcium phosphate ceramics: Preparation, properties and applications", *Journal of Materials Science: Materials in Medicine*, 14 (2003) 201-209.
- [51] Kay M.I., Young R.A., Posner A.S., "Crystal structure of hydroxyapatite", *Nature*, 204 (1964) 1050-1052.
- [52] <http://www.pentax.jp/english/lifecare/newceramics/apaceram/index.html>, last visited on 20 September 2010.
- [53] Helson L.L., Wilson J., "An Introduction to Bioceramics", *World Scientific*, (1993) 139-180.
- [54] Ramesh S., Tan C.Y., Sopyan I., Hamdi M., Teng W.D., "Consolidation of nanocrystalline hydroxyapatite powder", *Science and Technology of Advanced Materials*, 8 (2007) 124-130.

- [55] Kalita S.J., Bhardwaj A., Bhatt H.A., “Nanocrystalline calcium phosphate ceramics in biomedical engineering”, *Materials Science and Engineering C*, 27 (2007) 441–449.
- [56] Fernández E., Gil F.J., Ginebra M.P., Driessens F.C.M., Planell J.A., Best S.M., “Calcium phosphate bone cements for clinical applications. Part I: Solution chemistry”, *Journal of Materials Science: Materials in Medicine*, 10 (1999) 169–176.
- [57] Webster T.J., Ergun C., Doremus R.H., Siegel R.W., Bizios R., “Enhanced osteoclast-like cell functions on nanophase ceramics”, *Biomaterials*, 22 (2001) 1327–1333.
- [58] Webster T.J., Ergun C., Doremus R.H., Siegel R.W., Bizios R., “Enhanced functions of osteoblasts on nanophase ceramics”, *Biomaterials*, 21 (2000) 1803–1810.
- [59] Catros S., Guillemot F., Lebraud E., Chanseau C., Perez S., Bareille R., Amedee J., Fricain J.C., “Physico-chemical and biological properties of a nano hydroxyapatite powder synthesized at room temperature”, *Ingénierie et Recherche Biomédicale (BioMedical Engineering and Research)*, 31 (2010) 226–233.
- [60] Chu C., Xue X., Zhu J., Yin Z., “Mechanical and biological properties of hydroxyapatite reinforced with 40 vol.% titanium particles for use as hard tissue replacement”, *Journal of Materials Science: Materials in Medicine*, 15 (2004) 665–670.
- [61] Evis Z., Doremus R.H., “Coatings of hydroxyapatite-nanosize alpha alumina composites on Ti-6Al-4V”, *Materials Letters*, 59 (2005) 3824–3827.
- [62] He L.-H., Standard O.C., Huang T.T.Y., Latella B.A., Svain M.V., “Mechanical behavior of porous hydroxyapatite”, *Acta Biomaterialia*, 4 (2008) 577–586.

- [63] Bezzi G., Celotti G., Landi E., La Torretta T.M.G., Sopyan I., Tampieri A., “A novel sol–gel technique for hydroxyapatite preparation”, *Materials Chemistry and Physics*, 78 (2003) 816–824.
- [64] Banerjee A., Bandyopadhyay A., Bose S., “Hydroxyapatite nanopowders: Synthesis, densification and cell–materials interaction”, *Materials Science and Engineering C*, 27 (2007) 729–735.
- [65] Hench L.L., “Bioceramics: From concept to clinic” *Journal of the American Ceramic Society*, 74 (1991) 1487-1510.
- [66] Legeros R.Z., Legeros J.P., in *An Introduction to Bioceramics*, edited by Hench L.L. and Wilson J., World Scientific, Singapore (1993) 33-39.
- [67] Ahn E.S., Gleason N.J., Nakahira A., Ying J.Y., “Nanostructure processing of hydroxyapatite-based bioceramics”, *Nano Letters*, 1 (2001) 149-153.
- [68] Meyers M.A., Chen P.Y., Lin A.Y.M., Seki Y., “Biological materials: Structure and mechanical properties”, *Progress in Materials Science*, 53 (2008) 1-206.
- [69] Huang J., Best S.M., Bonfield W., Buckland T., “Development and characterization of titanium-containing hydroxyapatite for medical applications”, *Acta Biomaterialia* 6 (2010) 241–249.
- [70] Ergun C., “Effect of Ti ion substitution on the structure of hydroxylapatite”, *Journal of the European Ceramic Society*, 28 (2008) 2137-2149.
- [71] Ergun C., Doremus R.H., Lanford W., “Hydroxylapatite and titanium: Interfacial reactions”, *Journal of Biomedical Materials Research Part A*, 65A (2003) 336-343.
- [72] Kanchana P., Sekar C., “Influence of sodium fluoride on the synthesis of hydroxyapatite by gel method”, *Journal of Crystal Growth*, 312 (2010) 808–816.

- [73] Machoy-Mokrzynska A., "Fluoride- magnesium interaction", *Fluoride, Journal of the International Society for Fluoride Research*, 28 (1995) 175-177.
- [74] Eslami H., Solati-Hashjin M., Tahriri M., "The comparison of powder characteristics and physicochemical, mechanical and biological properties between nanostructure ceramics of hydroxyapatite and fluoridated hydroxyapatite", *Materials Science and Engineering A*, 29 (2009) 1387-1398.
- [75] Okazaki M., Miake Y., Tohda H., Yanagisawa T., Matsumoto T., Takahashi J., "Functionally graded fluoridated apatites", *Biomaterials*, 20 (1999) 1421-1426.
- [76] Cheng K., Weng W., Wang H., Zhang S., "In vitro behavior of osteoblast-like cells on fluoridated hydroxyapatite coatings", *Biomaterials*, 26 (2005) 6288–6295.
- [77] Gross K.A., Rodriguez-Lorenzo L.M., "Sintered hydroxyfluorapatites Part II: mechanical properties of solid solutions determined by microindentation" *Biomaterials*, 25 (2004) 1385–1394.
- [78] Evis Z., Doremus R.H., "Effect of MgF_2 on hot pressed hydroxylapatite and monoclinic zirconia composites", *Journal of Materials Science*, 42 (2007) 3739-3744.
- [79] Kuwahara H., Mazaki N., Takahashi M., Watanabe T., Yang X., Aizawa T., *Materials Science and Engineering A* 319-321 (2001) 687-691.
- [80] Ponton C.B, Rawlings R.D., "Vickers indentation fracture toughness test part 1: Review of literature and formulation of standardized indentation toughness equation", *Materials Science and Technology*, 5 (1989) 865-872.
- [81] Kalita S.J., Bhatt H.A, "Nanocrystalline hydroxyapatite doped with magnesium and zinc: Synthesis and characterization", *Materials Science and Engineering C*, 27 (2007) 837-848.

- [82] http://en.wikipedia.org/wiki/Dicalcium_phosphate last visited on July 2010.
- [83] Gross K.A., Rodriguez-Lorenzo L.M., “Sintered hydroxyfluorapatites Part I: Sintering ability of precipitated solid solution powders”, *Biomaterials*, 25 (2004) 1375–1384.
- [84] Chenglin C., Jingchuan Z., Zhongda Y., Shidong W., “Hydroxyapatite–Ti functionally graded biomaterial fabricated by powder metallurgy”, *Materials Science and Engineering A271* (1999) 95–100.
- [85] Fang Y., Agrawal D.K., Roy D.M., “Fabrication of transparent hydroxyapatite ceramics by ambient-pressure sintering”, *Materials Letters*, 23 (1995) 147-151.
- [86] Basar B., Tezcaner A., Keskin D., Evis Z., “Improvements in microstructural, mechanical, and biocompatibility properties of nano-sized hydroxyapatites doped with yttrium and fluoride”, *Ceramics International*, 36 (2010) 1633-1643.
- [87] Azami M., Jalilifiroozinezhad S., Mozafari M., Rabiee M., “Synthesis and solubility of calcium fluoride/hydroxy-fluorapatite for dental application”, *Ceramics International*, 37 (2011) 2007-2014.
- [88] Slosarczyk A., Paluszkievicz C., Gawlicki M., Paszkiewicz Z., “The FTIR spectroscopy and QXRD studies of calcium phosphate based materials produced from the powder precursors with different Ca/P ratios”, *Ceramics International*, 23 (1997) 297-304.
- [89] Torrent-Burgues J., Rodriguez-Clemente R., “Hydroxyapatite precipitation in a semibatch process”, *Crystal Research and Technology*, 36 (2001) 1075-1082.
- [90] Kannan S., Ferreira J.M., “Synthesis and thermal stability of hydroxyapatite-beta-tricalcium phosphate composites with cosubstituted sodium, magnesium, and fluorine”, *Chemistry of Materials*, 18 (2006) 198-203.

- [91] Azami M., Jalilifiroozinezhad S., Mozafari M., Rabiee M., "Synthesis and solubility of calcium fluoride/hydroxy-fluorapatite for dental application", *Ceramics International*, 37(2011) 2007-2014.
- [92] Ozek S.N., Tuna S., Erson-Bensan A.E., Severcan F., "Characterization of microRNA-125b expression in MCF7 breast cancer cells by ATR-FTIR spectroscopy", *Analyst*, 135 (2010) 3094–3102.
- [93] Qu H., Wei M., "Effect of fluorine content on mechanical properties of sintered hydroxyapatite", *Materials Science and Engineering C*, 26 (2006) 46-53.
- [94] Linghong G., Hui L., "Phase transformations and structure characterization of calcium polyphosphate during sintering process", *Journal of Materials Science*, 39 (2004) 7041-7047.
- [95] Toker S.M., Evis Z., Tezcaner A., "Investigation of microstructure, microhardness and biocompatibility characteristics of yttrium and fluoride doped hydroxyapatite", 15th National Biomedical Engineering Meeting, Turkey (2010) 1-5.
- [96] Bertoni E., Bigi A., Cojazzi G., Gandolfi M., Panzavolta S., Roveri N., "Nanocrystals of magnesium and fluoride substituted hydroxyapatite", *Journal of Inorganic Biochemistry*, 72 (1998) 29-35.
- [97] Shannon R.D., "Revised effective ionic-radii and systematic studies of interatomic distances in halides and chalcogenides", *Acta Crystallographica Section A*, 32 (1976) 751-767.
- [98] Jha L.J., Best M., Knowles J.C., Rehman I., Santos J.D., Bonfield W., "Preparation and characterization of fluoride substituted apatites", *Journal of Materials Science: Materials in Medicine*, 8 (1997) 185-191.

- [99] Ribeiro, C.C., Gibson I., Barbosa M.A., “The uptake of titanium ions by hydroxyapatite particles — structural changes and possible mechanisms”, *Biomaterials*, 27 (2006) 1749.
- [100] El Kady A., Mohamed K.R., El-Bassyouni G.T., “Fabrication, characterization and bioactivity evaluation of calcium pyrophosphate/polymeric biocomposites”, *Ceramics International*, 35 (2009) 2933–2942.
- [101] Douard N., Detsch R., Ghodsina R.C., Damia C., Deisinger U., Champion E., “Processing, physico-chemical characterisation and in vitro evaluation of silicon containing β -tricalcium phosphate ceramics”, *Materials Science and Engineering C*, 31 (2011) 531-539.
- [102] Chen L., Wang Z., Lin C., “Preparation and characterization of nano-sized HA particles and HA/chitosan naano-composite for use in biomedical materials”, *Materials Letters*, 57 (2002) 858-861.
- [103] Oliveira Ugarte J.F., Sena L.A., Castro Perez C.A., Aguiar P.F., Rossi A.M., Soares G.A., “Influence of processing parameters on structural characteristics of porous calcium phosphate samples: A study using an experimenta design method”, *Materials Research*, 8 (2005) 71-76.
- [104] Sanosh K.P., Chu M.C., Balakrishnan A., Lee Y.J., Kim T.N., Cho S.J., “Preparation and characterization of nano-hydroxyapatite powder using sol-gel technique”, *Current Applied Physics*, 9 (2009) 1459-1462.
- [105] Pushpakanth S., Srinivasan B., Sreedhar B., Sastry T.P., “An in situ approach to prepare nanorods of titania-hydroxyapatite (TiO₂-HAp) nanocomposite by microwave hydrothermal technique”, *Material Chemical Physics*, 107 (2008) 492-498.

- [106] Ergun C., Evis Z., Webster T. J., Sahin F. C., "Synthesis and microstructural characterization of nano-size calcium phosphates with different stoichiometry", *Ceramics International*, 37 (2011) 971-977.
- [107] Kannan S., Rocha J.H.G, Ventura J.M.G., Lemos A.F., Ferreira J.M.F., "Effect of Ca/P ratio of precursors on the formation of different apatitic ceramics-an X-ray diffraction study", *Scripta Materialia*, 53 (2005) 1259-1262.
- [108] Bandyopadhyay A., Withey E.A., Moore J., Bose S., "Influence of ZnO doping in calcium phosphate ceramics", *Materials Science and Engineering C*, 27 (2007) 14-17.
- [109] Maciejewski M., Brunner T.J., Loher S.L., Stark W.J., Baiker A., "Phase transitions in amorphous calcium phosphates with different Ca/P ratios", *Thermochimica Acta*, 468 (2008) 75-80.
- [110] Petrov O.E., Dyulgerova E., Petrov L., Popova R., "Characterization of calcium phosphate phases obtained during the preparation of sintered biphasic Ca-P ceramics", *Materials Letters*, 48 (2001) 162-167.
- [111] Raynaud S., Champion E., Bernache-Assollant D., "Calcium phosphate apatites with variable Ca/P atomic ratio II. Calcination and sintering", *Biomaterials*, 23 (2002) 1073-1080.
- [112] Ergun C., Doremus R.H., "Thermal stability of hydroxylapatite-titanium and hydroxylapatite-titania composites", *Turkish Journal Engineering and Environmental Sciences*, 27 (2003) 423-429.
- [113] Wang Q.B., Wang Q.G., Wan C.X., "Effect of sintering time on the microstructure and properties of inorganic polyphosphate bioceramics", *Science of Sintering*, 42 (2010) 337-343.

- [114] Böhner M., Galea L., Doeblin N., “Calcium phosphate bone graft substitute: failures and hopes”, *Journal of the European Ceramic Society*, (2012) doi:10.1016/j.jeurceramsoc.2012.02.028.
- [115] Wu S.C., Hsu H.C., Hsu S.K., Wang W.S., Ho W.F., “Preparation and characterization of four different compositions of calcium phosphate scaffolds for bone tissue engineering”, *Materials Characterization*, 62 (2011) 526-534.
- [116] Klawitter J.J., Hulbert S.F., “Application of porous ceramics for the attachment of load bearing internal orthopedic applications”, *Journal of Biomedical Materials Research Symposium*, 2 (1971) 151-229.
- [117] Chou L., Marek B., Wagner W.R., “Effects of hydroxylapatite coating crystallinity on biosolubility, cell attachment efficiency and proliferation in vitro”, *Biomaterials*, 20 (1999) 977-985.
- [118] Słosarczyk A., Zima A., Paszkiewicz, Szczepaniak J., Aza A.H., Chrościcka A., “The influence of titanium on physicochemical properties of Ti-modified hydroxyapatite materials”, *Ceramic Materials*, 62 (2010) 369-375.
- [119] Graeve O.A., Kanakala R., Madadi A., Williams B.C., Glass K.C., “Luminescence variations in hydroxyapatites doped with Eu^{2+} and Eu^{3+} ions”, *Biomaterials*, 31 (2010) 4259-4267.
- [120] Cakmak G., Togan I., Severcan F., “ 17β - Estradiol induced compositional, structural and functional changes in rainbow trout liver, revealed by FTIR spectroscopy: A comparative study with nonylphenol”, *Aquatic Toxicology* 77 (2006)53-63.
- [121] Kim H.W., Noh Y.J., Koh Y.H., Kim H.E., “Enhanced performance of fluorine substituted hydroxyapatite composites for hard tissue engineering”, *Journal of Materials Science: Materials in Medicine* 14 (2003) 899-904.

VITA

Serap Güngör Geridönmez Güzeltepe Sok. 35 / 3 Demirlibahçe ANKARA sgungor@metu.edu.tr	
Personal Details	
Nationality	Turkish
Marital Status	Married
Education and Qualifications	
09.2002 – Today	Middle East Technical University, PhD. Student at Dept. of Engineering Sciences.
09.1997 – 09.2002	Ankara University. Bachelor degree, Dept. of Physics.
09.1991 – 01.1996	Milli Piyango Anatolian High School.
Publications/Conferences	
2007	Güngör-Geridönmez S., Birlik G., Sezgin Ö.C., ‘Response of Recumbent Persons to Random Vibrations’ Inter-Noise 2007, Istanbul, Turkey.
2008	Güngör-Geridönmez S., Birlik G., Sezgin Ö.C., ‘Vibration Exposure of Lying Persons in an Ambulance’ 16th Japan Conference on Human Response to Vibration, Yonago, Japan.
2009	Güngör-Geridönmez S., Birlik G., Sezgin Ö.C., ‘Vibration Exposure of Supine and Semi Supine Subjects’ 4th International Conference on Whole Body Vibration Injuries, Montreal, Canada.
2011	Maeda S., Güngör Geridönmez S., Miyashita K., Ishimatsu K., ‘Frequency weighting of Hand-Transmitted Vibration for Evaluating Comfort’ 12th International Conference on Hand-Arm Vibration, Ottawa, Canada.
2011	Maeda S., Güngör Geridönmez S., Miyashita K., Ishimatsu K., ‘Transition of Frequency-Weighting Curves of Hand-Arm Vibration Evaluation’ 19th Japan Conference on Human Response to Vibration, Nagoya, Japan.
2011	Maeda S., Güngör Geridönmez S., Miyashita K., Ishimatsu K., ‘Validation of Frequency Weightings of Hand-Transmitted Vibration for Evaluating Comfort’ Inter-noise 2011, Osaka, Japan.
2011	Kalyoncuoğlu, T., Yılmaz, B., Güngör-Geridönmez S., Kansu, G., ‘An attempt to improve clinical performance of dental implants: A pilot study’ European Prosthodontic Association (EPA) Congress, Bern, Switzerland.
2012	Güngör-Geridönmez S., Evis Z., ‘Synthesis and microstructural characterization of nano-sized hydroxyapatite doped with titanium and fluoride ions ’ Nanomaterials for Biomedical Technologies Conference, Frankfurt, Germany.
English, Dutch	Very Good, Good